CHAPTER 3

Acylpyrazolone ligands and their Neodymium metal complexes: Synthesis, Characterization and Structural Features.

Part (a): Structural Features, Emission Analysis, and Covalency Comparison of Neodymium Acylpyrazolone Complexes using Oscillator Strengths, Covalency and Judd-Ofelt Parameters.

3a.1 Introduction

The coordination chemistry of lanthanide ions has garnered significant attention over the past two decades owing to their advantageous magnetic, thermal, cytotoxic, redox, and optical properties, along with their large coordination numbers, facilitating the formation of highly complex dimensional networks [1–8]. Their diverse properties have led to applications in NMR imaging, sensors, lighting, fibers, display devices, lasers, and biological assays [7]. Lanthanides typically exhibit low covalency with ligands due to the shielding of their 4f electrons by $5s^2$ and $5p^6$ orbitals, along with ion-specific emission. The sharp electronic transitions of Ln(III) ions result from the modest stokes shift induced by the intrinsic nature of 4f electrons, which are protected from disruption by the ligand field. Understanding the bonding of lanthanide complexes relies on investigating the type and degree of covalency [9] despite limitations imposed by Laporte ($\Delta L=\pm1$) and Spin ($\Delta S=0$) rules for 4f-4f transitions. Certain spectral transitions, known as hypersensitive transitions, exhibit higher intensities and significantly influence covalency due to their sensitivity to the ligand environment. Judd-Ofelt intensity parameters (Ω_2, Ω_4, Ω_6) and oscillator strength calculations are crucial as they provide insight into the ligand's impact on intra-configurational transitions of Ln(III) ions based on factors such as covalency, number and magnitude of lines, and transition intensity ratios [10,11]. These factors offer information about the rigidity, long-range distance, symmetry, and coordination number of complexes.

Neodymium stands out among the lanthanides for its ability to form alloys, particularly in producing robust permanent magnets. Neodymium extraction techniques include ion exchange, flash pyrolysis [12], solvent extraction [13], and others. Neodymium compounds and nanomaterials exhibit a wide range of properties, including anticandidal [14], catalytic [15], chemo-selective [15], optical limiting [16], antibacterial [17], and wastewater treatment capabilities [18], as well as structural, optical, and electrical activities [19]. Perovskite strontium-doped neodymium manganite effectively removes Fast Green Dye [20]. Neodymium complexes featuring ligands with a β-diketone backbone typically favor a distorted square antiprism geometry [21]. Dynamic coupling mechanisms significantly influence the intensity of hypersensitive transitions in Nd-β-diketone complexes [22]. Ternary neodymium tris β-diketonate complexes emitting near-infrared light exhibit promising applications in organic light-emitting devices [23].

Acylpyrazolone ligands, along with additional ligands such as macrocycles, thiadiazols, cyclic multidentate groups, and naphthyl moieties [24–27], have attracted attention due to their ability to adopt variable 7 to 9 coordinated geometries high absorption coefficient values, efficient Antenna effects, luminous probe activities, and catalytic and biological recognition capabilities [28–30]. Understanding the properties of lanthanide-acylpyrazolone complexes relies on analyzing the covalent interactions between the metal and ligands. The extraction efficiency and effective Antenna effect of acylpyrazolones with lanthanides are intricately linked to the covalent nature of their metal-ligand interactions [28–30]. This study proposes a practical approach to determine the Judd-Ofelt intensity parameters and oscillator strengths of three Nd(III)-acylpyrazolone complexes—designated as 6, 7, and 8—in various solvents. These complexes have the general formula $[Nd(L)_3(H_2O)(EtOH)]$ and adopt a distorted square antiprismatic geometry.

3a.2 Experimental section

3a.2.1 Materials and Methods

The preparation of three ligands denoted as HL^1 (p-chlorobenzoyl 1-phenyl 3-methyl 5-pyrazolone), HL^2 (p-chlorobenzoyl 1-(m-chlorophenyl) 3-methyl 5-pyrazolone), and HL^3 (p-chlorobenzoyl 1-(p-tolyl) 3-methyl 5-pyrazolone), followed the reported procedure [31,32]. Neodymium(III) nitrate hexahydrate with a purity of 99.9% was acquired from SRL Pvt. Ltd.

3a.2.2 Neodymium-acylpyrazolone Complex Synthesis

A solution containing 3 mmol ligand in ethanol and 3 mmol $NaOH_{(aq)}$ was stirred for thirty minutes at 80–100 °C, as depicted in Figure 3a.1. Subsequently, a solution of 1 mmol neodymium(III) nitrate hexahydrate in ethanol was added dropwise. After 18 hours of refluxing, the solution was transferred to a container and evaporated slowly, yielding an eight-coordinated neodymium-acylpyrazolone complex.

Complex 6 Synthesis

Complex 6 was prepared using HL^1 ligand (0.9375 g), $NaOH_{(aq)}$ (0.12 g), and neodymium(III) nitrate hexahydrate (0.438 g). The bright pale-yellow prism-type crystals of complex 6 were obtained using a slow evaporation recrystallization technique. Yield (%): 93.14%, M.P.: >200 °C, Molecular formula: $C_{53}H_{43}Cl_3N_6NdO_8$, Formula wt: 1142.55. Mass peaks (see Figure 3a.2) (m/z) = 1141.14

($[C_{53}H_{43}Cl_3N_6NdO_8]^+$), 1124.15 ($[C_{59}H_{54}N_6NdO_6]^+$). **FTIR (KBr, cm^{-1}):** 3065 (w, $\upsilon_{O-H\ water}$), 2930 (w, $\upsilon_{O-H\ EtOH}$), 1612 (s, $\upsilon_{C=O\ PCB}$), 1592 (s, $\upsilon_{C=O\ acylpyz}$).

Complex 7 Synthesis

Complex 7 was prepared using HL^2 ligand (1.0416 g), $NaOH_{(aq)}$ (0.12 g), and neodymium(III) nitrate hexahydrate (0.438 g). Yield (%): 95.24%, M.P.: >200 °C, Molecular formula: $C_{53}H_{40}Cl_6N_6NdO_8$, Formula wt: 1245.88. **FTIR (KBr, cm^{-1}):** 3051 (w, $\upsilon_{O-H\ water}$), 2973 (w, $\upsilon_{O-H\ EtOH}$), 1612 (s, $\upsilon_{C=O\ PCB}$), 1589 (s, $\upsilon_{C=O\ acylpyz}$).

Complex 8 Synthesis

Complex 8 was prepared using HL^3 ligand (0.9795 g), $NaOH_{(aq)}$ (0.12 g), and neodymium(III) nitrate hexahydrate (0.438 g). Yield (%): 92.66%, M.P.: >200 °C, Molecular formula: $C_{56}H_{49}Cl_3N_6NdO_8$, Formula wt: 1184.63. Mass peaks (see Figure 3a.3) (m/z) = 1183.18 ($[C_{56}H_{49}Cl_3N_6NdO_8]^+$), 1166.18 ($[C_{62}H_{60}N_6NdO_6]^+$). **FTIR (KBr, cm^{-1}):** 3033 (w, $\upsilon_{O-H\ water}$), 2926 (w, $\upsilon_{O-H\ EtOH}$), 1615 (s, $\upsilon_{C=O\ PCB}$), 1599 (s, $\upsilon_{C=O\ acylpyz}$).

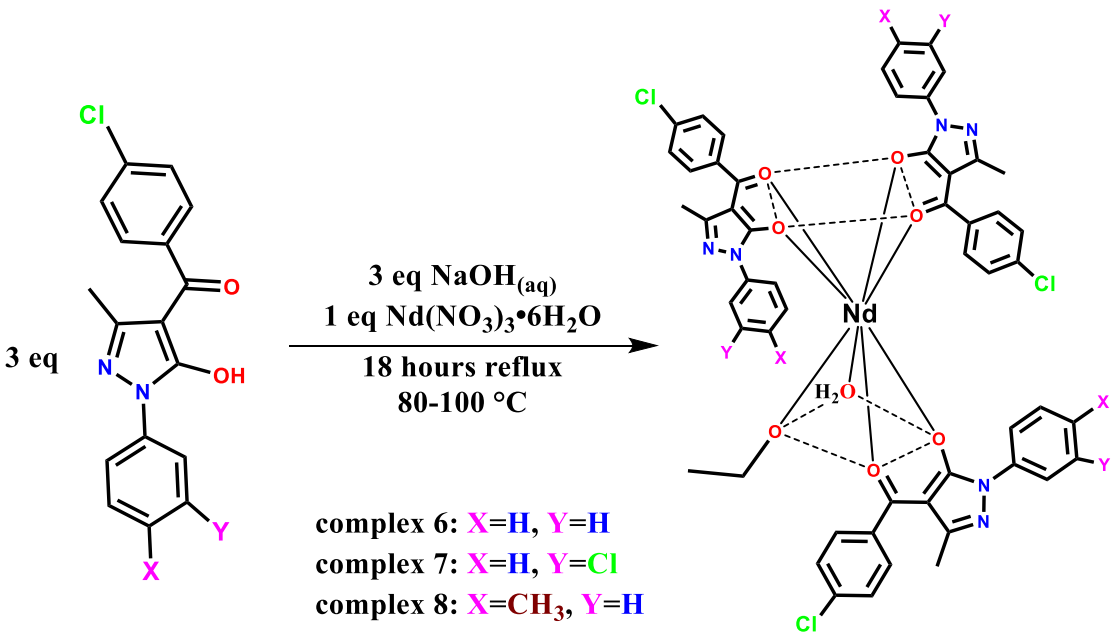

Figure 3a.1 Synthetic route for neodymium-acylpyrazolone complexes.

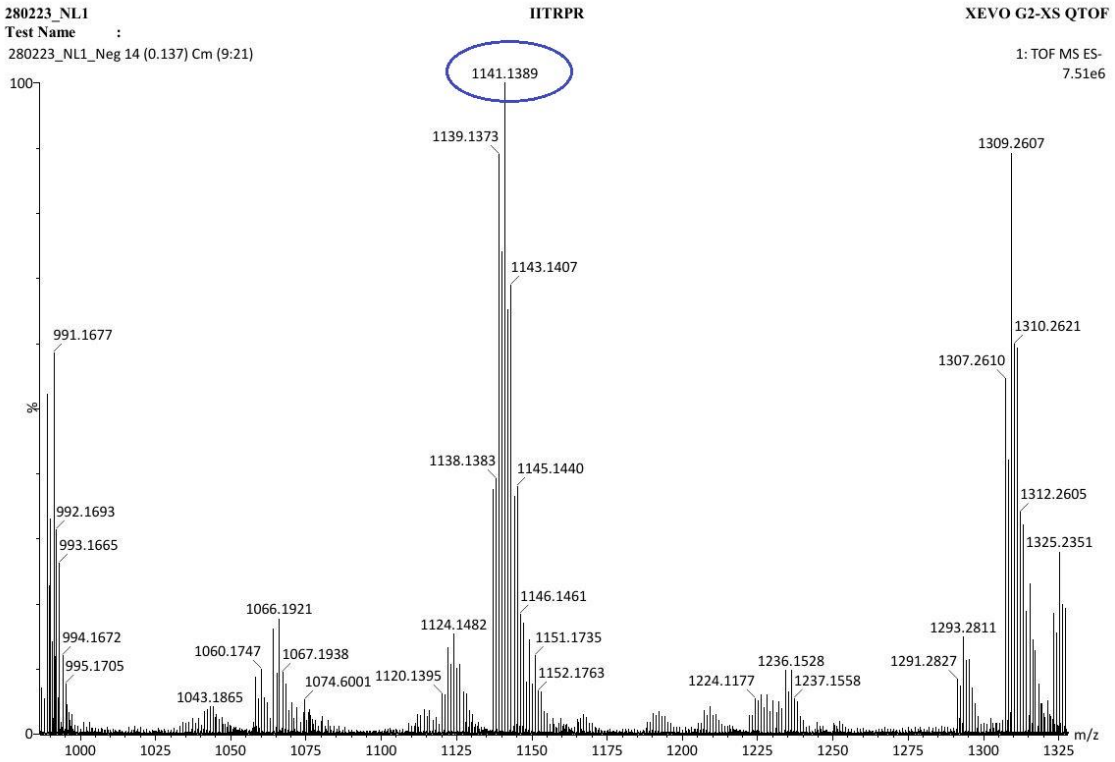

Figure 3a.2 Mass spectrum of complex 6.

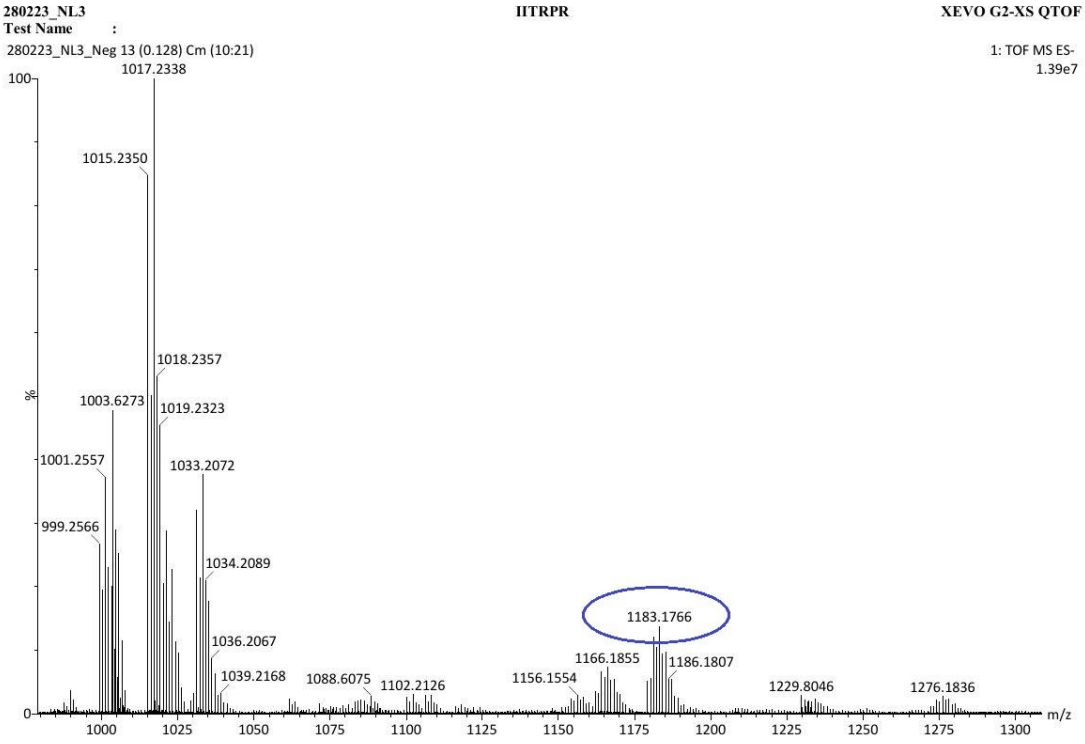

Figure 3a.3 Mass spectrum of complex 8.

3a.2.3 X-ray crystallographic examination

X-ray crystallographic analysis was conducted on complex 6 using Cu-K_α (λ = 1.54184 Å) radiation and graphite monochromator. The detection and refinement procedures were performed based on the methods outlined in previously published papers from our laboratory [33]. The diffraction data were solved using the SHELXT software [34], while computation was done using the crystallographic software SHELXL-2018/3 [35].

3a.2.4 Physical measurements and characterization techniques

Analogous methodologies, models, instruments, or instruments were employed to analyze the data of the synthesized compounds, using techniques such as FTIR, mass, UV-Vis, and TG-DTA following procedures outlined in previously published articles from our laboratory [33,36]. All mass spectra were collected via the XEVO G2-XS QTOF at IIT Ropar. KBr pellets were used in Bruker Alpha FT-IR spectrometer to obtain the FTIR spectra. Perkin Elmer Lambda 35 UV-Vis spectrometer was used to record the electronic spectra. On a SII-EXSTAR6000 TG-DTA 6300 apparatus, simultaneous TG-DTA was performed. The studies were conducted at a heating rate of 10 °C min^{-1} in a nitrogen environment over the 30-550 °C temperature range. Conductometer model EQ664A was used for molar conductivity measurement. The solid-state emission spectra were measured using a Jasco FP-6300 spectrofluorometer. Powder X-ray diffraction (XRD) analyses were measured on a Rigaku SmartLab SE (3kW) instrument from Japan using the SmartLab Studio II software. A Cu-Kα (0.154 nm) was used as the source in XRD, and data were collected using a D/teX Ultra 250 1D detector.

3a.3 Results and Discussion

For complexes 6, 7, and 8, the molar conductivity Λ_M values were found to be 10, 5, and 6 Ω^{-1} cm^2 mol^{-1}, respectively. These lower numbers demonstrate the behaviour is not electrolytic [37]. Furthermore, the subsequent section elucidates the extent of covalent bonding and crystal formations.

3a.3.1 FTIR spectral analysis

The neodymium complexes feature one CH_3CH_2OH and one H_2O molecule bound as monodentate ligands. The sharp single peak corresponding to the $\upsilon_{O\text{-}H}$ vibration of ethanol appeared within the range of 2920–2980 cm^{-1}, as indicated in Table 3a.1. Additionally, a broad band attributable to coordinated or hydrated water molecules was observed in the 3300–3600 cm^{-1} range. This observation can be attributed to using hexahydrate neodymium nitrate salt as the starting material and the exclusive use of 100% ethanol as the solvent throughout the synthesis process. A significant finding is the reduction in the stretching frequencies of $\upsilon_{C=O(4\text{-chlorobenzoyl})}$ and $\upsilon_{C=O(acyl\text{-}pyrazolone)}$ ligands upon complex formation, attributed to charge donation from the oxygen atoms of the acylpyrazolone ligands to the neodymium ion. Specifically, the $\upsilon_{C=O(4\text{-chlorobenzoyl})}$ stretching frequencies decreased from 1619 cm^{-1} of HL^1 to 1612 cm^{-1} for complex 6, from 1625 cm^{-1} of HL^2 to 1612 cm^{-1} for complex 7, and from 1619 cm^{-1} of HL^3 to 1615 cm^{-1} for complex 8. Similarly, the $\upsilon_{C=O(acyl\text{-}pyrazolone)}$ stretching frequencies also decreased upon complex formation. Analysis of the FTIR spectra of the complexes, depicted in Figures 3a.4-3a.6, revealed additional bands attributed to cyclic $\upsilon_{C=N}$, $\upsilon_{C=C}$, υ_{N-N}, and υ_{C-H} in-plane deformations for all complexes.

Table 3a.1 The FTIR values for neodymium complexes (in cm^{-1}).

Code	HL^1 Ligand	Complex 6	HL^2 Ligand	Complex 7	HL^3 Ligand	Complex 8
$\nu_{(C=O)}$ benzoyl	1620	1612	1624	1612	1694	1615
$\nu_{(C=O)}$ acyl	1590	1592	1590	1589	1601	1599
cyclic $\nu_{(C=N)}$	1484	1475	1484	1478	1446	1475
$\nu_{C\text{-}C}$ aromatic	1357	1366	1348	1394	1381	1361
$\nu_{(N\text{-}N)}$	1213	1155	1210	1157	1178	1156
C-H in plane deformation	1085	941	1080	957	1071	942

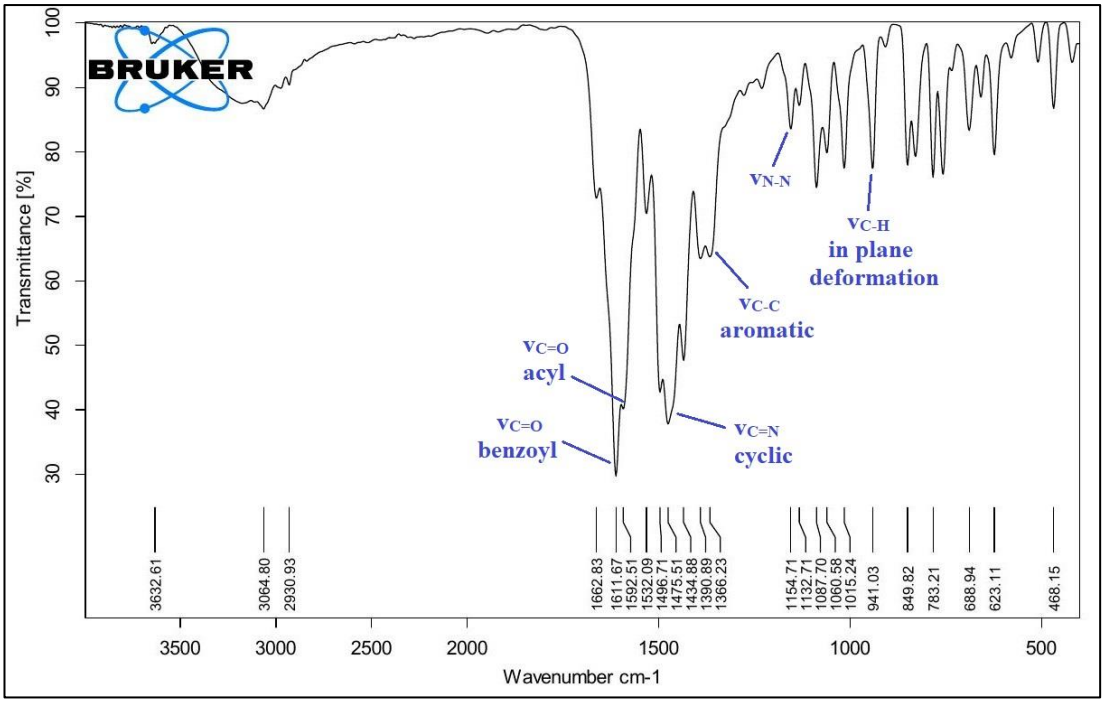

Figure 3a.4 FTIR spectrum of complex 6.

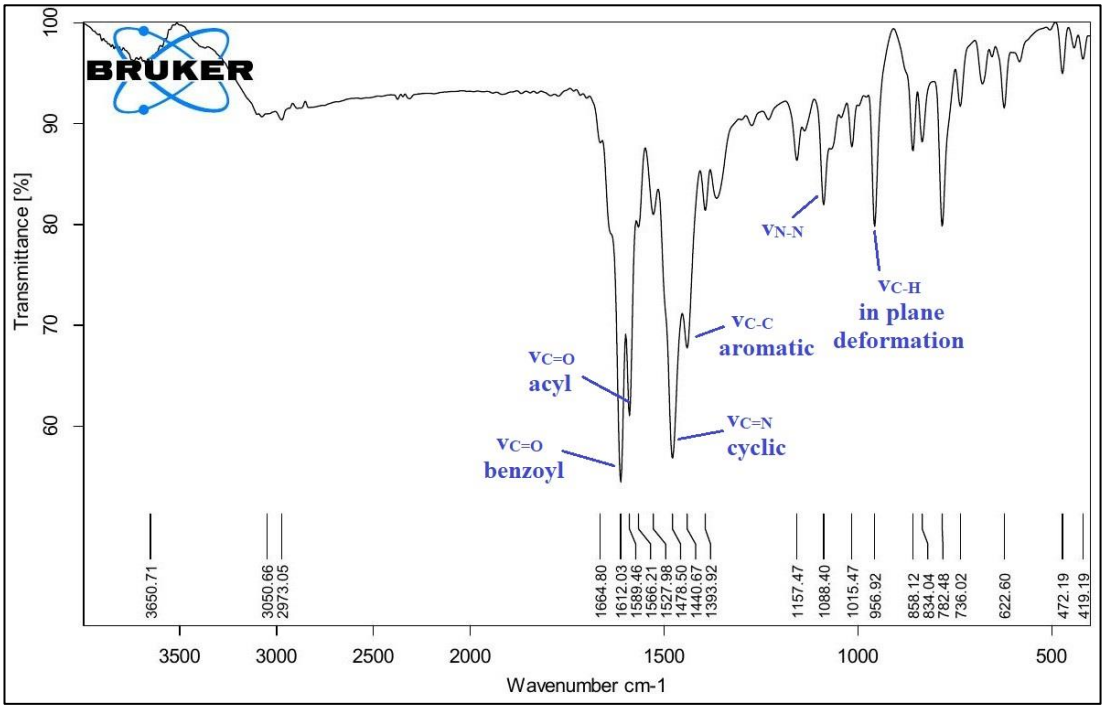

Figure 3a.5 FTIR spectrum of complex 7.

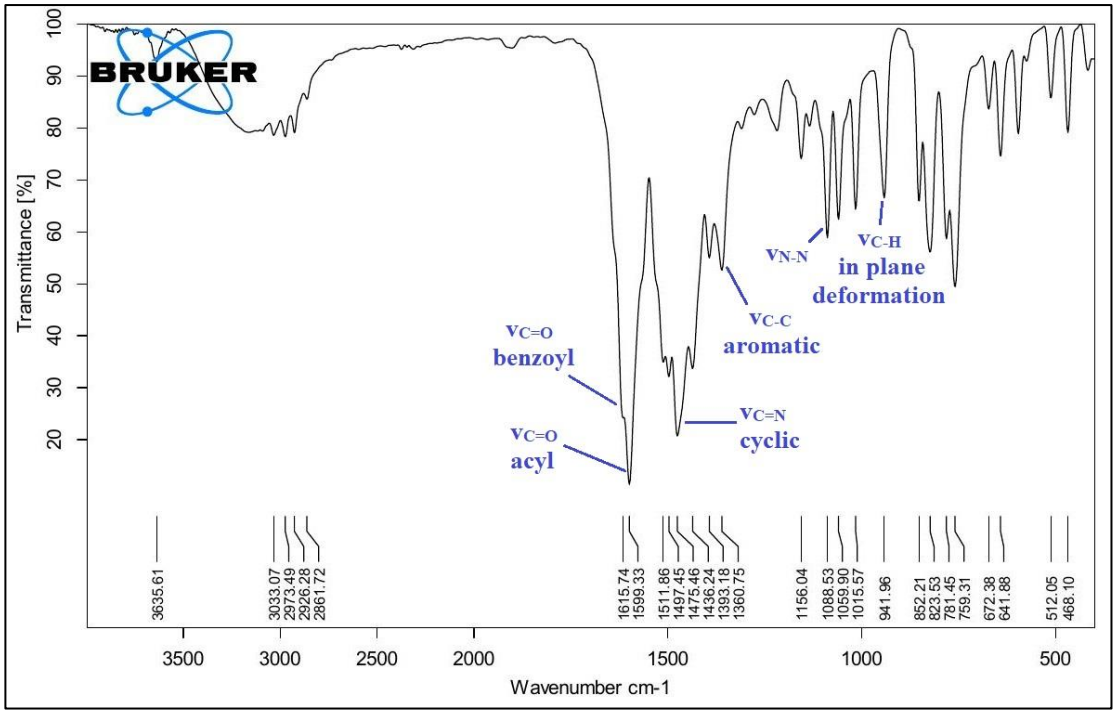

Figure 3a.6 FTIR spectrum of complex 8.

3a.3.2 Thermogravimetric analysis

The complexes underwent thermal analysis to assess their thermal stability, a crucial factor in determining their volatility. For complexes 6, 7, and 8, the thermogravimetric analysis (TGA) revealed two degradation steps, resulting in overall mass losses of 67.27%, 46.92%, and 60.98%, respectively. The residual substance Nd_2O_3 remained after degradation. In the first degradation stage, complex 6 lost 22.85% of its mass, complex 7 lost 8.36%, and complex 8 lost 22.86%. This loss primarily involved removing 15, 6, and 15 H_2O molecules for complexes 6, 7, and 8. However, the actual degradation of the complexes occurred above their respective melting points [38]. The second degradation stage involved mass losses of 44.42% for complex 6, 38.56% for complex 7, and 38.12% for complex 8, attributed to removing three acylpyrazolone units. The peak of maximum mass loss for complexes 6, 7, and 8 was observed at 424.1°C, 425.7°C, and 421.8°C, respectively, as depicted in Figures 3a.7-3a.9, illustrating all thermogravimetric curves.

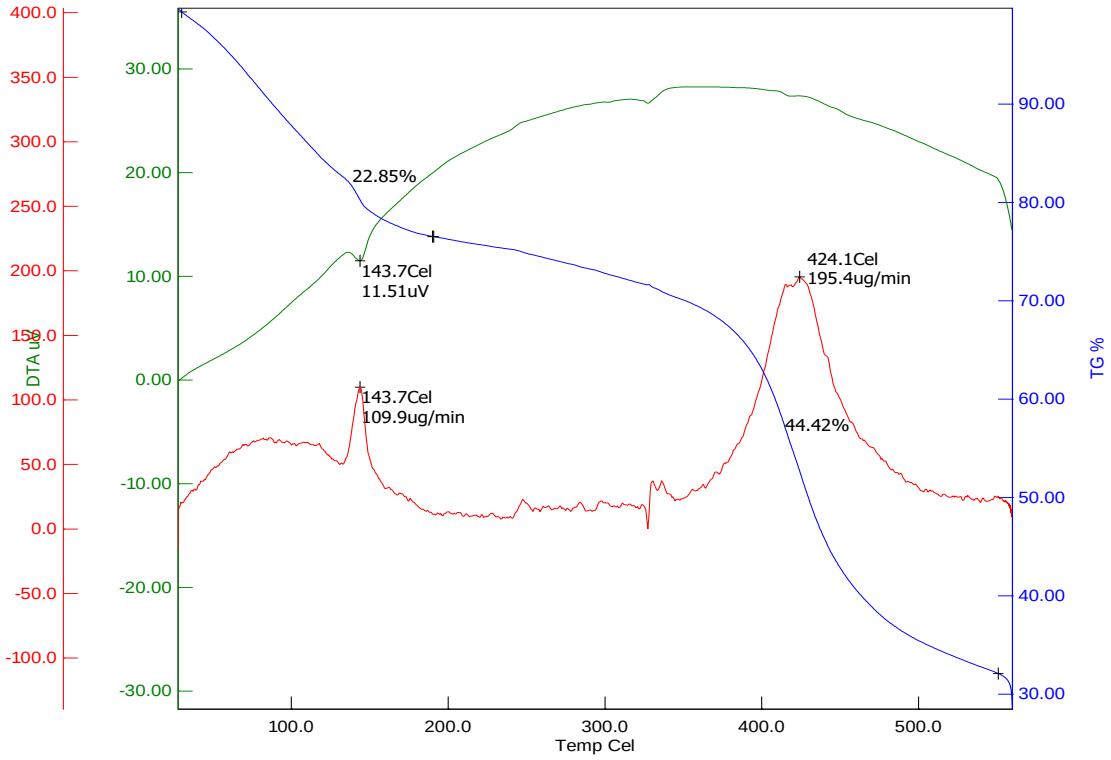

Figure 3a.7 Thermogravimetric curve of complex 6.

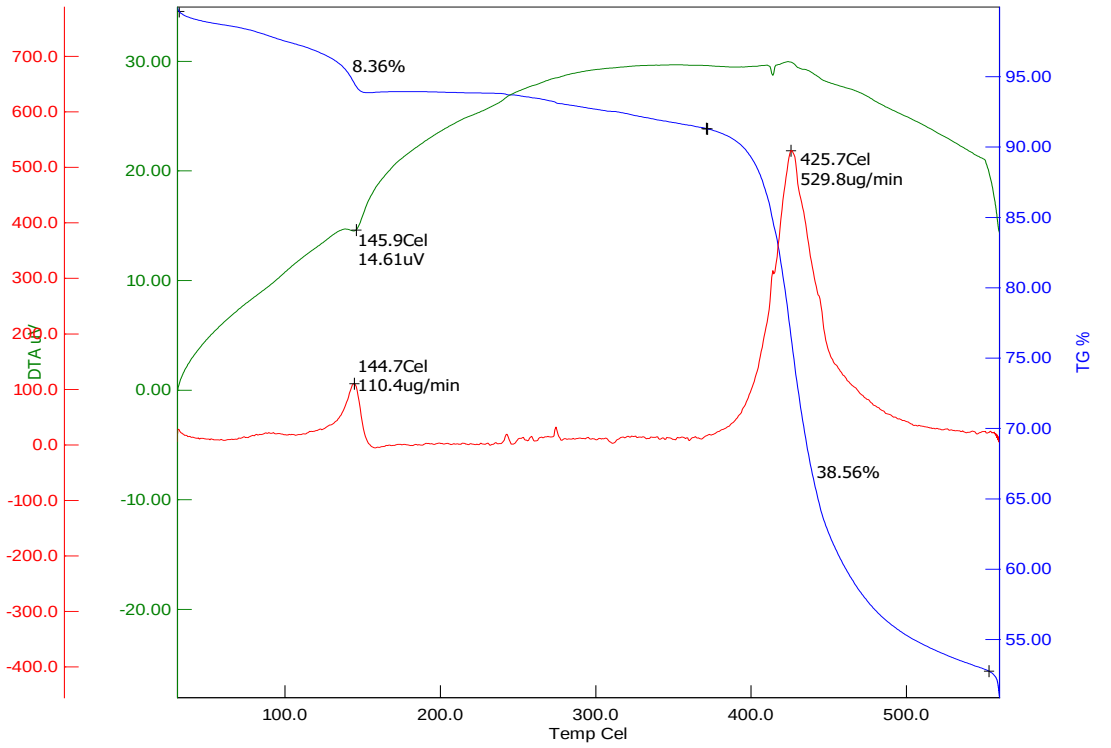

Figure 3a.8 Thermogravimetric curve of complex 7.

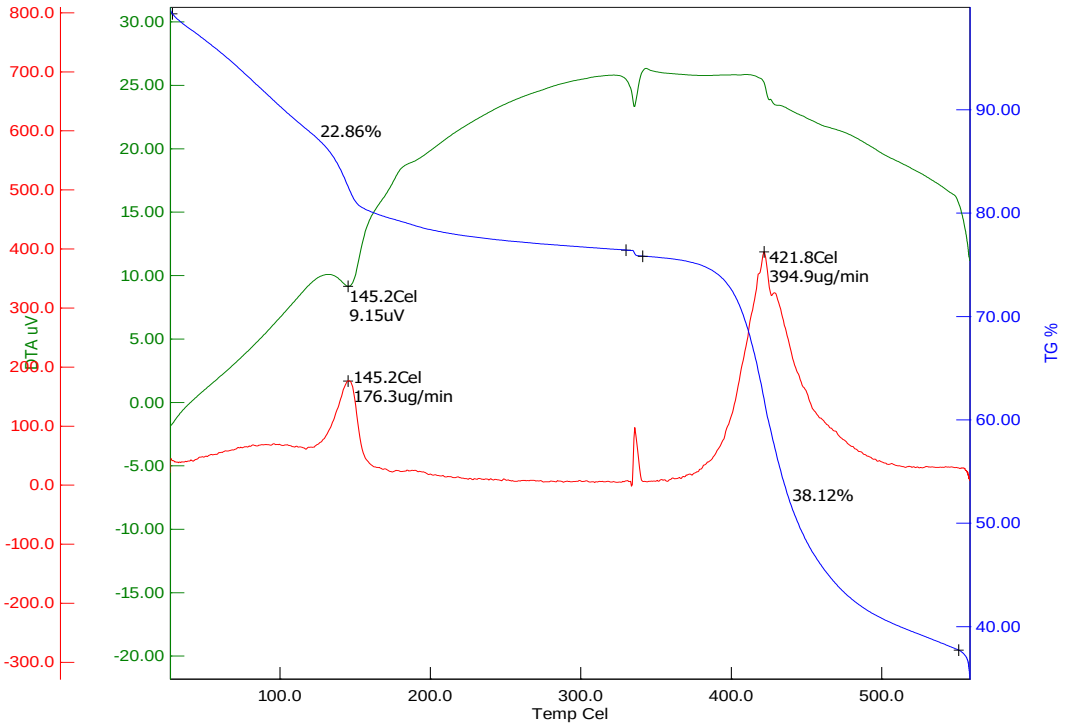

Figure 3a.9 Thermogravimetric curve of complex 8.

3a.3.3 Single crystal X-ray diffraction analysis

After obtaining pale yellow prismatic single crystals suitable for X-ray analysis, solid-state X-ray diffraction was employed to determine the structure of complex 6. Similar to previous reports on neodymium acylpyrazolone complexes [23,39–43], complex 6 exhibited an eight-coordinated core with a Nd(III) ion. The optimized structure, illustrated as the ORTEP diagram shown in Figure 3a.10, revealed two molecules with unit cell dimensions of a=14.5931(5) Å, b=15.9902(5) Å, c=24.7739(7) Å, α=89.718(2)°, β= 74.488(3)°, and γ=75.625(3)°. The crystal exhibited distortions, leading to the identification of identity and inversion center operations with orders of 1 and 2, respectively. In the plot, side A featured Nd1, surrounded by six L^1 ligand O-atoms (O1A, O2A, O3A, O4A, O5A, and O6A) and two water O-atoms (O1WA and O2WA). Side B contained Nd2, surrounded by six L^1 ligand O-atoms (O1B, O2B, O3B, O4B, O5B, and O6B), one water O-atom (O1WB), and one ethanol O-atom (O1M). The coordination polyhedron around the central Nd(III) ion was a distorted square-antiprism, with the complex crystallizing in the *P−1* space group of the triclinic system with centrosymmetric symmetry (see Figure 3a.10(a) and 3a.10(b)). Figure 3a.10(c) shows one potential ligand configuration centered on the central atom [29]. The crystal

packing of the complex facilitated low-energy movement between metal ions, with an Nd-Nd distance of 9.8126(9) Å [44]. Three ligands (L^1) interacted with the central neodymium ion as bidentate ligands, forming three chelating rings [45,46]. The atoms O1A and O2A (or O1B and O2B) of one L^1 ligand are positioned almost coplanar in the top plane, while the atoms O3A and O4A (or O3B and O4B) of another L^1 ligand reside in the bottom plane. Conversely, the remaining oxygen atoms of the third L^1 ligand are oriented perpendicular to the plane of the ring. On side A, the top plane is formed with O2WA from the coordinating water molecule, O1A, and O2A from one L^1 ligand, and O5A from another L^1 ligand's pyrazolone moiety. Similarly, the bottom plane on side A comprises O3A and O4A from the L^1 ligand, O6A from another L^1 ligand, and O1WA from the coordinating water molecule. On side B, an 'anti' arrangement is observed, where the top plane consists of O1B and O2B from the L^1 ligand, O6B from another L^1 ligand, and O1WB from the coordinating water molecule. Meanwhile, the bottom plane on side B comprises O3B and O4B from the L^1 ligand, O5B from another L^1 ligand, and O1M from the coordinating ethanol molecule.

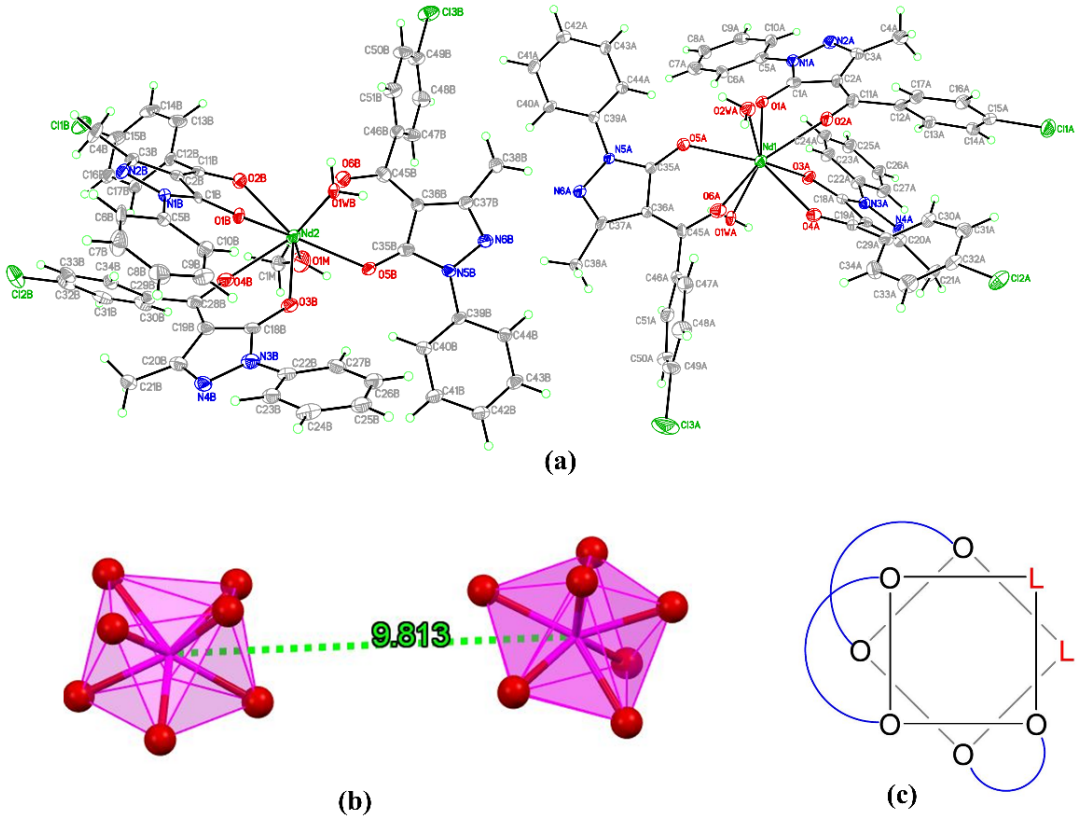

Figure 3a.10 (a) ORTEP illustration of complex 6 with 50% ellipsoid probability, **(b)** Polyhedral style presentation, and **(c)** square antiprism arrangement.

Table 3a.2 Structural refinement data for complex 6.

Code	Complex 6
CCDC number	2257746
Empirical formula	$C_{103}H_{82}Cl_6N_{12}Nd_2O_{16}$
Formula weight	2244.98
Temperature	100(2) K
Wavelength	1.54184 Å
Crystal system	Triclinic
Space group	*P −1*
Unit cell dimensions	a = 14.5931(5) Å, b = 15.9902(5) Å, c = 24.7739(7) Å, α= 89.718(2)°, β= 74.488(3)°, γ=75.625(3)°.
Volume	5384.2(3) $Å^3$
Z	2
Density (calculated)	1.385 Mg/m^3
Absorption coefficient	9.186 mm^{-1}
F(000)	2268
Final R indices [I>2sigma(I)]	R_1 = 0.1004, wR_2 = 0.2367
R indices (all data)	R_1 = 0.1294, wR_2 = 0.2604
Theta range for data collection	3.271 to 79.190°.
Index ranges	−17<=h<=18, −20<=k<=20, −31<=l<=29
Reflection collected	20893
Independent reflections	20893 [$R_{(int)}$ = 0.1152]
Completeness to theta = 25.242°	93.8 %
Absorption correction	Analytical
Refinement method	Full-matrix least-squares on F^2
Goodness-of-fit on F^2	1.072
Data / restraints / parameters	20893 / 228 / 1311

Table 3a.2 provides an overview of the crystallographic and refinement information, while Table 3a.3 details the selected bond lengths and bond angles. Distortion in the square antiprism occurs due to slight deviations: atoms O1A and O2WA (or O2B and O1WB) are positioned slightly above the upper plane, O2A and O5A (or O1B and O6B) are slightly below and on the opposite side, O4A and O1WA (or O4B and O5B) are slightly below the bottom plane, and O3A and O6A (or O3B and O1M) are slightly above. The complex exhibits a higher melting point attributed to π–π stacking interaction between two 5-membered pyrazole rings at a distance of 3.570 Å.

The bond lengths of C(11A)–O(2A), C(28A)–O(4A), C(45A)–O(6A), C(11B)–O(2B), C(28B)–O(4B), and C(45B)–O(6B) in the acyl group measure 1.282(12) Å, 1.264(12) Å, 1.241(11) Å, 1.272(12) Å, 1.271(12) Å, and 1.230(14) Å, respectively, slightly exceeding the typical C–O distance in ketones (1.23 Å) due to O→Nd bonding [47]. In comparison to Nd-O(acyl) bond lengths (ranging from 2.410(7) Å to 2.506(7) Å), Nd-O(pyrazolone) bond lengths (ranging from 2.389(8) Å to 2.441(7) Å) are marginally longer, indicating stronger covalency attributed to the acyl group oxygen atoms. This elongation in bonds results in a reduction in the average bond order between neodymium and oxygen atoms, thereby enhancing covalency. The bond lengths observed include Nd1-O1WA (2.470(7) Å), Nd2-O1WB (2.441(7) Å), Nd1-O2WA (2.468(8) Å), and Nd2-O1M (2.46(1) Å), revealing the solvent's impact on the complex's covalent nature.

When coordinating with the neodymium ion in its enol state, the L^1 ligands form stable six-membered rings, with internal angle sums of approximately 707.1°, 714.51°, and 705.48° for side A, and 712.72°, 708.06°, and 716.41° for side B. These angles approach 720°, indicating nearly planar six-membered rings and suggesting electron delocalization during complexation. The average $C{=}C_{pyz\text{-}ring}$ distance measures 1.437 Å (side A) / 1.425 Å (side B), falling between typical C=C (1.33 Å) and C-C (1.54 Å) bond distances, indicating some electron delocalization. Figure 3a.11 illustrates the organization of polyhedral units along the b-axis, demonstrating the arrangement to maintain stability through secondary interactions [5]. As indicated in Table 3a.4, the NdO_8 polyhedra are structurally linked by O-H···N hydrogen bonds, with varying symmetry transformations spanning distances of 2.06–2.35 Å. These hydrogen bonds primarily form between H-atoms in water molecules and N-atoms of ligands. Additionally, C-H···O, O-H···Cl, C-H···Cl, and C-H···N interactions contribute to the crystal's resilience, with H···O, H···Cl, H···Cl, and H···N distances ranging from 2.20-2.66 Å, 2.89 Å, 2.66-2.79 Å, and 2.69 Å, respectively.

Table 3a.3 Bond parameters in complex 6.

Atoms	Bond lengths	Atoms	Bond lengths	Atoms	Bond angles	Atoms	Bond angles
Nd(1)-O(1A)	2.409(6)	Nd(2)-O(1B)	2.405(7)	O(1A)-Nd(1)-O(2A)	72.7(2)	O(1B)-Nd(2)-O(4B)	77.2(3)
Nd(1)-O(2A)	2.410(7)	Nd(2)-O(2B)	2.469(7)	O(2A)-Nd(1)-O(4A)	74.8(2)	O(5B)-Nd(2)-O(1WB)	78.9(2)
Nd(1)-O(3A)	2.436(7)	Nd(2)-O(3B)	2.441(6)	O(1A)-Nd(1)-O(5A)	78.8(2)	O(1B)-Nd(2)-O(1WB)	69.1(2)
Nd(1)-O(4A)	2.417(7)	Nd(2)-O(4B)	2.427(8)	O(1A)-Nd(1)-O(3A)	71.3(2)	O(5B)-Nd(2)-O(3B)	76.1(2)
Nd(1)-O(5A)	2.429(7)	Nd(2)-O(5B)	2.389(7)	O(2A)-Nd(1)-O(3A)	75.0(2)	O(1B)-Nd(2)-O(3B)	73.4(2)
Nd(1)-O(6A)	2.472(7)	Nd(2)-O(6B)	2.506(7)	O(4A)-Nd(1)-O(3A)	73.0(2)	O(4B)-Nd(2)-O(3B)	72.2(3)
Nd(1)-O(1WA)	2.469(7)	Nd(2)-O(1WB)	2.440(8)	O(1A)-Nd(1)-O(2WA)	91.5(2)	O(1WB)-Nd(2)-O(3B)	89.8(3)
Nd(1)-O(2WA)	2.469(8)	Nd(2)-O(1M)	2.462(11)	O(2A)-Nd(1)-O(2WA)	69.7(2)	O(5B)-Nd(2)-O(1M)	75.6(3)
O(1A)-C(1A)	1.267(12)	O(1B)-C(1B)	1.261(10)	O(4A)-Nd(1)-O(2WA)	103.5(2)	O(4B)-Nd(2)-O(1M)	72.3(3)
O(2A)-C(11A)	1.282(12)	O(2B)-C(11B)	1.272(12)	O(5A)-Nd(1)-O(2WA)	77.4(2)	O(1M)-Nd(2)-O(2B)	85.1(3)
O(3A)-C(18A)	1.263(11)	O(3B)-C(18B)	1.267(12)	O(1A)-Nd(1)-O(1WA)	102.1(2)	O(5B)-Nd(2)-O(6B)	73.0(2)
O(4A)-C(28A)	1.264(12)	O(4B)-C(28B)	1.271(12)	O(4A)-Nd(1)-O(1WA)	88.1(2)	O(4B)-Nd(2)-O(6B)	136.9(3)
O(6A)-C(45A)	1.241(11)	O(6B)-C(45B)	1.230(14)	O(5A)-Nd(1)-O(1WA)	74.7(2)	O(1WB)-Nd(2)-O(6B)	71.9(3)
O(5A)-C(35A)	1.250(11)	O(5B)-C(35B)	1.225(13)	O(3A)-Nd(1)-O(1WA)	70.1(2)	O(3B)-Nd(2)-O(6B)	146.5(3)
C(35A)-C(36A)	1.449(11)	C(35B)-C(36B)	1.463(13)	O(4A)-Nd(1)-O(6A)	73.9(2)	O(1M)-Nd(2)-O(6B)	74.5(3)
C(1A)-C(2A)	1.427(14)	C(1B)-C(2B)	1.400(13)	O(5A)-Nd(1)-O(6A)	71.2(2)	O(2B)-Nd(2)-O(6B)	75.9(2)
C(18A)-C(19A)	1.443(12)	C(18B)-C(19B)	1.435(16)	O(2WA)-Nd(1)-O(6A)	77.8(2)	O(1WB)-Nd(2)-O(1M)	142.5(3)
C(36A)-C(37A)	1.435(14)	C(36B)-C(37B)	1.413(14)	O(1WA)-Nd(1)-O(6A)	74.7(2)	O(1B)-Nd(2)-O(6B)	122.1(3)
C(2A)-C(3A)	1.449(13)	C(2B)-C(3B)	1.424(14)	O(2WA)-Nd(1)-O(1WA)	145.8(2)	O(1B)-Nd(2)-O(2B)	72.7(2)
C(19A)-C(20A)	1.427(14)	C(19B)-C(20B)	1.437(14)	O(1A)-Nd(1)-O(4A)	136.5(2)	O(4B)-Nd(2)-O(2B)	74.7(2)

Table 3a.4 Hydrogen bonds for complex 6 [Å and °].

D-H···A	d(D-H)	d(H···A)	d(D···A)	<(DHA)
O(1WA)-H(1W1)…N(4A)#1	0.81(2)	2.09(3)	2.855(11)	158(8)
O(1WA)-H(1W2)…N(6B)	0.80(2)	2.21(3)	2.881(11)	142(5)
O(2WA)-H(2W1)…Cl(3A)#2	0.83(2)	2.89(8)	3.477(9)	130(9)
C(6A)-H(6AA)…O(1A)	0.95	2.28	2.899(12)	122.5
C(21A)-H(21B)…Cl(1B)#3	0.98	2.79	3.380(11)	119.5
C(44A)-H(44A)…O(5A)	0.95	2.33	2.877(11)	116.5
O(1WB)-H(1W3)…N(6A)	0.82(2)	2.06(2)	2.791(11)	148(4)
O(1WB)-H(1W4)…N(2B)#4	0.82(2)	2.35(9)	2.854(11)	121(9)
C(1M)-H(1MC)…Cl(3B)#5	0.98	2.66	3.201(11)	114.9
C(4B)-H(4BA)…O(1WB)#4	0.98	2.66	3.463(15)	139.5
C(4B)-H(4BC)…Cl(2A)#6	0.98	2.69	3.437(12)	133.3
C(10B)-H(10B)…O(1B)	0.95	2.22	2.857(13)	123.9
C(27B)-H(27B)…O(3B)	0.95	2.35	2.935(14)	119.4
C(40B)-H(40B)…O(5B)	0.95	2.20	2.842(13)	124.2
C(44B)-H(44B)…N(4A)#1	0.95	2.69	3.543(13)	149.8

Symmetry transformations used to generate equivalent atoms:
#1 -x+1,-y+1,-z+1 #2 -x+1,-y,-z+1 #3 x,y,z+1
#4 -x+1,-y,-z #5 -x+1,-y+1,-z #6 x,y,z-1

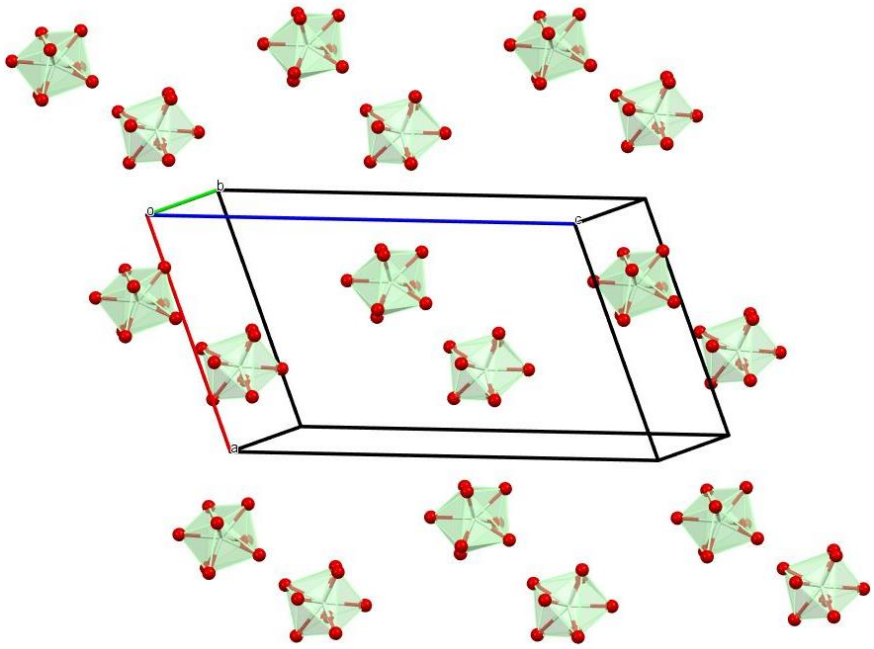

Figure 3a.11 The packing arrangement between polyhedral units of complex 6.

Bright pale-yellow prismatic crystals of complex 6 were obtained using a slow evaporation technique. However, attempts to obtain x-ray quality crystals of complexes 7 and 8 were unsuccessful. Consequently, a simulated pattern for complex 6 was generated from the single crystal data and compared with the experimental pattern obtained from the powder XRD experiment. The simulated pattern closely matched the experimental pattern for all three complexes, as depicted in Figure 3a.12. This verification confirms the similarity in geometry and structure among all the complexes. It ensures that the structure obtained from a single crystal is representative of the bulk of the complexes. In the XRD graph, a sharp band with maxima in the range of 2θ = 5 to 10° indicates the crystalline nature of the complexes.

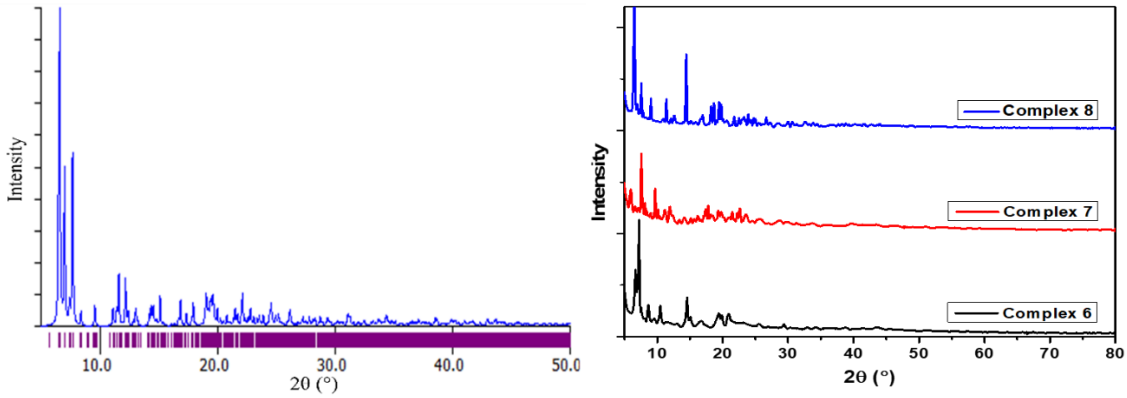

Figure 3a.12 Comparison between (a) simulated powder XRD pattern for complex 6 crystal and (b) experimental powder XRD patterns for complexes 6, 7, and 8.

3a.3.4 Hirshfeld surface area analysis

Using the Crystal Explorer 17.5 program [48,49], the donor-acceptor interaction sites and intermolecular contacts for complex 6 can be visualized. The crystal of complex 6 was utilized to generate Hirshfeld surfaces (HS), which were subsequently analyzed by applying the d_{norm} to assess exterior and interior distances (d_e and d_i). Figure 3a.13 elucidates the 2D-FP plot and 3D representations of d_{norm}, d_i, d_e, curvedness, shape index, and fragment patch surfaces. Red dots on the d_{norm} HS indicate hydrogen bonding. The total number of HS interactions with nearby complex 6 molecules (NBs) is depicted in a 2D-FP plot, where the interactions H(HS)···H(NBs), H(HS)···All(NBs), and All(HS)···H(NBs) are the most prevalent, contributing 46.5%, 67.3%, and 71.9%, respectively. Carbon-hydrogen contacts, constituting 9.5% of the entire HS region, are the next most prevalent. These interactions are graphically represented in Figure 3a.14, with additional 2D-FP graphs provided in Figure 3a.15. The curvedness map's curved area situated amid the 5-membered pyrazole rings, suggests π-π stacking, enhancing lattice strength, along with the presence of red dots in d_{norm} indicating hydrogen bonding. Neodymium exhibits no further interactions with adjacent molecules, as evidenced by the absence of Nd-all, all-Nd, or Nd-Nd interactions within the complex. The shape-index plot illustrates the concave appearance of ligand oxygen atoms with an opaque orange tint, indicative of coordination interactions and a shape-index value lower than zero.

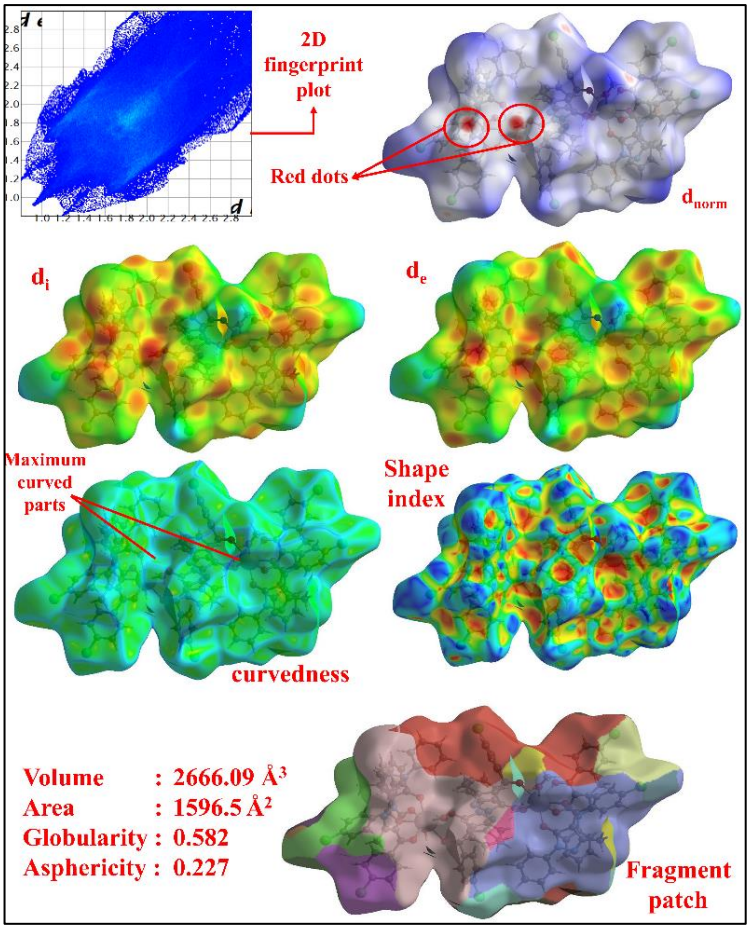

Figure 3a.13 The molecular HS for complex 6.

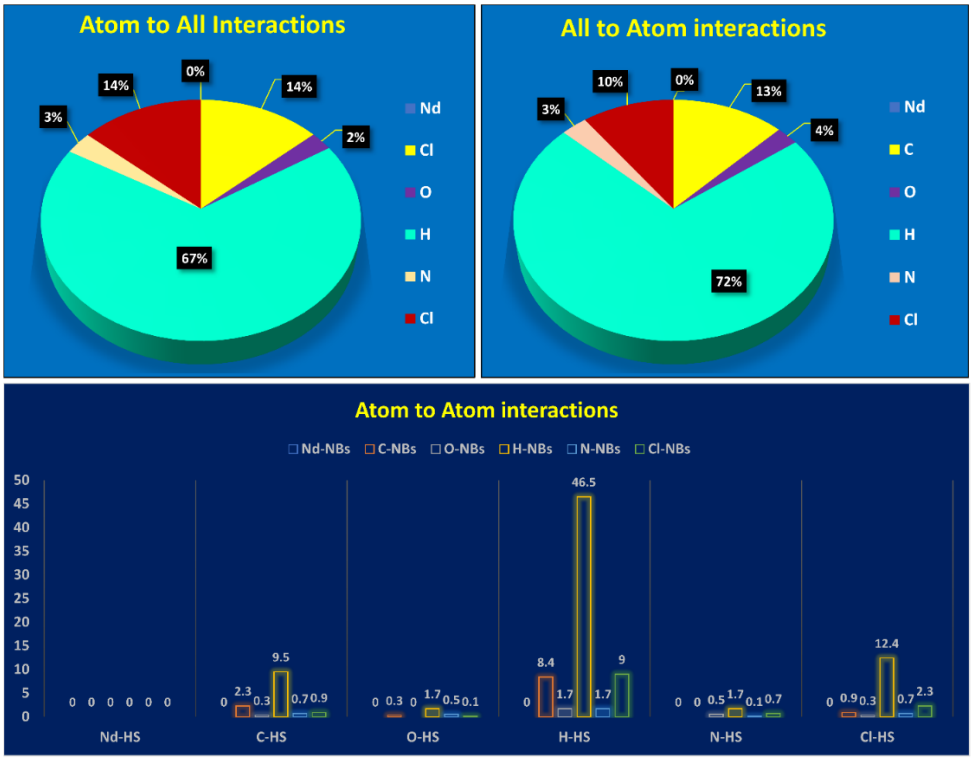

Figure 3a.14 Graphical presentation of Hirshfeld Percentage interactions.

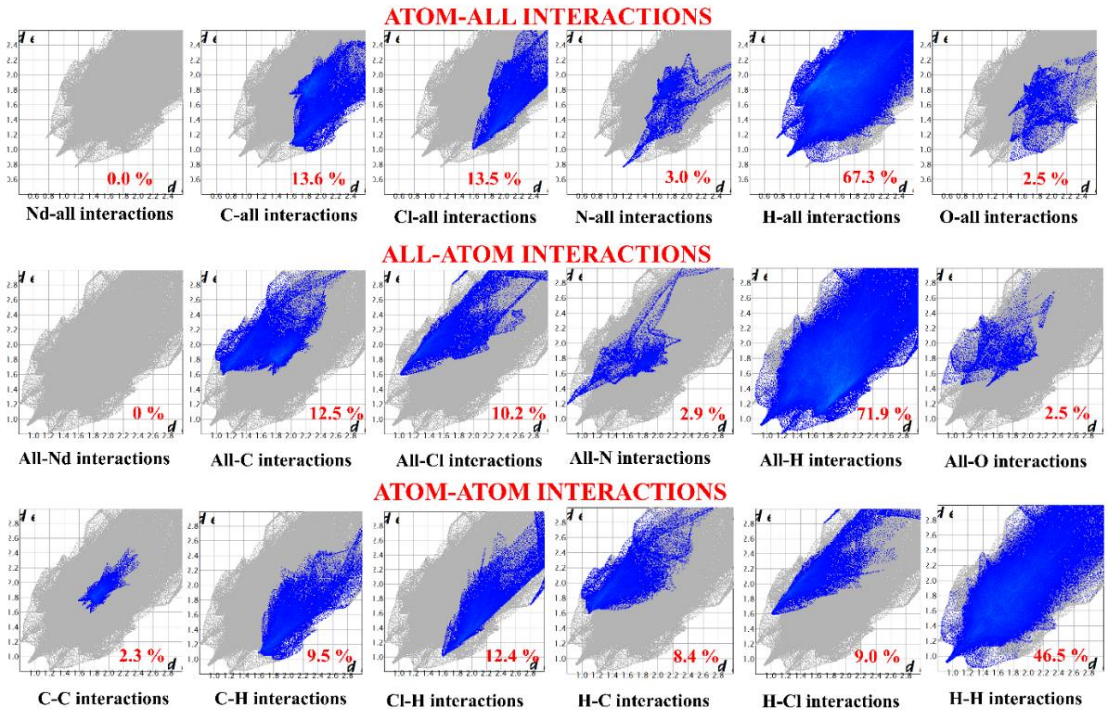

Figure 3a.15 2D Fingerprint map for complex 6.

3a.3.5 Absorption and Emission Spectral Analysis

All three synthesized compounds demonstrate solubility in various solvents. Electronic spectra of 10^{-2} M solutions of these complexes were recorded in chloroform, ethanol, nitrobenzene, pyridine, DMF, and DMSO solvents. The results of the 4f-4f electronic spectra and oscillator strength measurements of the complexes in different solvents, along with hexa-hydrated $Ln(NO_3)_3$ in water, are depicted in Figure 3a.16 and Table 3a.5, respectively. Lanthanide complexes, characterized by their rapid solvent transfer rate and remarkably low crystal field stabilization energy, can attain superior coordination geometries [50,51]. Within visible wavelengths, these complexes exhibit frequent parity-forbidden transitions in the 4f-4f bands, originating from the $^4I_{9/2}$ ground state to distinctive excited states of the Nd(III) ion [38]. The observed transitions include $^4F_{3/2} \leftarrow {}^4I9/2$, $^4F_{5/2} \leftarrow {}^4I_{9/2}$, $^4F_{7/2} \leftarrow {}^4I_{9/2}$, $^4F_{9/2} \leftarrow {}^4I_{9/2}$, $^4G_{5/2} \leftarrow {}^4I_{9/2}$, $^4G_{7/2} \leftarrow {}^4I_{9/2}$, and $^4G_{9/2} \leftarrow {}^4I_{9/2}$. The spectral intensity of the absorption band is characterized by oscillator strengths (P) [52], experimentally linked to the integral area of the absorption band, and expressed as:

$$\mathbf{f_{exp}\ or}\ \boldsymbol{P} = \mathbf{4.31} \times \mathbf{10^{-19}} \left[\frac{\boldsymbol{9\eta}}{\boldsymbol{\eta^2 + 2}}\right] \int \boldsymbol{\varepsilon_{max}(\bar{\nu})d\bar{\nu}} \qquad (1)$$

Where, $\varepsilon_{max} = \frac{\boldsymbol{Absorbance\ (A)}}{\boldsymbol{Concentration\ (c) \times \text{path length of the cell in cm (b = 1 cm)}}}$, ν = transition wave number, η = Refractive index.

Considering the studied Nd(III) transitions, the absorption intensity of the $^4G_{5/2}$, $^4G_{7/2} \leftarrow {}^4I_{9/2}$ pair, situated near the center of the visible region (17300-17900 cm^{-1}), displays a notable sensitivity to the ligand environment surrounding the Nd(III) ion. Hence, it serves as a suitable ion for research employing visible absorption spectroscopy. Both transitions adhere to the principles of electric quadrupolar selection ($\Delta J \leq 2$, $\Delta L \leq 2$, $\Delta S = 0$) and are identified as hypersensitive transitions [10,11]. The transitions $^4F_{3/2} \leftarrow {}^4I_{9/2}$, $^4F_{5/2} \leftarrow {}^4I_{9/2}$, and $^4F_{7/2} \leftarrow {}^4I_{9/2}$ of Nd(III) are termed pseudohypersensitive transitions. Despite not strictly adhering to the selection criterion for hypersensitive transitions, these transitions demonstrate significant sensitivity in the complexes. Upon transitioning from the $Nd^{3+}_{aqua-ion}$ to the complex across all solvents used, the oscillator strength of the $^4G_{5/2} \leftarrow {}^4I_{9/2}$ transition increases by a factor of 4 to 6 times (hypersensitive). For complexes 6 and 8 (see Table 3a.5), the intensification is typically observed in the following order: Pyridine > DMF > DMSO > Ethanol > Chloroform > Nitrobenzene. Pyridine promotes the intensity of the 4f-4f electric dipole in both complexes due to the strong coordination of the Nd(III)-ion, enhancing bond covalency and oscillator strength [38]. The unusual behaviour of complex 7 may be attributed to the electron-withdrawing m-chloro phenyl group attached to the N of the 5-membered pyrazolone ring. Furthermore, in three solvents with strong coordination (pyridine, DMF, DMSO), the complexes exhibit the sequence 6 > 7 > 8. Complex 6 demonstrates less molecular symmetry and higher covalency than the other two complexes, attributed to the increased polarizable interaction of the L^1 ligand with the Nd(III)-ion, resulting in larger values of oscillator strengths for complex 6.

The qualitative identification of symmetry has been facilitated by analyzing both the band shape and strength of the hypersensitive transition [38]. Consistently, similar band shapes across all hypersensitivity transitions indicate an eight-coordination geometry. Notably, the band morphologies in pyridine, DMF, and DMSO solvents reveal increasingly distinct and intense hypersensitive peaks. This enhancement in asymmetries can be attributed to the strong coordinating nature of these solvents, increasing oscillator strength.

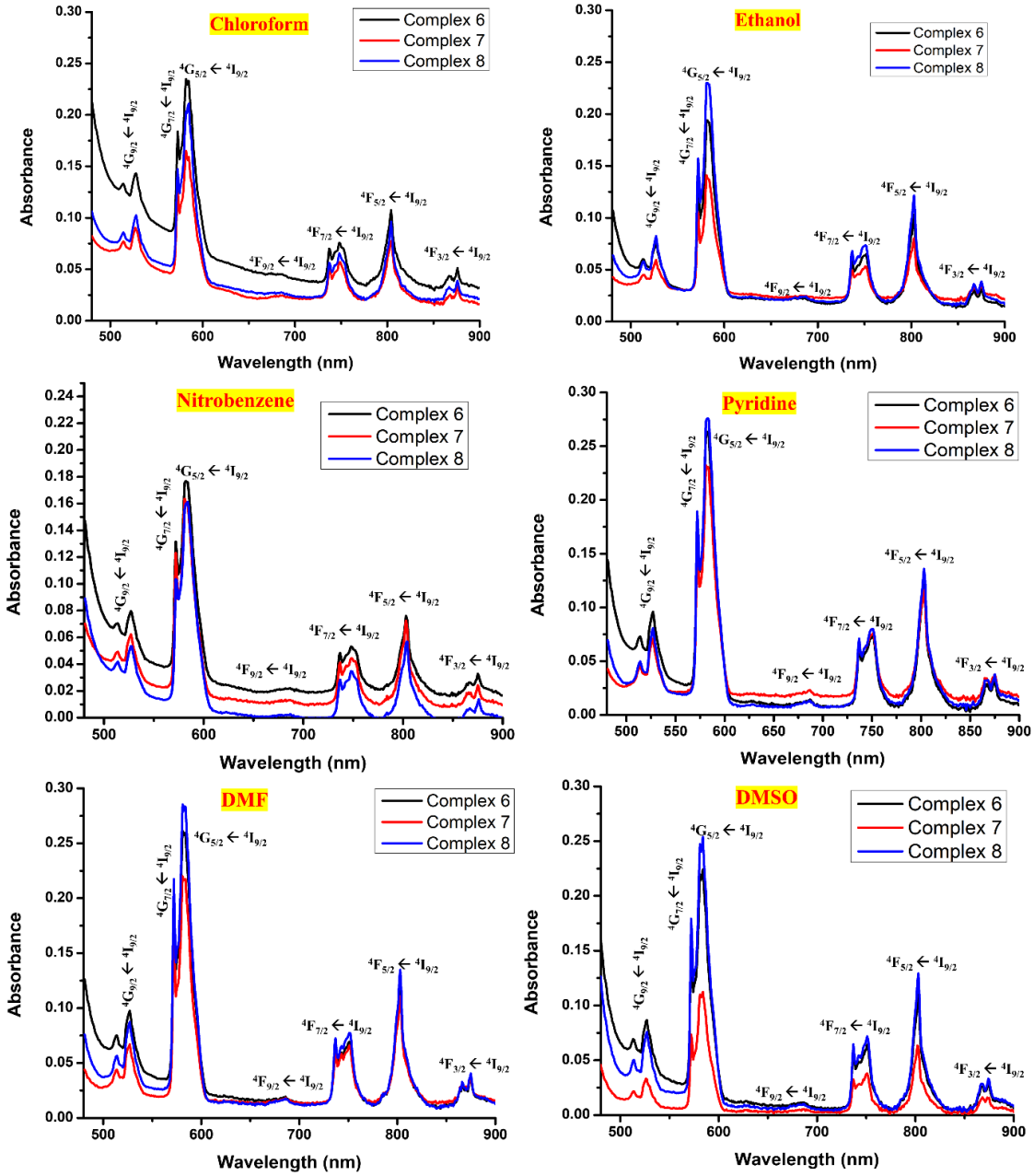

Figure 3a.16 4f-4f electronic spectra of complexes 6, 7, and 8 in various solvents.

Table 3a.5 Measurements of experimental oscillator strengths (f_{exp}), theoretical oscillator strengths (f_{calcu}), and root mean square deviation (δ_{RMS}) for complexes 6, 7, and 8 in various solvents.

Transitions			$^4F_{3/2} \leftarrow {}^4I_{9/2}$	$^4F_{5/2} \leftarrow {}^4I_{9/2}$	$^4F_{7/2} \leftarrow {}^4I_{9/2}$	$^4F_{9/2} \leftarrow {}^4I_{9/2}$	$^4G_{5/2} \leftarrow {}^4I_{9/2}$	$^4G_{7/2} \leftarrow {}^4I_{9/2}$	$^4G_{9/2} \leftarrow {}^4I_{9/2}$	δ_{RMS}
Spectra ranges [cm^{-1}][a]			11700-11200	12820-12050	13800-12900	15400-14200	17900-16450	17700-17300	19200-18400	
Nd^{3+} aqua ion ($P \times 10^{-6}$)			1.94	7.63	7.71	0.41	9.4	3.54	2.22	
Oscillator Strength $P \times 10^{-6}$ in different solvents for complex 6	A	f_{exp}	1.27	8.04	5.9	0.15	31.54	5.11	5.98	0.509
		f_{calcu}	1.929	4.340	3.043	0.263	16.227	1.560	0.503	
	B	f_{exp}	1.56	7.88	7.27	0.68	32.58	5.14	6.91	0.511
		f_{calcu}	1.75	4.72	3.53	0.30	16.80	1.54	0.51	
	C	f_{exp}	1.19	5.6	5.51	0.39	30.15	4.78	4.81	0.504
		f_{calcu}	1.34	3.49	2.57	0.22	15.53	1.28	0.39	
	D	f_{exp}	1.85	10.88	9.71	0.23	47.3	7.43	9.6	0.509
		f_{calcu}	2.46	6.41	4.74	0.40	24.43	2.19	0.71	
	E	f_{exp}	1.67	9.39	9.63	0.61	45.16	7.24	9.95	0.514
		f_{calcu}	2.14	5.99	4.52	0.38	23.34	2.02	0.65	
	F	f_{exp}	1.52	9.38	8.26	0.17	38.99	6.06	7.77	0.506
		f_{calcu}	2.02	5.45	4.07	0.34	20.22	1.82	0.59	
Oscillator Strength $P \times 10^{-6}$ in different solvents for complex 7	A	f_{exp}	0.97	6.23	5.12	0.57	24.61	4.19	7.55	0.536
		f_{calcu}	1.69	3.68	2.55	0.22	12.71	1.30	0.43	
	B	f_{exp}	1.31	5.28	4.61	0.06	25.66	3.6	5.75	0.514
		f_{calcu}	1.41	3.18	2.23	0.19	13.23	1.20	0.37	
	C	f_{exp}	1.26	6.2	5.95	0.04	29.2	5.02	6.33	0.514
		f_{calcu}	1.59	3.88	2.80	0.24	15.11	1.37	0.44	
	D	f_{exp}	1.77	9.77	9.1	0.35	40.9	6.5	10.81	0.523
		f_{calcu}	2.34	5.97	4.39	0.37	21.12	1.99	0.66	
	E	f_{exp}	1.72	8.68	8.04	0.37	38.78	6.58	10.07	0.523
		f_{calcu}	2.31	5.40	3.84	0.33	20.05	1.91	0.62	
	F	f_{exp}	1.97	10.19	10.43	0.22	41.75	6.39	10.19	0.514
		f_{calcu}	2.09	6.38	4.94	0.41	21.71	1.95	0.66	
Oscillator Strength $P \times 10^{-6}$ in different solvents for complex 8	A	f_{exp}	1.25	6.83	6.37	0.19	31.85	4.98	7.35	0.514
		f_{calcu}	1.68	4.18	3.04	0.26	16.52	1.48	0.47	
	B	f_{exp}	1.76	9.47	8.77	0.36	39.52	6.14	9.99	0.518
		f_{calcu}	2.22	5.76	4.25	0.36	20.50	1.91	0.63	
	C	f_{exp}	1.18	5.92	5.68	0.22	31.24	5.56	5.89	0.506
		f_{calcu}	1.63	3.76	2.66	0.23	16.29	1.43	0.44	
	D	f_{exp}	2.02	11.8	10.88	0.19	51.2	8.07	11.36	0.512
		f_{calcu}	2.69	7.10	5.27	0.45	26.56	2.40	0.78	
	E	f_{exp}	1.98	10.92	9.89	0.49	48.58	8.58	11.24	0.517
		f_{calcu}	2.84	6.67	4.76	0.41	25.11	2.36	0.76	
	F	f_{exp}	2.27	10.51	9.35	0.18	45.73	7.09	9.1	0.505
		f_{calcu}	2.49	6.23	4.55	0.39	23.75	2.16	0.70	

A = Chloroform, B = Ethanol, C = Nitrobenzene, D = Pyridine, E = DMF, F = DMSO

[a]The values presented here are merely intended to provide an indication of the general position since the spectral ranges reported for the transition vary from solvent to solvent.

The impact of covalency with the Judd-Ofelt parameters (Ω_2, Ω_4, Ω_6) can be elucidated through the following equation [53]:

$$f_{ed} = \frac{8\pi^2 mc\sigma}{3h(2J+1)} \cdot x \sum_{\lambda=2,4,6} \Omega_\lambda \left|\langle a \| U^\lambda \| b \rangle\right|^2 \qquad (2)$$

Where m, c, h, n, σ, and 2J+1 are electron mass, light speed, Planck's constant, refractive index, transition's wave number, and degeneracy of |a⟩, respectively. X = field correction factor $\left(x = \frac{(n^2+2)^2}{9n}\right)$. The refractive index can be determined from the band gap energy value using Tauc's equation [54,55]. After obtaining the band gap energy (E_g) using Tauc's equation, the refractive index is calculated using the following relation:

$$\frac{(n^2-1)}{(n^2+1)} = 1 - \sqrt{\frac{E_g}{20}} \quad (3)$$

Equation (2) yields a new, more straightforward equation (4) of the b = Ax type matrix once constant values are added.

$$\frac{f_{e_d}}{c} = \sum_{\lambda=2,4,6} \Omega_\lambda \left|\langle a \| U^\lambda \| b \rangle\right|^2 \quad (4)$$

Judd-Ofelt parameters have been identified (see Table 3a.6) for all synthesized compounds using the least square approach using $\left|\langle a \| U^\lambda \| b \rangle\right|^2$ values from the Carnall publication [52]. By Judd-Ofelt theory, the calculated value of oscillator strength (f_{cal}) was computed from initial (a) to excited state (b) transitions by applying equation (2). To find the accuracy of the fitting procedure, the root mean square deviation (δ_{rms}) of f_{exp} with respect to f_{cal} was calculated using the formula given below.

$$\delta = \sqrt{\frac{\sum(f_{cal}-f_{exp})^2}{\sum f_{exp}^2}} \quad (5)$$

The quality of the fitting result improves with a lower value of the root mean square deviation. Comparative values of the calculated oscillator strength (f_{cal}) and root mean square deviation (δ_{rms}) are provided in Table 3a.5.

The amplitudes of the Judd-Ofelt parameters Ω_λ (λ = 2, 4, 6) reflect the enhancement of 4f-4f band transitions, particularly hypersensitive ($^4G_{5/2} \leftarrow {}^4I_{9/2}$) and pseudohypersensitive transitions ($^4F_{5/2}$, $^4F_{7/2} \leftarrow {}^4I_{9/2}$). As covalency is introduced into the metal-ligand interaction, the oscillator strength and magnitude of Ω_2 increase, indicating the strengthening of transitions. Ω_4 and Ω_6 parameters can predict the oscillator strength for Nd(III) complexes. However, Ω_2 values can specifically demonstrate how solvents or ligands affect the intensity of a hypersensitive transition.

Compared to the Ω_2 parameter, the Ω_4 and Ω_6 parameters, which are linked to alterations in the symmetry characteristics of the complex species, are slightly influenced. Specific solvents have been observed to impact the Ω_4 and Ω_6 parameters significantly. With coordinating solvents entering the system, the degree of mixing between the $4f^n$ and 5d orbitals changes, leading to higher values of the Ω_6 parameter. Consequently, coordinating solvents exhibit larger values of Ω_6 in Table 3a.6. Meanwhile, Ω_4 values remain consistently low across all complexes in various solvents, suggesting that long-ranging secondary interactions such as π···π stacking or H-bonding remain unaffected.

Table 3a.6 Judd-Ofelt intensity parameters for complexes 6, 7, and 8.

Complex	J-O Parameter [$\Omega/10^{-20}$ cm^2]	A	B	C	D	E	F
6	Ω_2	5.07	5.46	5.17	7.96	7.74	6.61
	Ω_4	1.88	1.45	1.16	2.11	1.72	1.69
	Ω_6	3.92	4.63	3.36	6.19	5.94	5.33
7	Ω_2	3.87	4.22	4.86	6.76	6.32	7.20
	Ω_4	1.68	1.37	1.46	2.06	2.19	1.50
	Ω_6	3.28	2.87	3.64	5.72	4.97	6.52
8	Ω_2	5.36	6.60	5.27	8.65	7.96	7.66
	Ω_4	1.51	1.92	1.56	2.29	2.68	2.23
	Ω_6	3.96	5.55	3.44	6.89	2.16	5.92

A = Chloroform, B = Ethanol, C = Nitrobenzene, D = Pyridine, E = DMF, F = DMSO

In order to demonstrate the covalency of complexes, equations (6) to (9) were used to compute the Nephelauxetic ratio (β), Sinha parameter (δ%), bonding parameter ($b^{1/2}$), and angular overlap parameter (η). In Nephelauxetic ratio calculation, $\bar{\nu}_{\text{complex}}$ and $\bar{\nu}_{\text{free ion}}$ was identified by taking peak center values for all transitions in the absorption spectra of complexes. All covalency parameters are provided in Tables 3a.7-3a.10.

$$\text{Nephelauxetic ratio } \boldsymbol{\beta} = \frac{\bar{\nu}_{complex}}{\bar{\nu}_{free\ ion}} \tag{6}$$

$$\text{Sinha parameter } \boldsymbol{\delta}\% = \left[\frac{1-\beta}{\beta}\right] \times 100 \tag{7}$$

$$\text{Bonding parameter } b^{\frac{1}{2}} = \left(\frac{1-\beta}{2}\right)^{1/2} \tag{8}$$

$$\text{Angular overlap parameter } \eta = \frac{1-\sqrt{\beta}}{\sqrt{\beta}} \tag{9}$$

Table 3a.7 Calculation of Nephelauxetic ratio β for complexes 6, 7, and 8.

Nephelauxetic ratio β						
Transitions	Chloroform	Ethanol	Nitrobenzene	Pyridine	DMF	DMSO
Complex 6						
$^4F_{3/2} \leftarrow {}^4I_{9/2}$	0.9874	0.9886	0.9886	0.9886	0.9897	0.9886
$^4F_{5/2} \leftarrow {}^4I_{9/2}$	0.9875	0.9888	0.9888	0.9888	0.9888	0.9888
$^4F_{7/2} \leftarrow {}^4I_{9/2}$	0.9893	0.984	0.9893	0.9854	0.9854	0.9854
$^4F_{9/2} \leftarrow {}^4I_{9/2}$	0.9898	0.9898	0.9883	0.9883	0.9898	0.9898
$^4G_{5/2} \leftarrow {}^4I_{9/2}$	0.9879	0.9897	0.9879	0.9879	0.9897	0.9845
$^4G_{7/2} \leftarrow {}^4I_{9/2}$	0.989	0.9908	0.9908	0.9908	0.9908	0.9908
$^4G_{9/2} \leftarrow {}^4I_{9/2}$	0.9886	0.9905	0.9905	0.9905	0.9905	0.9905
Complex 7						
$^4F_{3/2} \leftarrow {}^4I_{9/2}$	0.9874	0.9886	0.9886	0.9886	0.9886	0.9965
$^4F_{5/2} \leftarrow {}^4I_{9/2}$	0.9875	0.9888	0.9888	0.9888	0.9888	0.99
$^4F_{7/2} \leftarrow {}^4I_{9/2}$	0.9893	0.9854	0.988	0.9854	0.9854	0.9854
$^4F_{9/2} \leftarrow {}^4I_{9/2}$	0.9927	0.9956	0.9912	0.9883	0.9898	0.9883
$^4G_{5/2} \leftarrow {}^4I_{9/2}$	0.9879	0.9897	0.9897	0.9897	0.9897	0.9845
$^4G_{7/2} \leftarrow {}^4I_{9/2}$	0.989	0.9908	0.9908	0.9908	0.9908	0.9908
$^4G_{9/2} \leftarrow {}^4I_{9/2}$	0.9905	0.9905	0.9905	0.9905	0.9905	0.9924
Complex 8						
$^4F_{3/2} \leftarrow {}^4I_{9/2}$	0.9874	0.9886	0.9874	0.9886	0.9886	0.9897
$^4F_{5/2} \leftarrow {}^4I_{9/2}$	0.9875	0.9888	0.9875	0.9888	0.9888	0.9888
$^4F_{7/2} \leftarrow {}^4I_{9/2}$	0.9893	0.9854	0.9893	0.9854	0.9854	0.9854
$^4F_{9/2} \leftarrow {}^4I_{9/2}$	0.9883	0.9883	0.9883	0.9883	0.9898	0.9898
$^4G_{5/2} \leftarrow {}^4I_{9/2}$	0.9829	0.9879	0.9845	0.9862	0.9897	0.9845
$^4G_{7/2} \leftarrow {}^4I_{9/2}$	0.989	0.9908	0.9908	0.9908	0.9908	0.9908
$^4G_{9/2} \leftarrow {}^4I_{9/2}$	0.9886	0.9905	0.9886	0.9905	0.9905	0.9905

Table 3a.8 Calculation of Sinha Parameter δ for complexes 6, 7, and 8.

Sinha parameter δ						
Transitions	Chloroform	Ethanol	Nitrobenzene	Pyridine	DMF	DMSO
Complex 6						
$^4F_{3/2} \leftarrow {}^4I_{9/2}$	1.2711	1.1544	1.1544	1.1544	1.0415	1.1544
$^4F_{5/2} \leftarrow {}^4I_{9/2}$	1.2614	1.1346	1.1346	1.1346	1.1346	1.1346
$^4F_{7/2} \leftarrow {}^4I_{9/2}$	1.0843	1.6253	1.0843	1.4866	1.4866	1.4866
$^4F_{9/2} \leftarrow {}^4I_{9/2}$	1.0301	1.0301	1.1794	1.1794	1.0301	1.0301
$^4G_{5/2} \leftarrow {}^4I_{9/2}$	1.22	1.045	1.22	1.22	1.045	1.5701
$^4G_{7/2} \leftarrow {}^4I_{9/2}$	1.1099	0.9319	0.9319	0.9319	0.9319	0.9319
$^4G_{9/2} \leftarrow {}^4I_{9/2}$	1.151	0.9557	0.9557	0.9557	0.9557	0.9557
Complex 7						
$^4F_{3/2} \leftarrow {}^4I_{9/2}$	1.2711	1.1544	1.1544	1.1544	1.1544	0.3477
$^4F_{5/2} \leftarrow {}^4I_{9/2}$	1.2614	1.1346	1.1346	1.1346	1.1346	1.0078
$^4F_{7/2} \leftarrow {}^4I_{9/2}$	1.0843	1.4866	1.2185	1.4866	1.4866	1.4866
$^4F_{9/2} \leftarrow {}^4I_{9/2}$	0.7368	0.4433	0.8862	1.1794	1.0301	1.1794
$^4G_{5/2} \leftarrow {}^4I_{9/2}$	1.22	1.045	1.045	1.045	1.045	1.5701
$^4G_{7/2} \leftarrow {}^4I_{9/2}$	1.1099	0.9319	0.9319	0.9319	0.9319	0.9319
$^4G_{9/2} \leftarrow {}^4I_{9/2}$	0.9557	0.9557	0.9557	0.9557	0.9557	0.7675
Complex 8						
$^4F_{3/2} \leftarrow {}^4I_{9/2}$	1.2711	1.1544	1.2711	1.1544	1.1544	1.0415
$^4F_{5/2} \leftarrow {}^4I_{9/2}$	1.2614	1.1346	1.2614	1.1346	1.1346	1.1346
$^4F_{7/2} \leftarrow {}^4I_{9/2}$	1.0843	1.4866	1.0843	1.4866	1.4866	1.4866
$^4F_{9/2} \leftarrow {}^4I_{9/2}$	1.1794	1.1794	1.1794	1.1794	1.0301	1.0301
$^4G_{5/2} \leftarrow {}^4I_{9/2}$	1.7385	1.22	1.5701	1.3951	1.045	1.5701
$^4G_{7/2} \leftarrow {}^4I_{9/2}$	1.1099	0.9319	0.9319	0.9319	0.9319	0.9319
$^4G_{9/2} \leftarrow {}^4I_{9/2}$	1.151	0.9557	1.151	0.9557	0.9557	0.9557

Table 3a.9 Calculation of Bonding parameter $b^{1/2}$ for complexes 6, 7, and 8.

Bonding parameter $b^{1/2}$						
Transitions	Chloroform	Ethanol	Nitrobenzene	Pyridine	DMF	DMSO
Complex 6						
$^4F_{3/2} \leftarrow {}^4I_{9/2}$	0.0792	0.0755	0.0755	0.0755	0.0718	0.0755
$^4F_{5/2} \leftarrow {}^4I_{9/2}$	0.0789	0.0749	0.0749	0.0749	0.0749	0.0749
$^4F_{7/2} \leftarrow {}^4I_{9/2}$	0.0732	0.0894	0.0732	0.0856	0.0856	0.0856
$^4F_{9/2} \leftarrow {}^4I_{9/2}$	0.0714	0.0714	0.0763	0.0763	0.0714	0.0714
$^4G_{5/2} \leftarrow {}^4I_{9/2}$	0.0776	0.0719	0.0776	0.0776	0.0719	0.0879
$^4G_{7/2} \leftarrow {}^4I_{9/2}$	0.0741	0.0679	0.0679	0.0679	0.0679	0.0679
$^4G_{9/2} \leftarrow {}^4I_{9/2}$	0.0754	0.0688	0.0688	0.0688	0.0688	0.0688
Complex 7						
$^4F_{3/2} \leftarrow {}^4I_{9/2}$	0.0792	0.0755	0.0755	0.0755	0.0755	0.0416
$^4F_{5/2} \leftarrow {}^4I_{9/2}$	0.0789	0.0749	0.0749	0.0749	0.0749	0.0706
$^4F_{7/2} \leftarrow {}^4I_{9/2}$	0.0732	0.0856	0.0776	0.0856	0.0856	0.0856
$^4F_{9/2} \leftarrow {}^4I_{9/2}$	0.0605	0.047	0.0663	0.0763	0.0714	0.0763
$^4G_{5/2} \leftarrow {}^4I_{9/2}$	0.0776	0.0719	0.0719	0.0719	0.0719	0.0879
$^4G_{7/2} \leftarrow {}^4I_{9/2}$	0.0741	0.0679	0.0679	0.0679	0.0679	0.0679
$^4G_{9/2} \leftarrow {}^4I_{9/2}$	0.0688	0.0688	0.0688	0.0688	0.0688	0.0617
Complex 8						
$^4F_{3/2} \leftarrow {}^4I_{9/2}$	0.0792	0.0755	0.0792	0.0755	0.0755	0.0718
$^4F_{5/2} \leftarrow {}^4I_{9/2}$	0.0789	0.0749	0.0789	0.0749	0.0749	0.0749
$^4F_{7/2} \leftarrow {}^4I_{9/2}$	0.0732	0.0856	0.0732	0.0856	0.0856	0.0856
$^4F_{9/2} \leftarrow {}^4I_{9/2}$	0.0763	0.0763	0.0763	0.0763	0.0714	0.0714
$^4G_{5/2} \leftarrow {}^4I_{9/2}$	0.0924	0.0776	0.0879	0.0829	0.0719	0.0879
$^4G_{7/2} \leftarrow {}^4I_{9/2}$	0.0741	0.0679	0.0679	0.0679	0.0679	0.0679
$^4G_{9/2} \leftarrow {}^4I_{9/2}$	0.0754	0.0688	0.0754	0.0688	0.0688	0.0688

Table 3a.10 Calculation of Angular Overlap parameter η for complexes 6, 7, and 8.

Angular Overlap parameter η						
Transitions	Chloroform	Ethanol	Nitrobenzene	Pyridine	DMF	DMSO
Complex 6						
$^4F_{3/2} \leftarrow {}^4I_{9/2}$	0.0063	0.0058	0.0058	0.0058	0.0052	0.0058
$^4F_{5/2} \leftarrow {}^4I_{9/2}$	0.0063	0.0057	0.0057	0.0057	0.0057	0.0057
$^4F_{7/2} \leftarrow {}^4I_{9/2}$	0.0054	0.0081	0.0054	0.0074	0.0074	0.0074
$^4F_{9/2} \leftarrow {}^4I_{9/2}$	0.0051	0.0051	0.0059	0.0059	0.0051	0.0051
$^4G_{5/2} \leftarrow {}^4I_{9/2}$	0.0061	0.0052	0.0061	0.0061	0.0052	0.0078
$^4G_{7/2} \leftarrow {}^4I_{9/2}$	0.0055	0.0046	0.0046	0.0046	0.0046	0.0046
$^4G_{9/2} \leftarrow {}^4I_{9/2}$	0.0057	0.0048	0.0048	0.0048	0.0048	0.0048
Complex 7						
$^4F_{3/2} \leftarrow {}^4I_{9/2}$	0.0063	0.0058	0.0058	0.0058	0.0058	0.0017
$^4F_{5/2} \leftarrow {}^4I_{9/2}$	0.0063	0.0057	0.0057	0.0057	0.0057	0.005
$^4F_{7/2} \leftarrow {}^4I_{9/2}$	0.0054	0.0074	0.0061	0.0074	0.0074	0.0074
$^4F_{9/2} \leftarrow {}^4I_{9/2}$	0.0037	0.0022	0.0044	0.0059	0.0051	0.0059
$^4G_{5/2} \leftarrow {}^4I_{9/2}$	0.0061	0.0052	0.0052	0.0052	0.0052	0.0078
$^4G_{7/2} \leftarrow {}^4I_{9/2}$	0.0055	0.0046	0.0046	0.0046	0.0046	0.0046
$^4G_{9/2} \leftarrow {}^4I_{9/2}$	0.0048	0.0048	0.0048	0.0048	0.0048	0.0038
Complex 8						
$^4F_{3/2} \leftarrow {}^4I_{9/2}$	0.0063	0.0058	0.0063	0.0058	0.0058	0.0052
$^4F_{5/2} \leftarrow {}^4I_{9/2}$	0.0063	0.0057	0.0063	0.0057	0.0057	0.0057
$^4F_{7/2} \leftarrow {}^4I_{9/2}$	0.0054	0.0074	0.0054	0.0074	0.0074	0.0074
$^4F_{9/2} \leftarrow {}^4I_{9/2}$	0.0059	0.0059	0.0059	0.0059	0.0051	0.0051
$^4G_{5/2} \leftarrow {}^4I_{9/2}$	0.0087	0.0061	0.0078	0.007	0.0052	0.0078
$^4G_{7/2} \leftarrow {}^4I_{9/2}$	0.0055	0.0046	0.0046	0.0046	0.0046	0.0046
$^4G_{9/2} \leftarrow {}^4I_{9/2}$	0.0057	0.0048	0.0057	0.0048	0.0048	0.0048

The bonding parameter's positive values and minimal alteration suggest covalent bonding with limited participation of 4f-orbitals in the synthesized complexes across all solvents, where the nephelauxetic effect values range between 0.9829 and 0.9965. Both the Sinha parameter (δ%) values and the angular overlap parameter (η) values, which illustrate electron delocalization across the 4f orbital and covalency, have been found to be positive for all complexes. This indicates a similar extent of covalent bonding, as expected due to the similar coordination number [51,56,57].

Figure 3a.17 presents a spectrum analysis of the recently synthesized compounds using solid-state emission spectra and electronic absorption in a 10^{-6} M ethanolic solution. Across the wavelengths specified in Table 3a.11, all three complexes display electronic n→π*, π→π*, and LMCT transitions. Additionally, each complex exhibits three emission peaks. The emission of light from $^2D_{3/2}$→$^4I_{9/2}$ causes the peaks observed at wavelengths of 331.4 nm (complex 6), 326.5 nm (complex 7), and 330.9 nm (complex 8). Similarly, peaks at 467.5 nm (complex 6), 466.7 nm (complex 7), and 468.8 nm (complex 8) indicate the $^4G_{11/2}$→$^4I_{9/2}$ transition, while those at 493.5 nm (complex 6), 493 nm (complex 7), and 492.7 nm (complex 8) denote the $^4G_{7/2}$→$^4I_{9/2}$ transition. Utilizing the emission spectrum bands and equations (1) and (2), the spectral strength (f_{exp} or P) and Judd-Ofelt parameters (Ω_t) were computed again. The calculated value of oscillator strength (f_{cal}) from initial (a) to excited state (b) transitions was determined using Judd-Ofelt theory, and the root mean square deviation (δ_{rms}) of f_{exp} with respect to f_{cal} was calculated using equation (5). The evaluated values for all complexes are presented in Table 3a.11. Based on the J-O parameters Ω_t, the probability of radiative transition, $A_{rad(\psi;\ \psi')}$, from the initial (ψ_J) to terminal state ($\psi'_{J'}$), was determined using the subsequent equation:

$$\boldsymbol{A_{\gamma ad}(\psi;\psi^*) = \frac{64\pi^4 e^2}{3h(2J+1)\lambda^3}\frac{n(n^2+2)^2}{9}[S_{ED}+S_{MD}]} \qquad (10)$$

S_{ED} and S_{MD} are electric and magnetic line strengths respectively. To calculate the probability of radiative transition, $A_{rad(\psi;\ \psi')}$ magnetic line strength is neglected, and equation (10) becomes:

$$\boldsymbol{A_{\gamma ad}(\psi;\psi^*) = \frac{64\pi^4 e^2}{3h(2J+1)\lambda^3}\frac{n(n^2+2)^2}{9}[S_{ED}]} \qquad (11)$$

Here, S_{ED} can be represented in the form of J-O parameters and a reduced square matrix by the following relation:

$$S_{ED} = \sum_{t=2,4,6} \Omega_t \left| \psi_J U^{(t)} \psi'_{J'} \right|^2 \quad (12)$$

The value of matrix elements was obtained from reference [52]. Further, the reciprocal of A_{rad} provides the value of radiative lifetime (τ_{rad}) as follows:

$$\tau_{rad} = \frac{1}{A_{rad}} \quad (13)$$

Table 3a.11 Oscillator Strength, Judd-Ofelt Parameters, root mean square deviation, Radiative transition rate, and Radiative lifetime of complexes 6, 7, and 8 from emission spectra.

Complex		6	7	8
Oscillator Strength × 10^{-6}	$^2D_{3/2} \rightarrow {}^4I_{9/2}$	35.56	36.66	30.07
	$^4G_{11/2} \rightarrow {}^4I_{9/2}$	29.62	37.89	21.72
	$^4G_{7/2} \rightarrow {}^4I_{9/2}$	38.33	33.87	38.33
J-O Parameter ($\Omega/10^{-20}$ cm^2)	Ω_2	17.16	16.80	14.98
	Ω_4	6.21	5.26	5.79
	Ω_6	7.32	11.79	4.59
root mean square deviation (δ_{rms})		0.9900	0.9896	0.9899
Radiative transition rate A_{rad} (s^{-1})		120.01	179.55	77.45
Radiative lifetime τ_{rad} (ms)		8.33	5.57	12.91

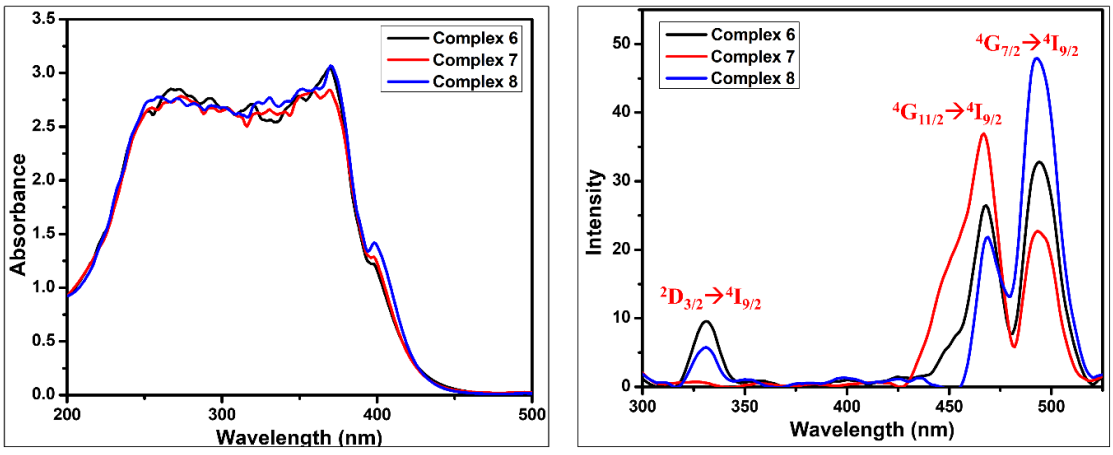

Figure 3a.17 The spectra of (a) Electronic absorption and (b) Emission for complexes 6, 7 and 8.

The stoke shift of these neodymium complexes was computed utilizing the absorption and emission spectrum peaks [58], following established protocols, and the results are outlined in Table 3a.12. These neodymium compounds exhibit a small Stoke shift, indicating primarily a vibrational shift without significant changes in energy levels.

Table 3a.12 Absorption and emission peak analysis for complexes 6, 7, and 8.

Complex	Absorption	Emission	Stoke shift
6	269.9 (n→π*)	331.4	61.5
	369.9 (π→π*)	467.5	97.6
	398.8 (LMCT)	493.5	94.7
7	273.7 (n→π*)	326.5	52.8
	369.9 (π→π*)	466.7	96.8
	397.7 (LMCT)	493	95.3
8	259.7 (n→π*)	330.9	71.2
	370 (π→π*)	468.8	98.8
	398.2 (LMCT)	492.7	94.5

The widely recognized energy diagram, shown in Figure 3a.18, illustrates how energy is absorbed by the acylpyrazolone ligand, known as the "CL (central ligand)", transferred to the metal ion, and then returned to the ground state [59]. The main ideas about the emission process of neodymium ions can be explained using this diagram. Because of its $4f^3$ configuration of Nd^{3+}, splitting of the spectrum states caused by interelectronic repulsion, spin-orbit coupling, and ligand field influence will take place to remove the J degeneracy partially or completely, making the transition "allowed" (See Figure 3a.18(a)). Energy travels through a path that begins with the central ligand absorbing energy into its excited singlet state. Then it is subsequently transferred to a triplet state by the ISC before arriving at the Nd(III) ion's energy levels. The functional group connected to the phenyl rings of acylpyrazolone, an NL (neutral ligand) that provides stability, fluorescence efficacy, absorption efficacy, and LMCT efficacy, is seen to have an impact on this light energy conversion diagram, which is also referred to as the "antenna effect" (See Figure 3a.18(b)).

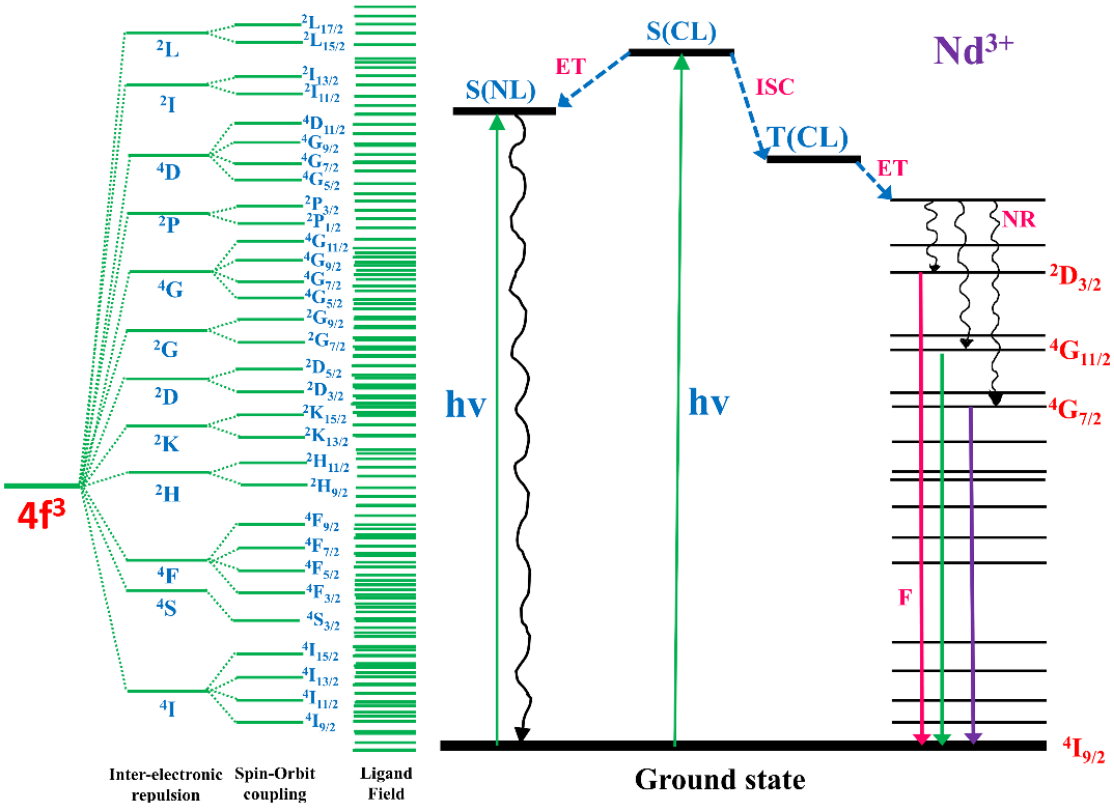

(a)

$4f^3$ configuration of a Nd(III) ion gives rise to several terms

(b)

Energy level diagram for Nd^{3+} complex, where CL = central ligand, NL = neutral ligand, S = singlet excited state, T = triplet excited state, ET = intramolecular energy transfer, ISC = intersystem crossing, F = Fluorescence decay, NR = Non-radiative pathway

Figure 3a.18 "Antenna effect" diagram showing the mechanism of the emission process in complexes 6, 7 and 8.

3a.4 Conclusions

The primary objectives of this study were to (i) assess the intensity of the hypersensitive transition peak in Nd(III)-acylpyrazolone complexes across various solvents, (ii) examine how structural variations in the ligand affect the hypersensitive transition (including oscillator strength, band shapes, and Judd-Ofelt parameters) in different complexes, (iii) investigate the influence of different coordinating and non-coordinating solvents, and (iv) determine the degree of covalency using various parameters. The three neodymium-acylpyrazolone complexes—designated as 6, 7, and 8—exhibited distorted square antiprism geometry with eight-coordination, stabilized by three σ-donating acylpyrazolone ligands and two solvent molecules. The structural analysis of all complexes included ESI-mass, FT-IR, thermogravimetric, and single-crystal X-ray diffraction methods. The $^4G_{5/2} \leftarrow {}^4I_{9/2}$ transition observed in the electronic

spectra of the complexes displayed hypersensitivity, evident from the higher values of oscillator strength and Ω_2 parameter. Notably, pyridine was found to enhance the 4f-4f strength the most among the solvents investigated. Furthermore, in solvents with strong coordination (pyridine, DMF, DMSO), the order of intensity among the complexes was consistently observed as complex 6 > 7 > 8. The presence of lower and consistent Ω_4 values and findings from Hirshfeld analysis suggested the involvement of long-ranging secondary $\pi\cdots\pi$ stacking or H-bonding interactions. Assessment of covalency parameters revealed positive values for electron delocalization across the 4f orbital and covalency in all complexes, indicating a similar level of covalent bonding. A lower root means square deviation, which indicates a better fitting result. The functional groups attached to the phenyl rings of acylpyrazolone, acting as neutral ligands (NL), significantly influenced the intensity of emission spectra, as evidenced by antenna effect energy diagrams. The potential for modifying the chemical and spectroscopic properties of acylpyrazolone to synthesize multi-dentate Nd(III) complexes holds promise for various applications in material sensing, scanning, and potentially in understanding biological mechanisms or diagnosing diseases.

References

[1] A. Cruz-Navarro, S. Rosete-Luna, J.M. Rivera, M. Rodríguez, A. Flores-Parra, S. Castillo-Blum, D. Morales-Morales, R. Colorado-Peralta, Heptacoordinated lanthanide(III) complexes based on 2,6-bis(1H-benzo[d]imidazol-2-yl)pyridine ligands (bbp, bmbp and bdmbp): Computational calculations, luminescent properties and cytotoxic evaluation., J Mol Struct 1283 (2023) 135345. https://doi.org/10.1016/j.molstruc.2023.135345.

[2] É. Böszörményi, O. Dömötör, B. Kutus, G. Varga, G. Peintler, P. Sipos, Coordination motifs of binary neodymium(III) D-gluconate, D-galactonate and L-gulonate complexes and the transition from inner- to outer-sphere coordination in neutral to strongly alkaline medium, J Mol Struct 1261 (2022) 132894. https://doi.org/10.1016/j.molstruc.2022.132894.

[3] U.P. Singh, R. Kumar, Structural and thermal properties of some neodymium (III) complexes, J Mol Struct 837 (2007) 214–223. https://doi.org/10.1016/j.molstruc.2006.10.022.

[4] L. Macalik, M. Wandas, W. Sąsiadek, J. Lorenc, R. Lisiecki, J. Hanuza, Molecular structure and spectroscopic properties of new neodymium complex with 3-bromo-2-chloro-6-picolinic N-oxide showing the ligand-to-metal energy transfer, J Mol Struct 1223 (2021) 128967. https://doi.org/10.1016/j.molstruc.2020.128967.

[5] Q. Liu, P. Cai, X. Wan, S. Zhang, K. Du, Q. Yin, Neodymium ternary complexes with 2,4,6-tri(2-pyridyl)-1,3,5-triazine: Synthesis, crystal structure and fluorescence property, J Mol Struct 1193 (2019) 151–157. https://doi.org/10.1016/j.molstruc.2019.05.008.

[6] S.S. Galley, S.A. Pattenaude, R.F. Higgins, C.J. Tatebe, D.A. Stanley, P.E. Fanwick, M. Zeller, E.J. Schelter, S.C. Bart, A reduction series of neodymium supported by pyridine(diimine) ligands, Dalton Trans 48 (2019) 8021–8025. https://doi.org/10.1039/c9dt00679f.

[7] B. Li, H. Li, P. Chen, W. Sun, C. Wang, T. Gao, P. Yan, Insight into the roles of structures and energy levels of mono- and bis-β-diketones on sensitizing Nd(III) NIR-luminescence, Dalton Trans 45 (2016) 11459–11470. https://doi.org/10.1039/c6dt01609j.

[8] J. Chakraborty, A. Ray, G. Pilet, G. Chastanet, D. Luneau, R.F. Ziessel, L.J. Charbonnière, L. Carrella, E. Rentschler, M.S. El Fallah, S. Mitra, Syntheses, characterisation, magnetism and photoluminescence of a homodinuclear Ln(III)-Schiff base family, Dalton Trans (2009) 10263–10272. https://doi.org/10.1039/b908910a.

[9] M.L. Neidig, D.L. Clark, R.L. Martin, Covalency in f-element complexes, Coord Chem Rev 257 (2013) 394–406. https://doi.org/10.1016/j.ccr.2012.04.029.

[10] G.S. Opelt, Intensities of crystal spectra of rare-earth ions, J Chem Phys 37 (1962) 511–520. https://doi.org/10.1063/1.1701366.

[11] B.R. Judd, Optical Absorption Intensities of Rare-Earth Ions, Phys Rev 127 (1962) 750–761. https://doi.org/10.1103/PhysRev.127.750.

[12] X. Lei, H. Wang, L. Fu, J. Wang, S. Xu, Efficient Preparation of Rare Earth Oxides from Back Extraction Praseodymium Neodymium Chloride by Flash Pyrolysis, ChemistrySelect 7 (2022) e202200244. https://doi.org/10.1002/slct.202200244.

[13] H.-S. Yoon, C.-J. Kim, K.-W. Chung, S.-D. Kim, J.-Y. Lee, J.R. Kumar, Solvent extraction, separation and recovery of dysprosium (Dy) and neodymium (Nd) from aqueous solutions: Waste recycling strategies for permanent magnet processing, Hydrometallurgy 165 (2016) 27–43. https://doi.org/10.1016/j.hydromet.2016.01.028.

[14] S. Rehman, M.A. Almessiere, N. Tashkandi, A. Baykal, Y. Slimani, R. Jermy, V. Ravinayagam, C. Yaman, Fabrication of Spinel Cobalt Ferrite ($CoFe_2O_4$) Nanoparticles with Unique Earth Element Cerium and Neodymium for Anticandidal Activities, ChemistrySelect 4 (2019) 14329–14334. https://doi.org/10.1002/slct.201901811.

[15] Y.A. Tyula, P. Moradi, M. Nikoorazm, A New Neodymium Complex on Boehmite Nanoparticles with 1,3-Bis(pyridine-3-ylmethyl)thiourea as a Practical and Reusable Nanocatalyst for the Chemoselective Synthesis of Tetrazoles, ChemistrySelect 8 (2023) e202301674. https://doi.org/10.1002/slct.202301674.

[16] K.E. Sekhosana, R. Nkhahle, T. Nyokong, The Primary Demonstration of Exciton Coupling Effects on Optical Limiting Properties of Blue Double-Decker Lanthanide Phthalocyanine Salts, ChemistrySelect 3 (2018) 6671–6682. https://doi.org/10.1002/slct.201800597.

[17] L. Fkhar, H.A. Oualid, A. Sayout, Y. Abdellaoui, Y. Brahmi, O. Mounkachi, A. Romane, M.A. Ali, Nd-Doping-Induced Enhancement in the Antibacterial Activity of Synthesized ZnO Heretostructures, ChemistrySelect 5 (2020) 11331–11339. https://doi.org/10.1002/slct.202002080.

[18] I. Badran, M.O. Al-Ejli, Efficient Multi-walled Carbon Nanotubes/Iron Oxide Nanocomposite for the Removal of the Drug Ketoprofen for Wastewater Treatment Applications, ChemistrySelect 7 (2022) e202202976. https://doi.org/10.1002/slct.202202976.

[19] A.S. Das, M. Roy, D. Roy, T. Kar, S. Rath, S. Bhattacharya, Investigations of Microstructure and Dc Conductivity of V_2O_5-Nd_2O_3 Glass Nanocomposites, ChemistrySelect 2 (2017) 11273–11280. https://doi.org/10.1002/slct.201701590.

[20] A. Bhoriya, Sachin, N. Bura, D. Yadav, J. Singh, N. Singh, H.K. Singh, N. Dilawar Sharma, Application of Perovskite Strontium Doped Neodymium Manganite ($Nd_{0.6}Sr_{0.4}MnO_3$) for Effective Removal of Fast Green Dye, A Toxic Wastewater Contaminant, ChemistrySelect 8 (2023) e202204632. https://doi.org/10.1002/slct.202204632.

[21] A.B. Ganaie, K. Iftikhar, Structure, optical absorption and NIR-Photoluminescence of ternary Neodymium (III) complexes with fluorinated β-diketone and heterocyclic Lewis bases, J Mol Struct 1273 (2023) 134352. https://doi.org/10.1016/j.molstruc.2022.134352.

[22] J.-Z. Gao, W.-D. Yang, W. Yang, J.-W. Kang, G.-B. Bai, G.-S. Yu, Studies on hypersensitive transitions of Nd(III) in Nd(III)-0-diketone-neutral ligand ternary compounds, Chin J Chem 11 (1993) 289–298. https://doi.org/10.1002/cjoc.19930110401.

[23] Z. Ahmed, H.C. Avila, R.S. Carvalho, J. Kai, J.A.L.C. Resende, E. Bandini, A. Barbieri, M. Cremona, Bright neodymium complexes for efficient near infra-red organic light emitting diodes, New J Chem 44 (2020) 14161–14170. https://doi.org/10.1039/d0nj00403k.

[24] N. Agarwal, I. Verma, N. Siddiqui, S. Javed, Experimental spectroscopic and quantum computational analysis of pyridine-2,6-dicarboxalic acid with molecular docking

studies, J Mol Struct 1245 (2021) 131046. https://doi.org/10.1016/j.molstruc.2021.131046.

[25] P. Bag, S. Dutta, U. Flörke, K. Nag, Solid state and solution properties of lanthanide(III) complexes of a tetraiminodiphenolate macrocyclic ligand. X-ray structure, 1H NMR and luminescence spectral studies, J Mol Struct 891 (2008) 408–419. https://doi.org/10.1016/j.molstruc.2008.04.028.

[26] Rohini, M. Baral, B.K. Kanungo, Structural effect on the central cavity of a pendent 12N3 macrocycle on bonding and photophysical properties of Eu^{3+} and Tb^{3+} complexes: Experimental and theoretical study, J Mol Struct 1184 (2019) 324–338. https://doi.org/10.1016/j.molstruc.2019.02.032.

[27] N. Łukasik, E. Luboch, J. Chojnacki, E. Wagner-Wysiecka, 1,3,4-Thiadiazole-based diamides: Synthesis and complexation properties, J Mol Struct 1146 (2017) 713–722. https://doi.org/10.1016/j.molstruc.2017.06.057.

[28] F. Marchetti, C. Pettinari, R. Pettinari, Acylpyrazolone ligands: Synthesis, structures, metal coordination chemistry and applications, Coord Chem Rev 249 (2005) 2909–2945. https://doi.org/10.1016/j.ccr.2005.03.013.

[29] F. Marchetti, R. Pettinari, C. Pettinari, Recent advances in acylpyrazolone metal complexes and their potential applications, Coord Chem Rev 303 (2015) 1–31. https://doi.org/10.1016/j.ccr.2015.05.003.

[30] F. Marchetti, C. Pettinari, C. Di Nicola, A. Tombesi, R. Pettinari, Coordination chemistry of pyrazolone-based ligands and applications of their metal complexes, Coord Chem Rev 401 (2019). https://doi.org/10.1016/j.ccr.2019.213069.

[31] I. Shaikh, R.N. Jadeja, R. Patel, Three mixed ligand mononuclear Zn(II) complexes of 4-acyl pyrazolones: Synthesis, characterization, crystal study and anti-malarial activity, Polyhedron 183 (2020) 114528. https://doi.org/10.1016/j.poly.2020.114528.

[32] I. Shaikh, R.N. Jadeja, R. Patel, V. Mevada, V.K. Gupta, 4-Acylhydrazone-5-Pyrazolones and their Zinc(II) Metal Complexes: Synthesis, Characterization, Crystal Feature and Antimalarial Activity, J Mol Struct 1232 (2021) 130051. https://doi.org/10.1016/j.molstruc.2021.130051.

[33] A.K. Patel, R.N. Jadeja, H. Roy, R.N. Patel, S.K. Patel, R.J. Butcher, Pseudo-tetrahedral copper(II) complex derived from N'-[(2E,3Z)-4-hydroxy-4-phenylbut-3-en-2-ylidene]acetohydrazide: Synthesis, molecular structure, quantum chemical investigations, antioxidant and antiproliferative properties, J Mol Struct 1185 (2019) 341–350. https://doi.org/10.1016/j.molstruc.2019.03.004.

[34] G.M. Sheldrick, SHELXT – Integrated space-group and crystal-structure determination, Acta Crystallogr A 71 (2015) 3–8. https://doi.org/10.1107/S2053273314026370.

[35] G.M. Sheldrick, Crystal structure refinement with SHELXL, Acta Crystallogr C 71 (2015) 3–8. https://doi.org/10.1107/S2053229614024218.

[36] I. Shaikh, R.N. Jadeja, R. Patel, Three mixed ligand mononuclear Zn(II) complexes of 4-acyl pyrazolones: Synthesis, characterization, crystal study and anti-malarial activity, Polyhedron 183 (2020) 114528. https://doi.org/10.1016/j.poly.2020.114528.

[37] W.J. Geary, The use of conductivity measurements in organic solvents for the characterisation of coordination compounds, Coord Chem Rev 7 (1971) 81–122. https://doi.org/10.1016/S0010-8545(00)80009-0.

[38] R. Ilmi, K. Iftikhar, Luminescent nine-coordinate lanthanide complexes derived from fluorinated β-diketone and 2,4,6-tris (2-pyridyl)-1,3,5-triazine, J Coord Chem 65 (2012) 403–419. https://doi.org/10.1080/00958972.2011.649737.

[39] E.C. Okafor, The Metal Chelates of Heterocyclic /3-Diketones and their Derivatives, Part IV New Mixed Ligand Tetrakis Complexes of Lanthanides Derived from tris-Acetylacetonates and Some 4-Acyl Pyrazolones, Zeitschrift für Naturforschung B 35 (1980) 715–718. https://doi.org/10.1515/znb-1980-0615.

[40] N.M. Shavaleev, R. Scopelliti, F. Gumy, J.C.G. Bünzli, Near-infrared luminescence of nine-coordinate neodymium complexes with benzimidazole-substituted 8-hydroxyquinolines, Inorg Chem 47 (2008) 9055–9068. https://doi.org/10.1021/ic8010585.

[41] G. Bombiere, A. Polo, W. Jia-Fu, W. Jinguang, X. Guang-Xian, Synthesis and characterization of a ytterbium complex with diphenylacetylpyrazolone

$Yb(DPAP)_3 \cdot (H_2O)_2 \cdot 3EtOH$, Inorganica Chim Acta 132 (1987) 263–271. https://doi.org/10.1016/S0020-1693(00)81753-3.

[42] E. Chukwuemeka Okafor, The metal complexes of heterocyclic β-diketones and their deriva-tives-IX. Lanthanon chelates of 3-methyl-l-phenyl-4-trifluoroacetylpyrazol-5-one (HPMTFP). ^{1}H, ^{13}C and ^{19}F NMR, i.r. and u.v.-visible spectral studies, Spectrochim. Acta A 38 (1982) 981–987. https://doi.org/10.1016/0584-8539(82)80049-4.

[43] V.F. Shul'Gin, S. V. Abkhairova, O. V. Konnik, S.B. Meshkova, Z.M. Topilova, E.B. Rusanov, G.G. Aleksandrov, I.L. Eremenko, Anionic lanthanide complexes with 3-methyl-4-formyl-1-phenyl-5-pyrazolone, Russian J Inorg Chem 58 (2013) 678–683. https://doi.org/10.1134/S0036023613060223.

[44] Z. Ahmed, R.E. Aderne, J. Kai, H.I.P. Chavarria, M. Cremona, Ytterbium β-diketonate complexes for near infra-red organic light-emitting devices, Thin Solid Films 620 (2016) 34–42. https://doi.org/10.1016/j.tsf.2016.07.076.

[45] D. Zhou, Q. Li, C. Huang, G. Yao, S. Umetani, M. Matsui, L. Ying, A. Yu, X. Zhao, Room-temperature fluorescence, phosphorescence and crystal structures of 4-acyl pyrazolone lanthanide complexes: $Ln(L)_3 \cdot 2H_2O$, Polyhedron 16 (1997) 1381–1389. https://doi.org/10.1016/S0277-5387(96)00382-8.

[46] Q. Liu, S. Zhang, K. Du, W. Li, Q. Yin, P. jun Cai, Structure and photoluminescence properties study of neodymium complexes containing fluorine ligands, J Fluor Chem 212 (2018) 161–165. https://doi.org/10.1016/j.jfluchem.2018.03.015.

[47] C.-F. Yao, Y.-S. Chen, W.-C. Chen, R.-S. Sheu, J.-K. Lai, C.-H. Ueng, 1,3-Diphenyl-2-tricyclo[3.3.1.1 3,7]dec-2-ylidenepropane-1,3-diimine, and its -1-imino-3-one and -1,3-dione Derivatives, Acta Crystallogr C 53 (1997) 956–959. https://doi.org/10.1107/S0108270197002746.

[48] C.F. Mackenzie, P.R. Spackman, D. Jayatilaka, M.A. Spackman, CrystalExplorer model energies and energy frameworks: extension to metal coordination compounds, organic salts, solvates and open-shell systems, IUCrJ 4 (2017) 575–587. https://doi.org/10.1107/S205225251700848X.

[49] P.R. Spackman, M.J. Turner, J.J. McKinnon, S.K. Wolff, D.J. Grimwood, D. Jayatilaka, M.A. Spackman, CrystalExplorer: a program for Hirshfeld surface analysis, visualization and quantitative analysis of molecular crystals, J Appl Crystallogr 54 (2021) 1006–1011. https://doi.org/10.1107/S1600576721002910.

[50] R. Ilmi, K. Iftikhar, Pyrazine bridged Ln_2 (La, Nd, Eu and Tb) complexes containing fluorinated β-diketone, Inorg Chem Commun 20 (2012) 7–12. https://doi.org/10.1016/j.inoche.2012.01.037.

[51] H. Debecca Devi, Ch. Sumitra, Th. David Singh, N. Yaiphaba, N. Mohondas Singh, N. Rajmuhon Singh, Calculation and Comparison of Energy Interaction and Intensity Parameters for the Interaction of Nd(III) with DL-Valine, DL-Alanine and β-Alanine in Presence and Absence of Ca^{2+}/Zn^{2+} in Aqueous and Different Aquated Organic Solvents Using 4f-4f Transition Spectra as Probe, Int J Spectrosc 2009 (2009) 1–9. https://doi.org/10.1155/2009/784305.

[52] W.T. Carnall, P.R. Fields, B.G. Wybourne, Spectral intensities of the trivalent lanthanides and actinides in solution. I. Pr^{3+}, Nd^{3+}, Er^{3+}, Tm^{3+}, and Yb^{8+}, J Chem Phys 42 (1965) 3797–3806. https://doi.org/10.1063/1.1695840.

[53] P. Goldner, F. Auzel, Application of standard and modified Judd-Ofelt theories to a praseodymium-doped fluorozirconate glass, J Appl Phys 79 (1996) 7972–7977. https://doi.org/10.1063/1.362347.

[54] P. Hervé, L.K.J. Vandamme, General relation between refractive index and energy gap in semiconductors, Infrared Phys Technol 35 (1994) 609–615. https://doi.org/10.1016/1350-4495(94)90026-4.

[55] P. Ahlawat, S. Bhayana, V. Lather, S. Khatri, P. Kumari, M. Kumar, M.S. Shekhawat, V.B. Taxak, S.P. Khatkar, R. Kumar, Judd-Ofelt, urbach energy and geometrical optimization study of orange light emitting samarium (III) complexes with heterocyclic ligands for application in optoelectronic devices, Opt Mater (Amst) 133 (2022) 112940. https://doi.org/10.1016/j.optmat.2022.112940.

[56] K. Iftikhar, Hypersensitivity in the 4f-4f Absorption Spectra of Lanthanide(II1) Complexes, Inorganica Chim Acta 129 (1987) 261–264. https://doi.org/10.1016/S0020-1693(00)86672-4.

[57] M.C. Chavan, P. V Vaidya, N.R. Lokhande, M.N. Ghoshal, Bonding and Energy Parameters for Some Praseodymium(III) Mixed Ligand Complexes, Indian J Chem Sect A: Inorg Phys Theor Anal 23 (2010) 530–532. http://inis.iaea.org/search/search.aspx?orig_q=RN:18050308.

[58] I. Ameen, A.K. Tripathi, R.L. Mishra, A. Siddiqui, U.N. Tripathi, Aging effect on bonding properties of fluorescent neodymium materials, Karbala International Journal of Modern Science 4 (2018) 258–273. https://doi.org/10.1016/j.kijoms.2018.05.001.

[59] N. Sabbatini, M. Guardigli, J.-M. Lehn, Luminescent lanthanide complexes supramolecular devices as photochemical, Coord Chem Rev 123 (1993) 201–228. https://doi.org/10.1016/0010-8545(93)85056-A.

CHAPTER 3

Part (b): Neodymium based acylpyrazolone complexes: Synthesis and physicochemical characterizations.

3b.1 Introduction

An introduction to the significance, characteristics, and applications of neodymium complexes in coordination chemistry was provided in section 3a.1 of chapter 3(a). Now, to predict the basis of the properties for complexes of neodymium-acylpyrazolones the covalency between metal-ligand closures can become important concept. As extraction ability and proficient Antenna effect of acylpyrazolones with lanthanoids can be examined through their metal-ligand covalent character [1–3], this study presents a practical technique for determining both the Judd-Ofelt intensity parameters and oscillator strengths of three Nd(III)-acylpyrazolone complexes, 9, 10, and 11, in different solvents which have the general formula $[Nd(L)_3(H_2O)(EtOH)]$ and distorted square antiprismatic geometry.

3b.2 Experimental section

3b.2.1 Materials and Methods

HL^4 (3,5-dimethyl benzoyl 1-phenyl 3-methyl 5-pyrazolone), HL^5 (3,5-dimethyl benzoyl 1-(m-chlorophenyl) 3-methyl 5-pyrazolone), and HL^6 (3,5-dimethyl benzoyl 1-(p-tolyl) 3-methyl 5-pyrazolone) ligands were directly prepared and used as mentioned in Chapter 2(a). Neodymium(III) nitrate hexahydrate with a purity of 99.9% was acquired from SRL Pvt. Ltd.

3b.2.2 Neodymium-acylpyrazolone Complex Synthesis

A solution containing 3 mmol ligand in ethanol and 3 mmol $NaOH_{(aq)}$ was stirred for thirty minutes at 80–100 °C, as shown in Figure 3b.1. Subsequently, a solution of 1 mmol neodymium(III) nitrate hexahydrate in ethanol was added dropwise. After 18 hours of refluxing, the solution was transferred to a container and evaporated slowly, yielding an eight-coordinated neodymium-acylpyrazolone complex.

Complex 9 Synthesis

Complex 9 was prepared using HL^4 ligand (0.92 g), $NaOH_{(aq)}$ (0.12 g), and neodymium(III) nitrate hexahydrate (0.438 g). Yield(%): 96.87 %, M.P.: 223-230 °C, Molecular formula: $C_{59}H_{58}N_6NdO_8$, Formula wt: 1123.39. Mass peaks (see Figure 3b.2) (m/z) = 1123.71 ($[C_{59}H_{58}N_6NdO_8]^+$), 1104.70 ($[C_{59}H_{56}N_6NdO_7]^+$), 305.24 ($[C_{19}H_{17}N_2O_2]^+$). **FTIR (KBr, cm^{-1}):** 3387 (w, $\upsilon_{O\text{-}H\ water}$), 2921 (w, $\upsilon_{O\text{-}H\ EtOH}$), 1611 (s, $\upsilon_{C=O\ DMB}$), 1580 (s, $\upsilon_{C=O\ acylpyz}$).

Complex 10 Synthesis

Complex 10 was prepared using HL^5 ligand (1.023 g), $NaOH_{(aq)}$ (0.12 g), and neodymium(III) nitrate hexahydrate (0.438 g). Yield(%): 93.01 %, M.P.: 212-220 °C, Molecular formula: $C_{59}H_{55}Cl_3N_6NdO_8$, Formula wt: 1226.72. **FTIR (KBr, cm^{-1}):** 3407 (w, $\upsilon_{O\text{-}H\ water}$), 2920 (w, $\upsilon_{O\text{-}H\ EtOH}$), 1614 (s, $\upsilon_{C=O\ DMB}$), 1587 (s, $\upsilon_{C=O\ acylpyz}$).

Complex 11 Synthesis

Complex 11 was prepared using HL^6 ligand (0.96 g), $NaOH_{(aq)}$ (0.12 g), and neodymium(III) nitrate hexahydrate (0.438 g). Yield(%): 95.34, M.P.: 208-215 °C, Molecular formula: $C_{62}H_{64}N_6NdO_8$, Formula wt: 1163.39. Mass peaks (see Figure 3b.3) (m/z) = 1163.77 ($[C_{62}H_{64}N_6NdO_8]^+$), 1145.77 ($[C_{62}H_{62}N_6NdO_7]^+$). **FTIR (KBr, cm^{-1}):** 3407 (w, $\upsilon_{O\text{-}H\ water}$), 2921 (w, $\upsilon_{O\text{-}H\ EtOH}$), 1596 (s, $\upsilon_{C=O\ DMB}$), 1577 (s, $\upsilon_{C=O\ acylpyz}$).

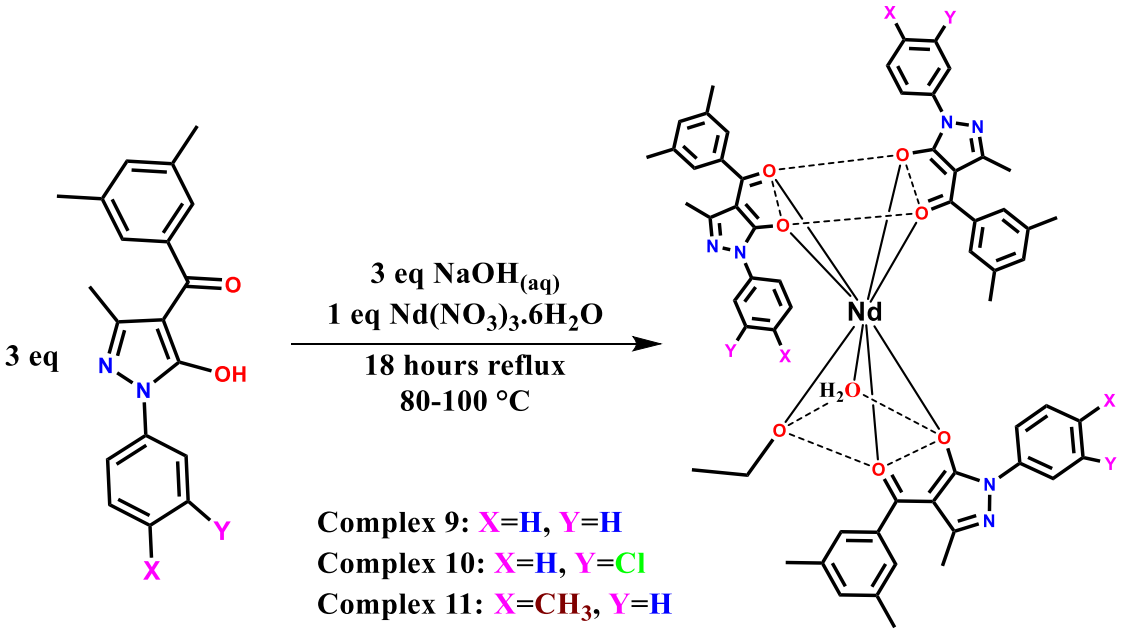

Figure 3b.1 Synthetic route for neodymium-acylpyrazolone complexes.

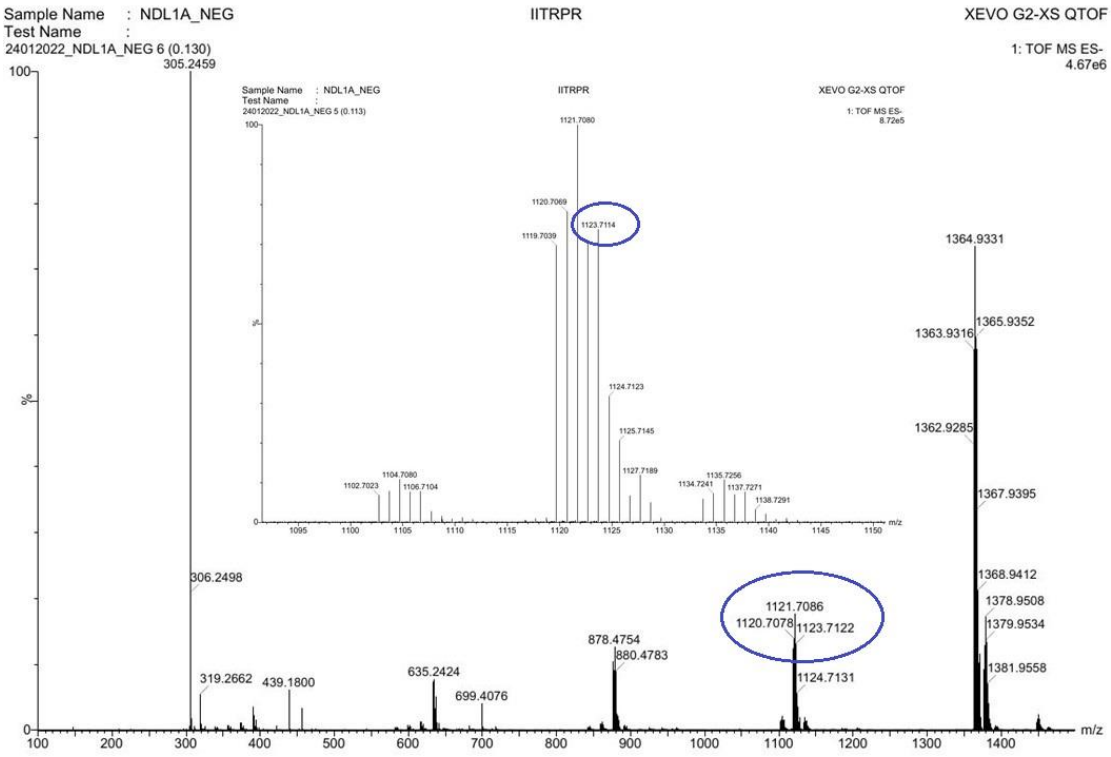

Figure 3b.2 Mass spectrum of complex 9.

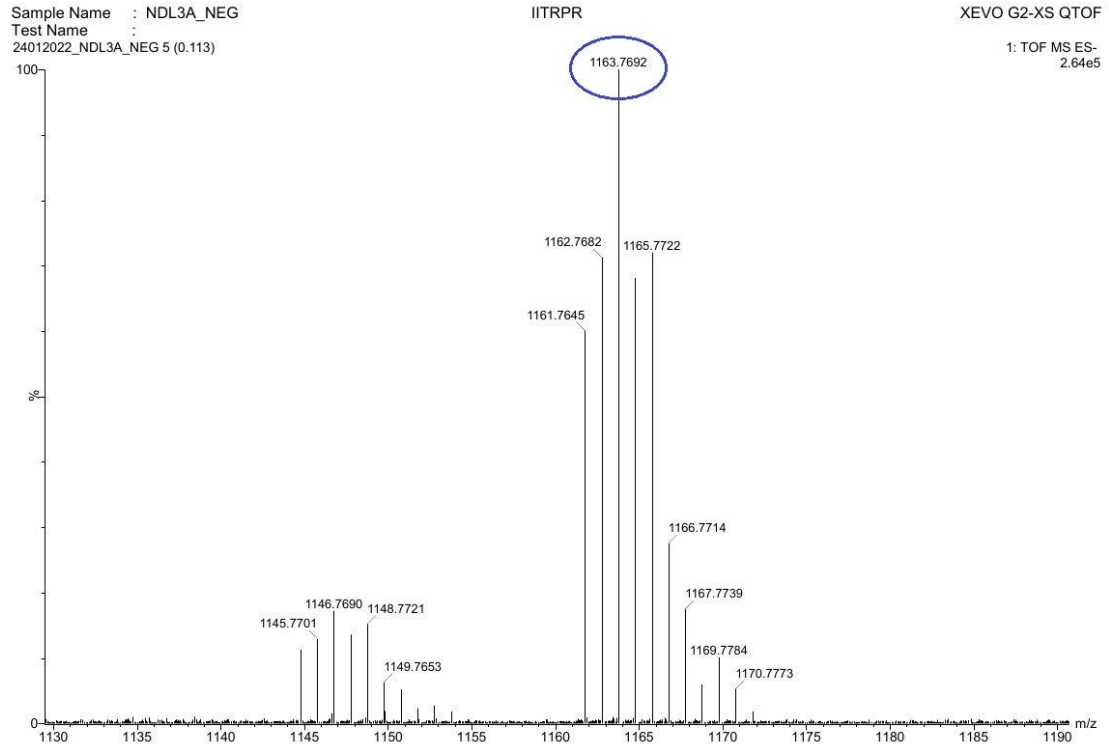

Figure 3b.3 Mass spectrum of complex 11.

3b.2.3 X-ray crystallographic examination

X-ray crystallographic analysis was conducted on complex 10 using a graphite monochromator and Mo-Kα (λ = 0.71073 Å) radiation. The detection and refinement procedures were performed based on the methods outlined in previously published papers from our laboratory [4]. The diffraction data were solved using the SHELXT software [5], while computation was done using the crystallographic software SHELXL-2018/3 [6].

3b.2.4 Physical measurements and characterization techniques

Similar methodologies, models, instruments, or instruments were employed to analyze the data of the synthesized compounds, using techniques such as FTIR, mass, UV-Vis, and TG-DTA as procedures outlined in Chapter 3(a) and previously published articles from our laboratory [4,7]. The solid-state emission spectra were captured utilizing a Jasco FP-6300 spectrofluorometer. Powder X-ray diffraction (XRD) was measured employing a Rigaku SmartLab SE (3kW) instrument from Japan, using the SmartLab Studio II software. The XRD used a Cu-K_α (0.154 nm) source, and data were collected using a D/teX Ultra 250 1D detector.

3b.3 Results and Discussion

For solution of complexes 9, 10, and 11 in DMF, the molar conductivity Λ_M values were found to be 11, 7, and 9 Ω^{-1} cm^2 mol^{-1}, respectively. These lower numbers demonstrate the behaviour is not electrolytic [8]. Furthermore, the subsequent section elucidates the extent of covalent bonding and crystal formations.

3b.3.1 FTIR spectral analysis

The FTIR bands of the $\upsilon_{O\text{-}H(ethanol)}$ and $\upsilon_{O\text{-}H(water)}$ ligands, respectively, serve as evidence for binding one CH_3CH_2OH and one H_2O as monodentate ligands in all neodymium complexes. These broad and low intense $\upsilon_{O\text{-}H(ethanol)}$ and $\upsilon_{O\text{-}H(water)}$ bands appear in the range 2900-3200 and 3200-3400 cm^{-1}, respectively, as given in Table 3b.1. This is because 100% ethanol was used as the solvent in the synthesis of all three complexes, which began with hexahydrate neodymium nitrate salt. The notable finding is decrease in $\upsilon_{C=O(3,5\text{-}dimethylbenzoyl)}$ and $\upsilon_{C=O(acyl\text{-}pyz)}$ stretching of ligands during complexation due to charge donation to Nd-ion by O-atoms of acylpyrazolones. $\upsilon_{C=O(3,5\text{-}dimethylbenzoyl)}$ is falling from 1621 cm^{-1} of HL^4 to 1611 cm^{-1} in complex 9, 1624 cm^{-1} of

HL^5 to 1614 cm^{-1} in complex 10, and 1622 cm^{-1} of HL^6 to 1596 cm^{-1} in complex 11. Similarly, $\upsilon_{C=O(acyl\text{-}pyz)}$ stretching becomes less when a complex is formed. Using the FTIR spectra of the complexes, which are shown in Figures 3b.4–3b.6, additional bands such as cyclic $\upsilon_{C=N}$, $\upsilon_{C=C}$, υ_{N-N}, and $\upsilon_{C-H\ in\ plane\ deformations}$ were also assigned to ligands and all complexes.

Table 3b.1 The FTIR values for neodymium complexes (in cm^{-1}).

Code	HL^4 Ligand	Complex 9	HL^5 Ligand	Complex 10	HL^6 Ligand	Complex 11
$\nu_{(C=O)}$ benzoyl	1621	1611	1624	1614	1622	1596
$\nu_{(C=O)}$ acyl	1605	1580	1589	1587	1607	1577
cyclic $\nu_{(C=N)}$	1511	1483	1554	1480	1511	1486
$\nu_{aromatic(C-C)}$	1307	1370	1344	1363	1356	1383
$\nu_{(N-N)}$	1175	1141	1176	1131	1175	1146
C-H in plane deformation	1067	1067	1080	1070	1066	1064

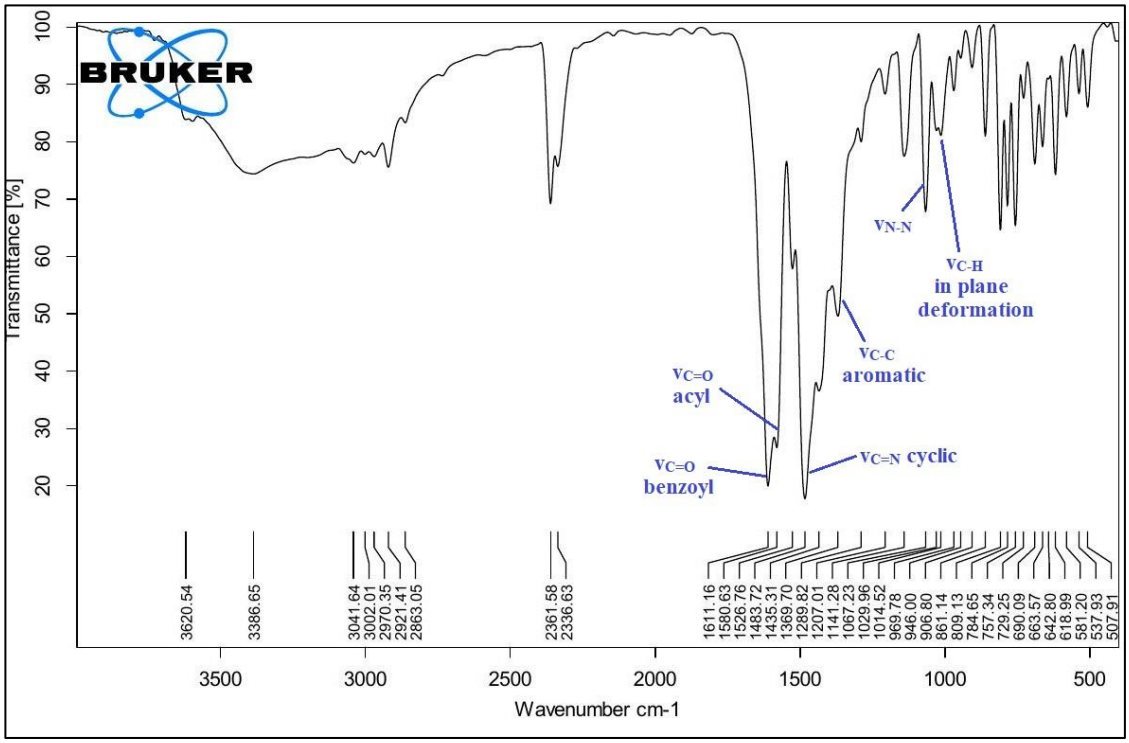

Figure 3b.4 FTIR spectrum of complex 9.

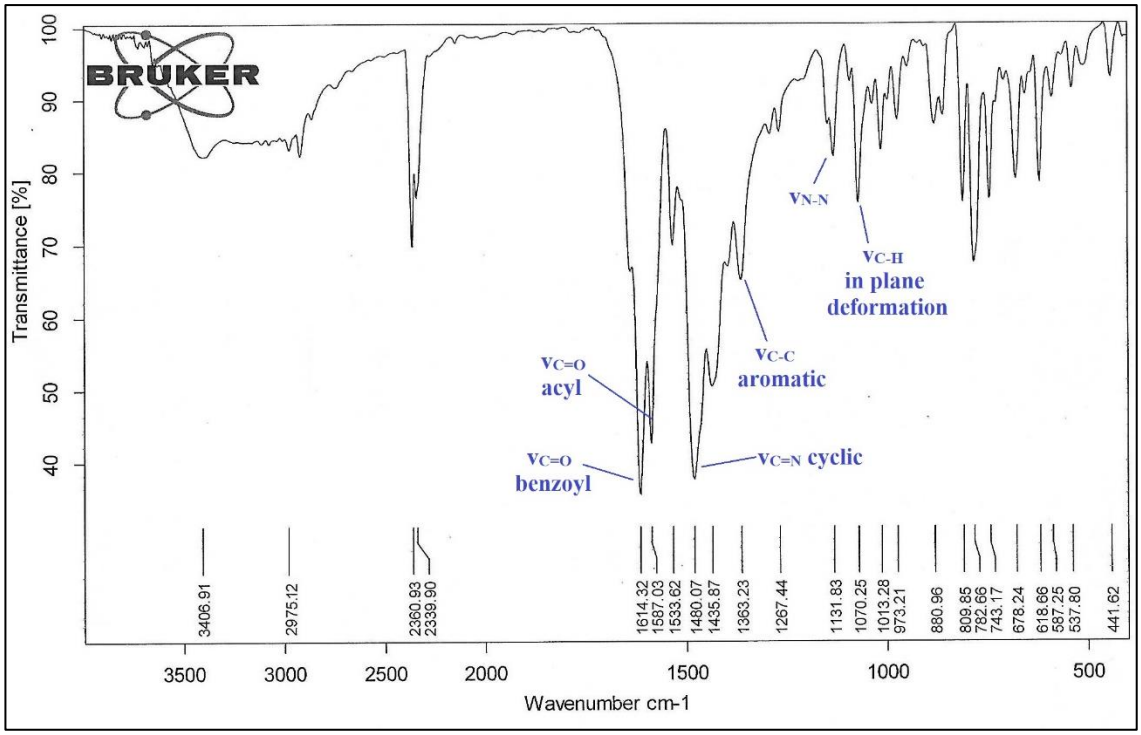

Figure 3b.5 FTIR spectrum of complex 10.

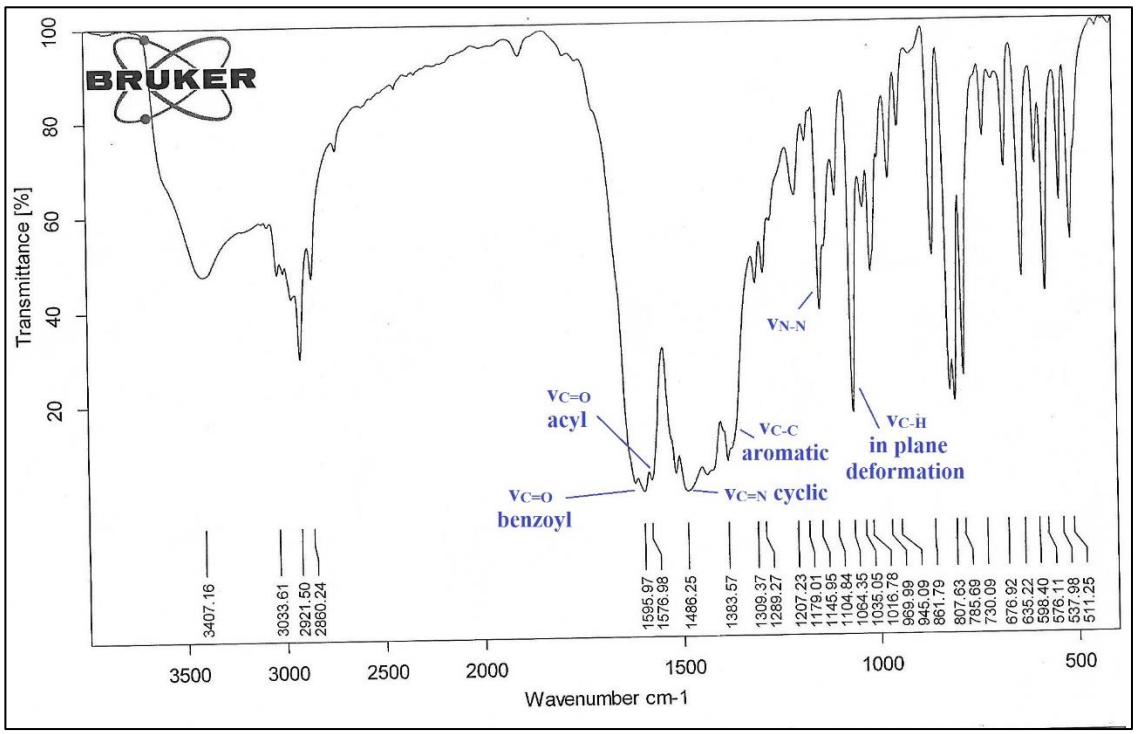

Figure 3b.6 FTIR spectrum of complex 11.

3b.3.2 Thermogravimetric analysis

Complexes were submitted for a thermal examination as the thermal stability of luminescent lanthanide complexes is an important factor in their use in photonics applications [9]. The TGA shows two degradation steps for complexes 9, 10, and 11, respectively, with overall mass losses of 56.1%, 49.6%, and 71.69%. The final substance, Nd_2O_3, is left behind. The first stage of degradation with mass loss of 15.7% for 9, 10.2% for 10, and 28.42% for 11 complexes in the 50-150 °C temperature range involve the loss of hydrated water or a coordinated solvent; however, actual complex degradation happens above their melting points [10]. The second stage of degradation, with mass loss of 40.4% for 9, 39.4% for 10, and 43.27% for 11 complexes in the 400-450 °C temperature range, is due to the removal of three acylpyrazolone units. Maximum loss for complexes 9, 10, and 11 is represented by the DTG curve at 424.3, 434.8, and 427.3 °C, respectively. Figures 3b.7–3b.9 contains all thermogravimetric curves.

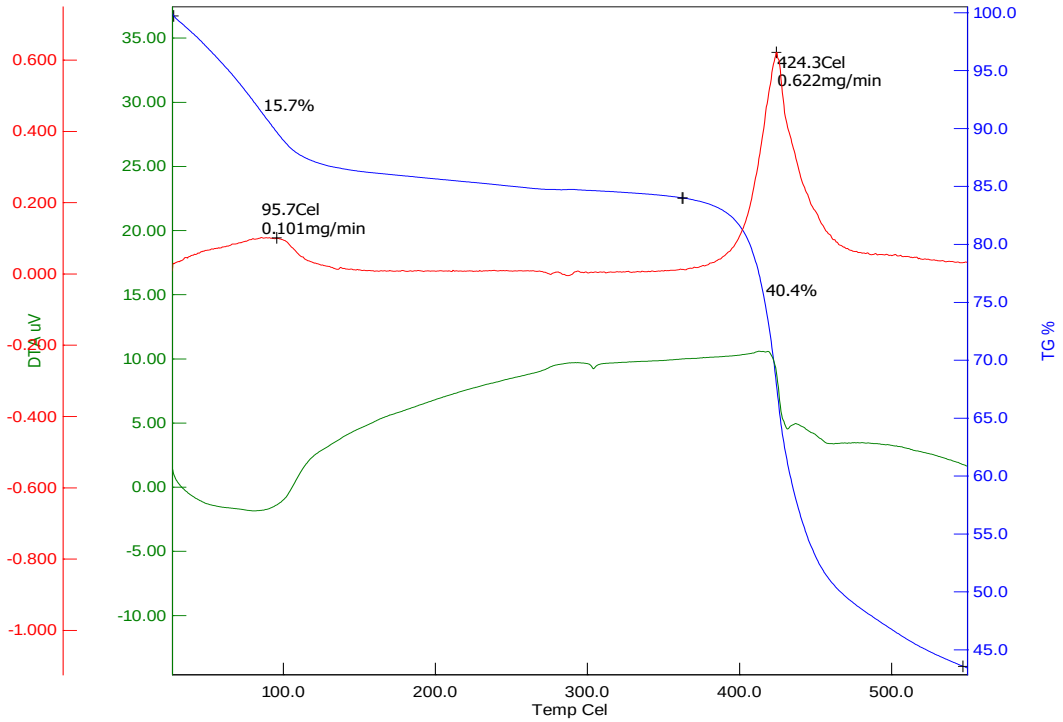

Figure 3b.7 Thermogravimetric curve of complex 9.

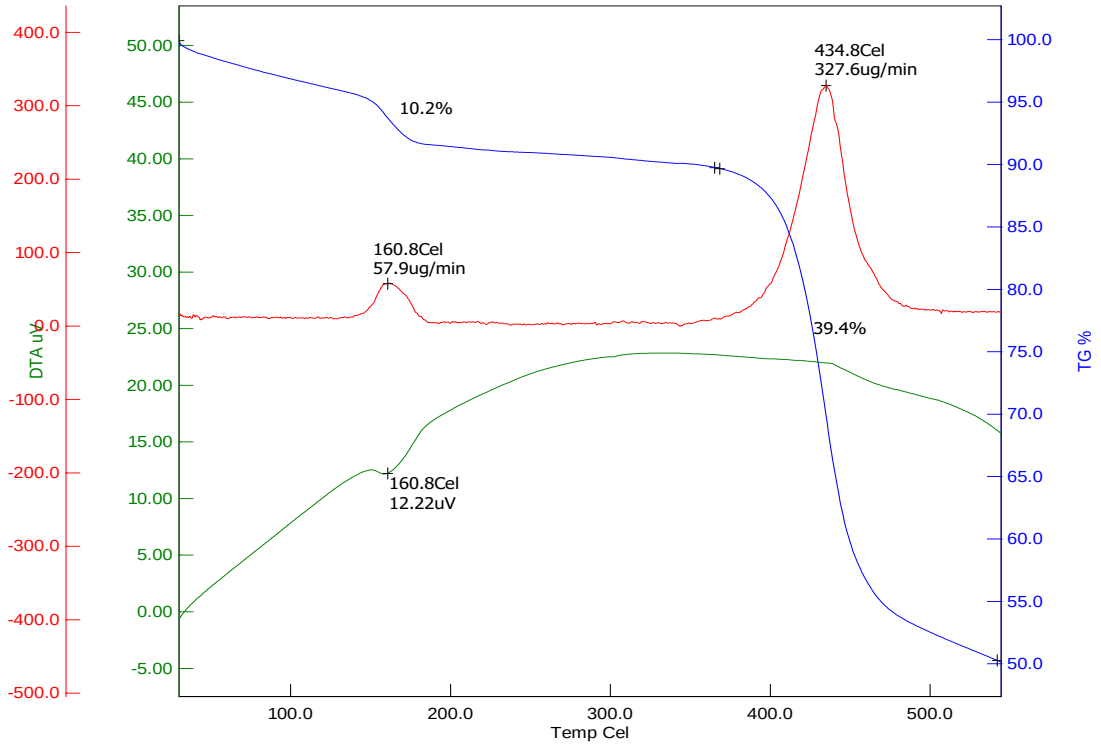

Figure 3b.8 Thermogravimetric curve of complex 10.

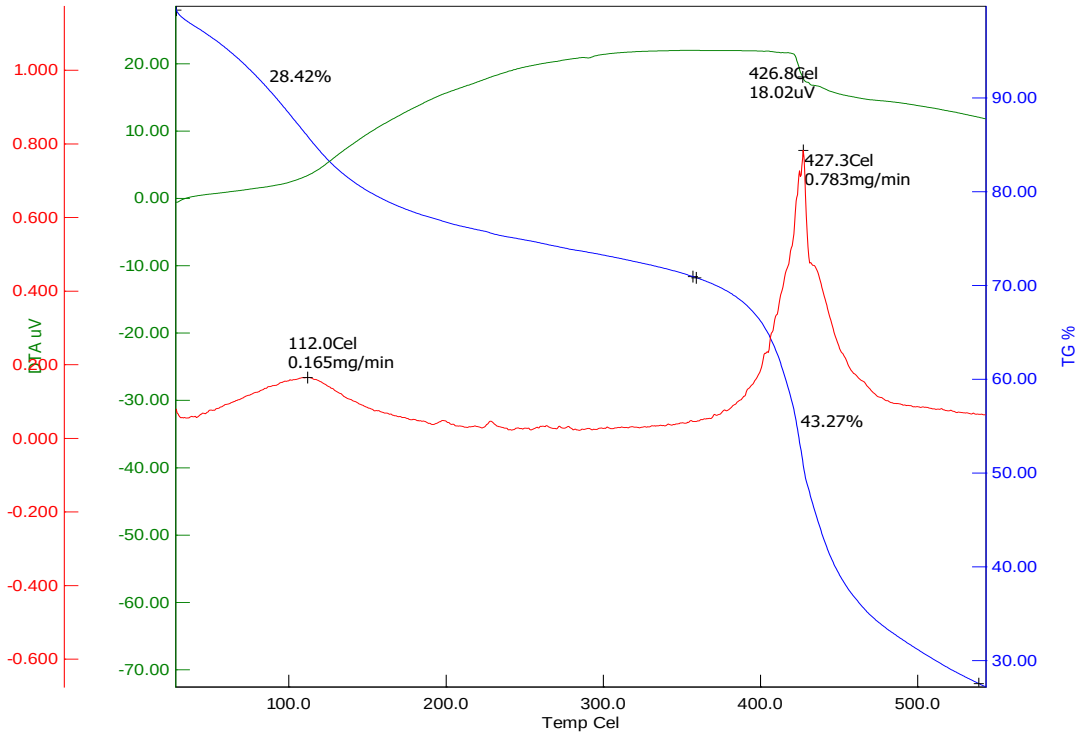

Figure 3b.9 Thermogravimetric curve of complex 11.

3b.3.3 Single crystal X-ray diffraction analysis

Through slow evaporation technique, bright pale-yellow prism-type crystals of complex 10 were obtained. Attempts to get x-ray quality crystals of complexes 9 and 11 were proved futile. After receiving the pale yellow prismatic single crystals necessary for X-ray measurement, solid-state X-ray diffraction was used to ascertain the structure of complex 10. Like the reports of the neodymium acylpyrazolone complexes [11–17], the mononuclear complex 10 features an eight-coordinated core Nd(III) ion, which is surrounded by six L^5 ligand O-atoms (O1, O2, O3, O4, O5, and O6), one O-atom (O1w) of water, and one O-atom (O7) of ethanol. Around the centre Nd(III) ion, the eight O-atoms organize into a warped square-antiprism coordination polyhedron and complex crystallized in the $P\,{-}1$ space group of the triclinic system (See Figure 3b.10(a) and 3b.10(b)). Complex 10 stabilises in the arrangement shown in Figure 3b.10(c) out of several feasible arrangements, as indicated in the Marchetti review [2]. The crystal packing of the complex satisfies the criteria of low energy movement between metal ions because the Nd-Nd distance is 12.3007(6) Å [18]. Three L^5 ligands come into contact with the central neodymium ion as bidentate ligands, forming three chelating rings [19,20]. The top plane can be formed by joining O1W of coordinating water, O7 of coordinating ethanol, O1 of the first ligand's pyrazolone moiety, and O5 of the second ligand's pyrazolone moiety. Similarly, the bottom plane can be formed by joining O2 of the first ligand's pyrazolone moiety, O6 of the second ligand's pyrazolone moiety, and O3, O4 atoms of the third acylpyrazolone ligand. For only one L^5 ligand, it’s both O3 and O4 atoms lie in the bottom plane.

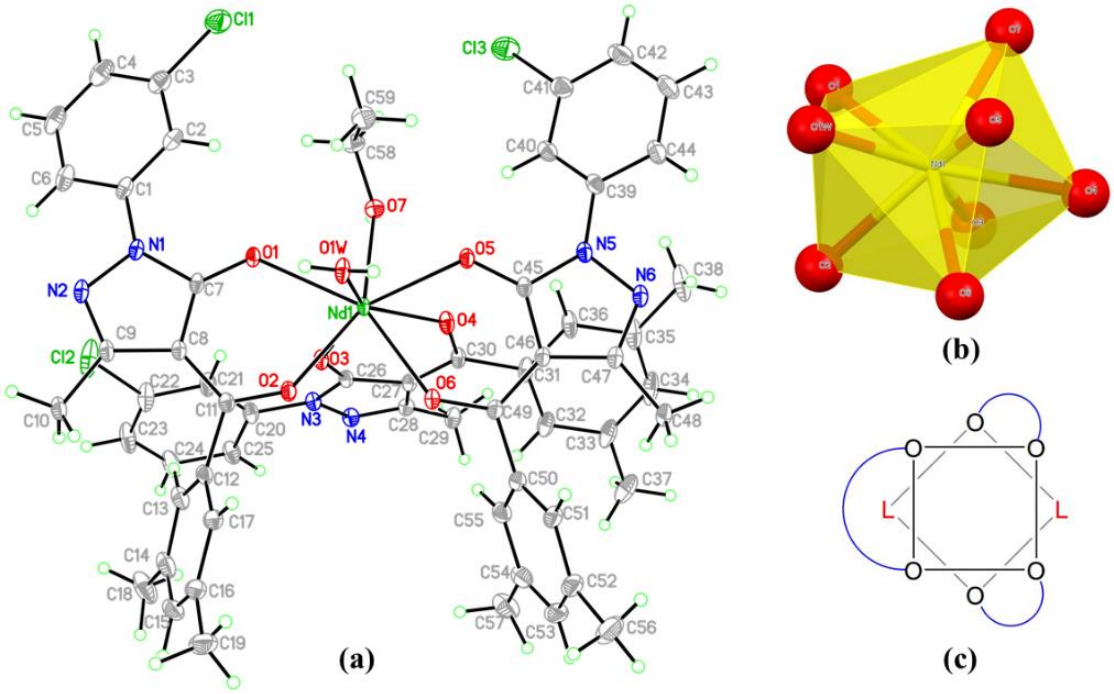

Figure 3b.10 (a) ORTEP illustration of complex 10 with 50% ellipsoid probability, **(b)** Polyhedral style presentation, and **(c)** square antiprism arrangement.

Table 3b.2 contains an overview of the crystallographic information as well as refinement information, while Table 3b.3 lists the chosen bond lengths and bond angles. Distortion in square antiprism is created as O7, O1W atoms are slightly above the upper plane, while O1, O5 atoms are slightly below and on the opposite side, O3, O6 atoms are slightly below the bottom plane, while O2, O4 atoms are slightly below. The lengths of the C(11)–O(2), C(30)–O(4), and C(49)–O(6) bonds in the acyl group are 1.253(2) Å, 1.251(3) Å, and 1.262(3) Å, respectively, that is slightly higher than typical for C–O distance in ketones [21] (1.23 Å) due to O→Nd bonding. In comparison to Nd-O(acyl) bond lengths (2.4061-2.4363), Nd-O(pyrazolone) bond lengths (2.4240-2.4474) are slightly higher, indicating stronger covalency caused by the acyl group O-atoms. This is because longer bonds lead to a drop in the average bond order between neodymium and O-atoms, increasing covalency. The greatest bond lengths are seen in the Nd-O1W (2.4792(15) Å) and Nd-O7 (2.5086(16) Å) bonds, which demonstrate weaker covalency with solvents compared to acylpyrazolone covalent binding and the influence of solvent on the covalent character of the complex. The L^5 ligands form stable six-membered rings when they coordinate to the neodymium ion in its enol state; the sum of the internal angles for the three ligands is, respectively, 715.85, 711.95, and 714.81°. These angles are very near 720°, indicating that the six-membered rings are almost planar. Figure 3b.11 depicts how complex units are organized and packed to

maintain stability due to interactions between 3,5-dimethyl benzoyl rings at 3.407 Å [22]. As shown in Table 3b.4, the NdO_8 polyhedron is structurally linked to one another by O-H···N hydrogen bonds that have various symmetry transformations and span a distance from 1.934 – 2.054 Å. The hydrogen bonds are formed between the H-atoms in water and ethanol molecules and the ligand's N-atoms. C-H···O interactions between methyl's H atoms and nearby N atoms, with an H···O distance range of 2.30-2.63 Å, also contribute to the crystal's improved resilience.

Table 3b.2 Crystallographic structural refinement for complex 10.

Code	Complex 10
CCDC number	2254186
Empirical formula	$C_{59}H_{56}Cl_3N_6NdO_8$
Formula weight	1227.68
Temperature	100(2) K
Wavelength	0.71073 Å
Crystal system	Triclinic
Space group	*P –1*
Unit cell dimensions	a = 14.2667(7) Å, b = 14.8966(8) Å, c = 15.6583(7) Å, α = 100.141(2)°, β = 108.461(2)°, γ =114.086(2)°
Volume	2696.7(2) $Å^3$
Z	2
Density (calculated)	1.512 Mg/m^3
Absorption coefficient	1.174 mm^{-1}
F(000)	1254
Final R indices [I>2sigma(I)]	R_1 = 0.0396, wR_2 = 0.0874
R indices (all data)	R_1 = 0.0558, wR_2 = 0.0968
Theta range for data collection	2.35 to 32.92°.
Index ranges	$-22 \leq h \leq 22$, $-23 \leq k \leq 23$, $-21 \leq l \leq 24$
Reflection collected	140101
Independent reflections	20662 [$R_{(int)}$ = 0.0804]
Completeness to theta = 25.242°	99.8 %
Absorption correction	None
Refinement method	Full-matrix least-squares on F^2
Goodness-of-fit on F^2	1.047
Data / restraints / parameters	20662 / 4 / 717

Table 3b.3 Selected bond lengths(Å) and bond angles(°) in complex 10.

Atoms	Bond lengths	Atoms	Bond angles	Atoms	Bond angles
Nd(1)-O(6)	2.4061(17)	O(6)-Nd(1)-O(2)	72.81(5)	O(6)-Nd(1)-O(3)	95.69(6)
Nd(1)-O(2)	2.4142(16)	O(2)-Nd(1)-O(3)	75.32(5)	O(2)-Nd(1)-O(4)	126.53(6)
Nd(1)-O(3)	2.4246(15)	O(3)-Nd(1)-O(4)	69.29(5)	O(5)-Nd(1)-O(1)	127.44(5)
Nd(1)-O(5)	2.4295(15)	O(6)-Nd(1)-O(4)	72.31(6)	O(1W)-Nd(1)-O(7)	109.56(6)
Nd(1)-O(4)	2.4363(16)	O(1)-Nd(1)-O(7)	75.43(5)	O(2)-Nd(1)-O(1)	73.93(5)
Nd(1)-O(1)	2.4474(15)	O(1)-Nd(1)-O(1W)	75.09(5)	O(3)-Nd(1)-O(1)	81.33(5)
Nd(1)-O(1W)	2.4792(15)	O(5)-Nd(1)-O(1W)	70.98(5)	O(5)-Nd(1)-O(4)	73.24(5)
Nd(1)-O(7)	2.5086(16)	O(5)-Nd(1)-O(7)	79.58(5)	O(6)-Nd(1)-O(5)	73.17(5)

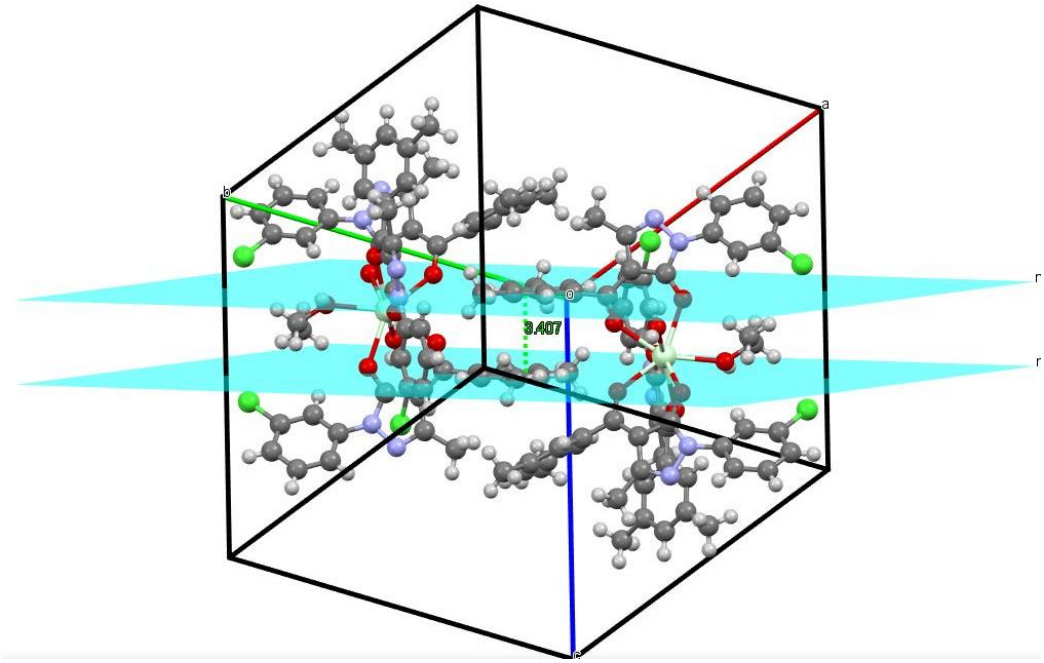

Figure 3b.11 The packing arrangement between complex units.

Table 3b.4 Hydrogen bonds for Complex 10 [Å and °].

D-H···A	d(D-H)	d(H···A)	d(D···A)	<(DHA)
O(7)-H(7O)...N(4)#1	0.818(18)	1.934(19)	2.745(2)	171(4)
O(1W)-H(1W1)...N(2)#2	0.826(17)	2.025(17)	2.845(2)	172(3)
O(1W)-H(1W2)...N(6)#3	0.815(17)	2.054(17)	2.869(2)	177(3)
C(2)-H(2A)...O(1)	0.95	2.38	2.928(3)	116.3
C(21)-H(21A)...O(3)	0.95	2.30	2.894(3)	120.3
C(29)-H(29A)...O(1)#1	0.98	2.63	3.565(3)	160.6
C(40)-H(40A)...O(5)	0.95	2.45	2.968(3)	113.8

Symmetry transformations used to generate equivalent atoms:
#1 -x+1,-y,-z+1 #2 -x+2,-y+1,-z+1 #3 -x+2,-y+1,-z+2

Bright pale-yellow prism-type crystals of the complex 10 were obtained through a slow evaporation technique. Attempts to get x-ray quality crystals of complexes 9 and 11 proved futile. Therefore, a simulated pattern was obtained for complex 10 from the single crystal data, and the same was compared with the pattern obtained experimentally from the powder XRD experiment. The simulated pattern matches well with the experimental pattern for all three complexes, as shown in Figure 3b.12. This confirms that all the complexes have similar geometry and structure. This also ensures the structure obtained from a single crystal represents the bulk of the complexes. In the XRD graph, a sharp band is observed with maxima in the range 2θ = 5 to 10°, indicating that the complexes are crystalline.

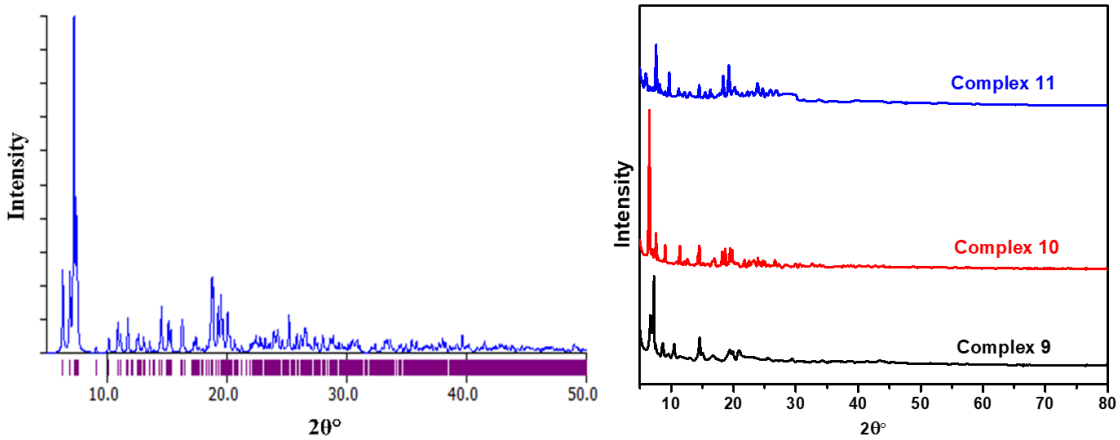

Figure 3b.12 Comparison between (a) simulated powder XRD pattern for complex 10 crystal and (b) experimental powder XRD patterns for complexes 9, 10, and 11.

3b.3.4 Hirshfeld surface area analysis

The Crystal Explorer 17.5 program was used to conduct a Hirshfeld surface study to illustrate the various interactions in a crystal structure [23,24]. The crystal of complex 10 is used to create HS, which is subsequently mapped by applying the d_{norm}, corresponding to the exterior and interior distances (de and di) and the van der Waals (vdW) radii of atoms. Figure 3b.13 explains the 2D-FP plot and 3D d_{norm}, di, de, curvedness, shape index, and fragment patch surfaces. H-bonding is indicated by red dots on d_{norm} HS. The total number of HS interactions with nearby complex 10 molecules (NBs) is depicted in a 2D-FP plot, with the interactions $H_{(HS)}\cdots H_{(NBs)}$, $H_{(HS)}\cdots All_{(NBs)}$, and $All_{(HS)}\cdots H_{(NBs)}$ showing the most frequent interactions, contributing respectively 54.6, 72.2, and 75.5%. Because of the tremendous amount of carbon and hydrogen in the HS, C···H contacts make up 9.7 % of the entire HS region

and are the next most prevalent contacts [25]. All these interactions are represented graphically in Figure 3b.14. All necessary 2d-FP graphs are shown in Figure 3b.15. The curvy area of the curvedness map located amid the phenyl rings suggests π-π stacking, which boosts the strength of the lattice together with red dots in d_{norm} [26]. Neodymium displays no further interactions with the adjacent molecules, as evidenced by the absence of Nd-all, all-Nd, or Nd-Nd contacts in the complex. According to shape-index maps, the concave appearance of O-atoms of ligands has manifested as an opaque orange tint having lower than zero shape-index value, providing proof of coordination interactions.

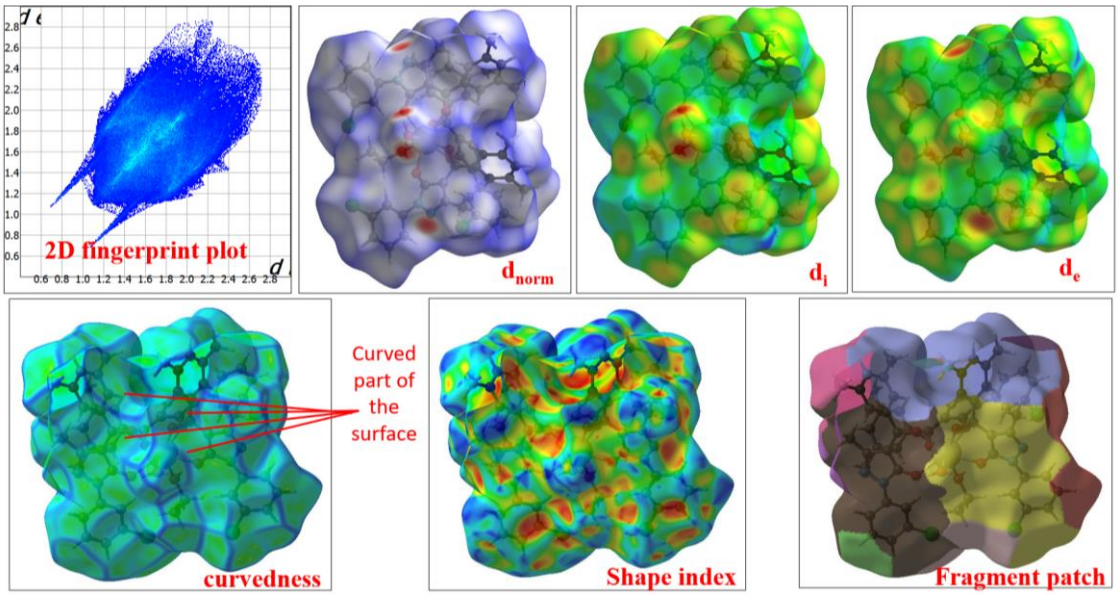

Figure 3b.13 2D-FP plot and 3D d_{norm}, d_i, d_e, curvedness, shape index, and fragment patch surfaces for complex 10.

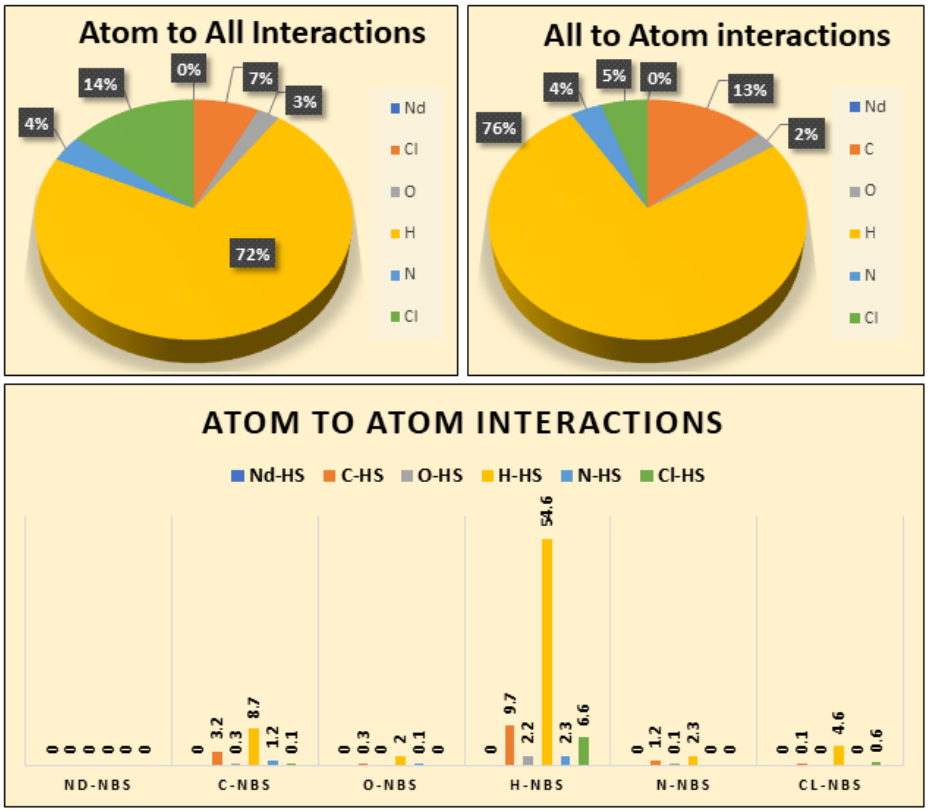

Figure 3b.14 Graphical presentation of Hirshfeld Percentage interactions.

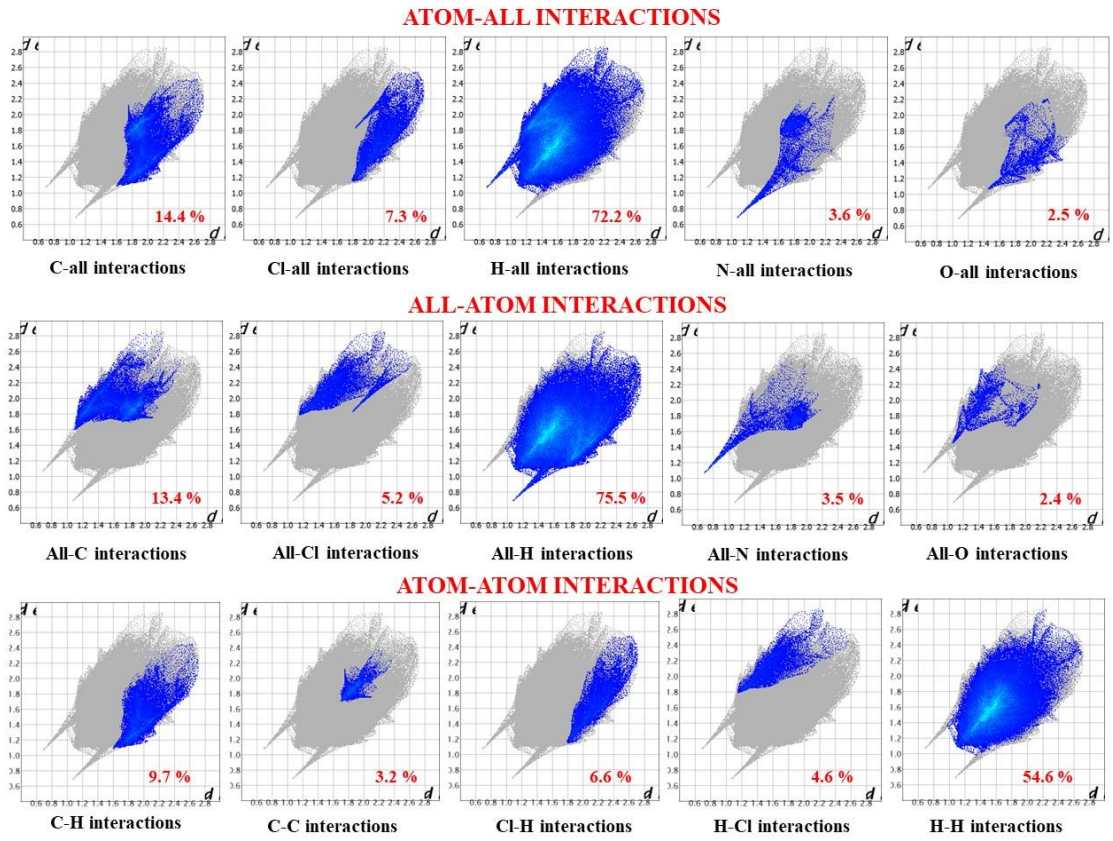

Figure 3b.15 2D Fingerprint map for complex 10.

3b.3.5 Optical transition property

All three of the synthesized compounds are soluble in various solvents, and the electronic spectra of 10^{-2} M solution of these complexes were captured in the acetonitrile, ethanol, nitrobenzene, pyridine, DMF, and DMSO solvents. The outcomes of the *4f-4f* electronic spectra and oscillator strength measurements of the complexes in various solvents, as well as for hexa-hydrated $Ln(NO_3)_3$ in water, are shown in Figure 3b.16 and Table 3b.5, respectively. With their quick solvent transfer rate and remarkably low crystal field stabilisation energy, lanthanoid complexes can achieve more excellent coordination geometries [27,28]. Complexes in the visible wavelengths display frequent parity-forbidden whittle *4f-4f* bands that travel through the $^4I_{9/2}$ ground state to the distinct excited states of the Nd(III) ion [29]. The transitions observed are $^4F_{3/2} \leftarrow {}^4I_{9/2}$, $^4F_{5/2} \leftarrow {}^4I_{9/2}$, $^4F_{7/2} \leftarrow {}^4I_{9/2}$, $^4F_{9/2} \leftarrow {}^4I_{9/2}$, $^4G_{5/2} \leftarrow {}^4I_{9/2}$, $^4G_{7/2} \leftarrow {}^4I_{9/2}$, and $^4G_{9/2} \leftarrow {}^4I_{9/2}$. The spectral strength of the absorption band is described by oscillator strengths (P) [30], which have been experimentally connected to the integral area of the absorption band and can be written as

$$P = 4.31 \times 10^{-9} \left[\frac{9\eta}{(\eta^2+2)^2}\right] \int \varepsilon_{max}(\bar{\nu})d\bar{\nu} \qquad (1)$$

Where, $\varepsilon_{max} = \frac{Absorbance\ (A)}{Concentration\ (c) \times \text{path length of the cell in cm (b = 1 cm)}}$, ν is the transition wavenumber, η is the Refractive index. The refractive index value can be identified from the band gap energy value using Tauc's equation [31,32]. After getting the value of band gap energy (E_g) using Tauc's equation [31,32], the refractive index is calculated using the relation [32]

$$\frac{(n^2-1)}{(n^2+1)} = 1 - \sqrt{\frac{E_g}{20}} \qquad (2)$$

With consideration to the Nd(III) transitions that have been studied, the $^4G_{5/2}$, $^4G_{7/2} \leftarrow {}^4I_{9/2}$ pair's absorption intensity, which is close to the visible region's centre (17857-18690 cm^{-1}), exhibits a distinctive sensitivity to the ligand environment surrounding the neodymium ion and consequently serves as an appropriate ion over research using visible absorption spectroscopy [33–36]. Both transitions are identified as being hypersensitive according to the electric quadrupolar selection ($\Delta J \leq 2$, $\Delta L \leq 2$, $\Delta S=0$) principles [37,38]. The transitions $^4F_{3/2} \leftarrow {}^4I_{9/2}$, $^4F_{5/2} \leftarrow {}^4I_{9/2}$, and $^4F_{7/2} \leftarrow {}^4I_{9/2}$ of Nd(III) are referred to as pseudohypersentive transitions because, while not adhering to the

selection criterion for hypersensitive transitions, it has been discovered that they demonstrate significant sensitivity in the complexes.

Moving from the $Nd^{3+}_{aqua-ion}$ to the complex across all of the used solvents raises the oscillator strength of $^4G_{5/2} \leftarrow {}^4I_{9/2}$ transition by a factor of 4 to 6 times (hypersensitive). During the formation of different solutions, ethanol and water will be replaced by the added solvents. For all the complexes in Table 3b.5, the intensification is typically observed in the following order: DMF > DMSO > Pyridine > Ethanol > Acetonitrile > Nitrobenzene. The intensity of the *4f-4f* electric dipole is particularly well-promoted by DMF in all three complexes due to strong coordination, which is responsible for more distinct and intense hypersensitive peaks, and the outcome is different from the reported complexes [29]. These highest values in DMF result from the Nd(III)-ion's strong coordination, which increases bond covalency and oscillator strength. Additionally, in three solvents with strong coordination (pyridine, DMF, DMSO), three complexes exhibit the sequence 9 > 10 > 11. Complex 9 exhibits less molecular symmetry and higher covalency than the other two complexes due to the L^4 ligand's increased polarizable interaction with the Nd(III)-ion, as seen by the bigger values of oscillator strengths for complex 9.

It has been utilized to qualitatively identify symmetry using both the band shape and strength of the hypersensitive transition [29]. The same band shapes of all hypersensitivity transitions consistently suggest the eight-coordination geometry. Hypersensitive peaks are becoming more distinct and intense in the band morphologies of DMF and DMSO. Asymmetries are increased by the strong coordinating nature of these solvents, which raises oscillator strength.

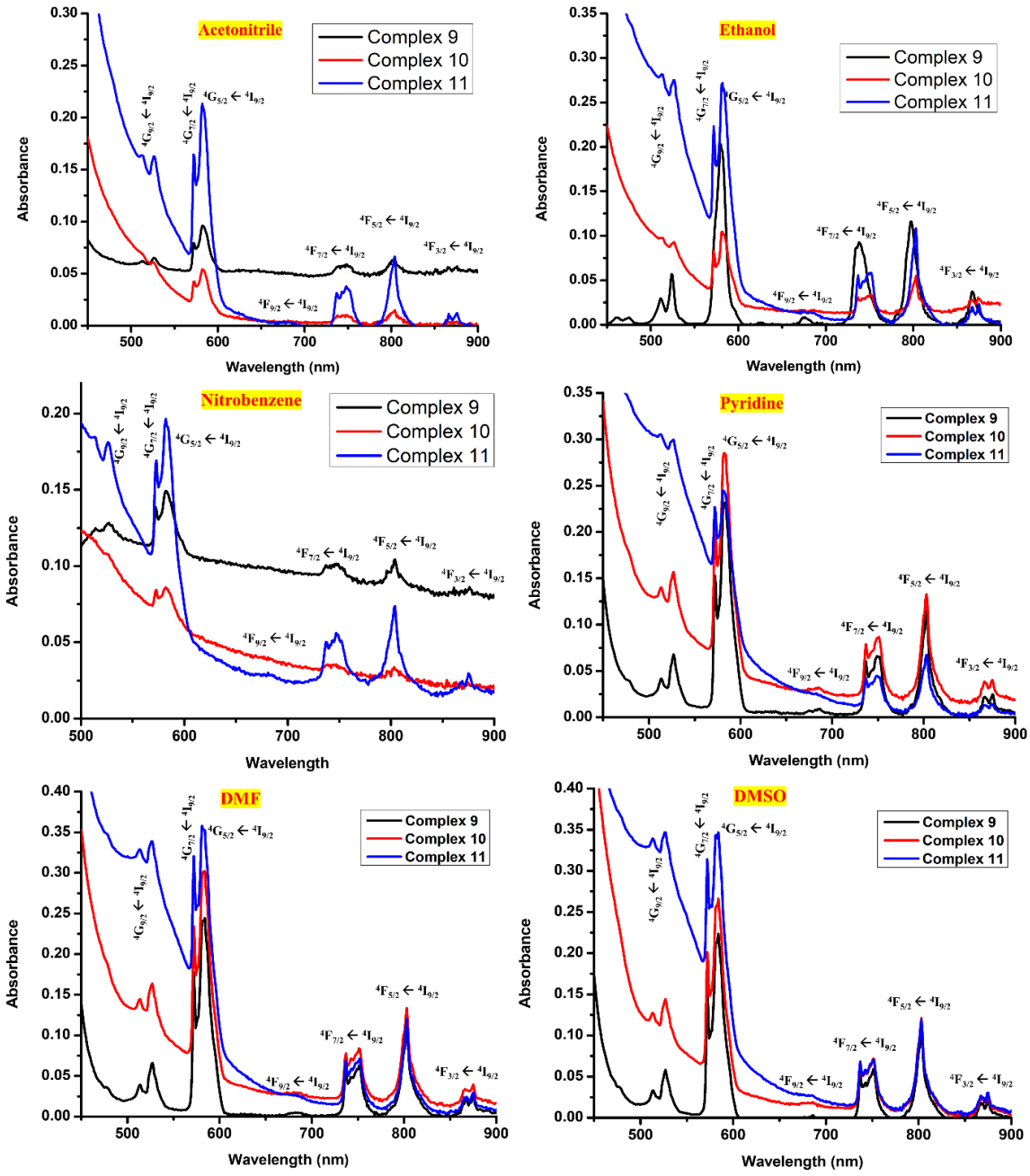

Figure 3b.16 4f-4f electronic spectra of complexes 9, 10, and 11 in various solvents.

Table 3b.5 Oscillator strength measurements of complexes 9, 10, and 11 in various solvents, as well as for hexa-hydrated $Ln(NO_3)_3$ in water.

Transitions	Spectra ranges (cm^{-1})[a]	Nd^{3+} aqua ion ($P \times 10^{-6}$)	Oscillator Strength $P \times 10^{-6}$ in different solvents					
			A	B	C	D	E	F
Complex 9								
$^4F_{3/2} \leftarrow {}^4I_{9/2}$	11628-11494	1.24	0.15	2.36	0.08	1.86	1.61	2.05
$^4F_{5/2} \leftarrow {}^4I_{9/2}$	12821-12048	7.08	1.27	12.58	1.13	10.12	9.42	9.47
$^4F_{7/2} \leftarrow {}^4I_{9/2}$	13793-12987	7.35	1.51	13.75	1.32	9.43	8.85	8.64
$^4F_{9/2} \leftarrow {}^4I_{9/2}$	15385-14286	0.11	0.04	0.8	0.029	0.22	0.0014	0.18
$^4G_{5/2} \leftarrow {}^4I_{9/2}$	17857-17390	8.37	9.26	37.21	8.71	49.78	53.76	48.16
$^4G_{7/2} \leftarrow {}^4I_{9/2}$	19230-18690	4.53	0.86	4.4	1.03	5.68	5.27	5.34
$^4G_{9/2} \leftarrow {}^4I_{9/2}$	19802-19230	0.45	0.19	2.14	0.23	0.98	0.79	1.01
Complex 10								
$^4F_{3/2} \leftarrow {}^4I_{9/2}$	11628-11494	1.24	0.11	0.59	0.022	1.79	1.89	2.12
$^4F_{5/2} \leftarrow {}^4I_{9/2}$	12821-12048	7.08	1.19	3.01	0.31	10.23	10.16	9.46
$^4F_{7/2} \leftarrow {}^4I_{9/2}$	13793-12987	7.35	1.21	2.71	0.59	9.67	9.41	8.74
$^4F_{9/2} \leftarrow {}^4I_{9/2}$	15385-14286	0.11	0.075	0.15	0.26	0.51	0.083	0.68
$^4G_{5/2} \leftarrow {}^4I_{9/2}$	17857-17390	8.37	7.34	14.89	3.85	49.26	53.23	46.09
$^4G_{7/2} \leftarrow {}^4I_{9/2}$	19230-18690	4.53	0.42	1.002	0.39	5.53	6.06	5.24
$^4G_{9/2} \leftarrow {}^4I_{9/2}$	19802-19230	0.45	0.33	0.3	0.58	0.96	0.94	1.12
Complex 11								
$^4F_{3/2} \leftarrow {}^4I_{9/2}$	11628-11494	1.24	1.52	1.56	0.66	1.03	1.502	1.64
$^4F_{5/2} \leftarrow {}^4I_{9/2}$	12821-12048	7.08	9.36	9.77	5.26	5.87	8.55	9.43
$^4F_{7/2} \leftarrow {}^4I_{9/2}$	13793-12987	7.35	6.53	8.32	5.51	5.102	8.07	8.29
$^4F_{9/2} \leftarrow {}^4I_{9/2}$	15385-14286	0.11	0.76	0.099	0.18	0.016	0.05	0.07
$^4G_{5/2} \leftarrow {}^4I_{9/2}$	17857-17390	8.37	35.35	39.71	24.72	25.74	48.21	43.96
$^4G_{7/2} \leftarrow {}^4I_{9/2}$	19230-18690	4.53	3.48	5.75	3.06	3.08	7.23	6.87
$^4G_{9/2} \leftarrow {}^4I_{9/2}$	19802-19230	0.45	0.702	0.96	1.81	1.48	1.37	1.35

A = Acetonitrile, B = Ethanol, C = Nitrobenzene, D = Pyridine, E = DMF, F = DMSO

[a]The values presented here are merely intended to provide an indication of the general position since the spectral ranges reported for the transition vary from solvent to solvent.

The Judd-Ofelt parameters (Ω_2, Ω_4, Ω_6) can be described by the following equation [39]

$$f_{ed} = \frac{8\pi^2 mc\sigma}{3h(2J+1)} \cdot x \sum_{\lambda=2,4,6} \Omega_\lambda \left|\langle a \| U^\lambda \| b \rangle\right|^2 \quad (3)$$

Where m is electron mass, c is the speed of light, h is Planck's constant and x is the field correction factor $\left(x = \frac{(n^2+2)^2}{9n}\right)$, n is the refractive index, σ is the transition's wavenumber, and 2J+1 is the degeneracy of $|a\rangle$.

Judd-Ofelt parameters have been identified (see Table 3b.6) for all synthesised compounds using the least square approach using $\left|\langle a\|U^{\lambda}\|b\rangle\right|^2$ values from the Carnall publication [30]. By Judd-Ofelt theory, the calculated value of oscillator strength (f_{cal}) was computed from initial (a) to excited state (b) transitions by applying equation (3). To find the accuracy of the fitting procedure, the root mean square deviation (δ_{rms}) of f_{exp} with respect to f_{cal} was calculated using formula given below.

$$\boldsymbol{\delta_{RMS}} = \sqrt{\frac{\Sigma(\boldsymbol{f_{exp}}-\boldsymbol{f_{calc}})^2}{\boldsymbol{M-3}}} \qquad (4)$$

The lower the root mean square deviation value, the better the fitting result. The comparative values of root mean square deviation (δ_{rms}) are given in Table 3b.6. The amplitude of Judd-Ofelt parameters Ω_λ (λ = 2, 4, 6) reflects the strengthening of *4f-4f* band transitions, particularly hypersensitive ($^4G_{5/2} \leftarrow {}^4I_{9/2}$) and pseudo hypersensitive transitions ($^4F_{5/2}$, $^4F_{7/2} \leftarrow {}^4I_{9/2}$). The oscillator strength and magnitude of Ω_2 increase with the increase in the nephelauxetic effect as covalency is introduced into the metal-ligand interaction. Ω_4 and Ω_6 can be used to indicate the oscillator strength for Nd(III) complexes; however, Ω_2 values can be used to show how solvent or ligand affects the intensity of a hypersensitive transition. Comparatively speaking to the Ω_2 parameter, the Ω_4 and Ω_6 parameters, which are connected to alterations in the symmetry characteristics of the complex species, are slightly influenced. The parameter Ω_4 is related to the electron density of the surrounding ligands, where an increase in Ω_4 parameter indicates a decreased electron density [40,41]. The relatively low value of the Ω_4 parameter indicates greater electron density on the ligands and a lower extent of charge transfer from the ligand to the Nd^{3+} ion. It has been found that the presence of specific solvents has a considerable impact on the Ω_4 and Ω_6 parameters [28]. As coordinating solvents enter the system, the degree of mixing between the $4f^n$ and *5d* orbitals changes, resulting in higher values of the Ω_6 parameter [28,42,43]. As a result, coordinating solvents have larger values of Ω_6 in Table 3b.6.

Table 3b.6 Judd-Ofelt intensity parameters and root mean square deviation for complexes 9, 10, and 11.

Complex			A	B	C	D	E	F
9	**J-O Parameter ($\Omega/10^{-20}$ cm^2)**	Ω_2	1.82	7.32	1.68	9.33	10.27	9.01
		Ω_4	0.16	1.00	0.08	0.11	0.13	0.31
		Ω_6	0.97	9.00	0.84	6.31	5.98	5.79
	δ_{RMS}		0.003	0.018	0.003	0.020	0.020	0.019
10	**J-O Parameter ($\Omega/10^{-20}$ cm^2)**	Ω_2	3.21	6.48	1.76	21.4	23.1	19.8
		Ω_4	0.32	0.26	0.12	0.13	0.44	0.69
		Ω_6	1.85	4.29	0.81	15	14.5	13.4
	δ_{RMS}		0.006	0.013	0.003	0.045	0.048	0.043
11	**J-O Parameter ($\Omega/10^{-20}$ cm^2)**	Ω_2	6.25	7.15	4.67	9.13	8.82	7.92
		Ω_4	0.61	0.54	0.12	0.62	0.68	0.83
		Ω_6	4.74	5.62	3.58	6.68	5.19	5.46
	δ_{RMS}		0.015	0.017	0.010	0.021	0.019	0.018

A = Acetonitrile, B = Ethanol, C = Nitrobenzene, D = Pyridine, E = DMF, F = DMSO

In order to demonstrate the covalency of complexes, equations (6) to (9) were used to compute the Nephelauxetic ratio (β), Sinha parameter (δ%), bonding parameter ($b^{1/2}$), and angular overlap parameter (η). In Nephelauxetic ratio calculation, $\bar{\nu}_{\text{complex}}$ and $\bar{\nu}_{\text{free ion}}$ was identified by taking peak centre values for all transitions in the absorption spectra of complexes. All covalency parameters are provided in Tables 3b.7-3b.10.

$$\text{Nephelauxetic ratio } \boldsymbol{\beta} = \frac{\bar{\nu}_{complex}}{\bar{\nu}_{free\ ion}} \quad (6)$$

$$\text{Sinha parameter } \boldsymbol{\delta}\% = \left[\frac{1-\beta}{\beta}\right] \times 100 \quad (7)$$

$$\text{Bonding parameter } b^{\frac{1}{2}} = \left(\frac{1-\beta}{2}\right)^{1/2} \quad (8)$$

$$\text{Angular overlap parameter } \boldsymbol{\eta} = \frac{1-\sqrt{\beta}}{\sqrt{\beta}} \quad (9)$$

Table 3b.7 Calculation of Nephelauxetic ratio β for complexes 9, 10, and 11.

Nephelauxetic ratio β					
Transitions	Acetonitrile	Ethanol	Pyridine	DMF	DMSO
Complex 9					
$^4F_{3/2} \leftarrow {}^4I_{9/2}$	0.9910	0.9998	0.9920	0.9928	0.9938
$^4F_{5/2} \leftarrow {}^4I_{9/2}$	0.9913	1.0000	0.9927	0.9946	0.9987
$^4F_{7/2} \leftarrow {}^4I_{9/2}$	0.9834	0.9997	0.9886	0.9910	0.9971
$^4F_{9/2} \leftarrow {}^4I_{9/2}$	1.0013	0.9987	0.9882	0.9953	0.9986
$^4G_{5/2} \leftarrow {}^4I_{9/2}$	0.9974	0.9996	0.9967	0.9972	0.9747
$^4G_{7/2} \leftarrow {}^4I_{9/2}$	0.9956	0.9998	0.9945	0.9944	0.9955
$^4G_{9/2} \leftarrow {}^4I_{9/2}$	0.9939	0.9996	0.9961	0.9971	0.9987
Complex 10					
$^4F_{3/2} \leftarrow {}^4I_{9/2}$	0.9930	0.9920	0.9923	0.9932	0.9935
$^4F_{5/2} \leftarrow {}^4I_{9/2}$	0.9912	0.9930	0.9929	0.9947	0.9986
$^4F_{7/2} \leftarrow {}^4I_{9/2}$	0.9844	0.9828	0.9874	0.9907	0.9979
$^4F_{9/2} \leftarrow {}^4I_{9/2}$	0.9910	0.9828	0.9895	0.9995	0.9996
$^4G_{5/2} \leftarrow {}^4I_{9/2}$	0.9974	0.9976	0.9972	0.9964	0.9744
$^4G_{7/2} \leftarrow {}^4I_{9/2}$	0.9975	0.9959	0.9947	0.9948	0.9954
$^4G_{9/2} \leftarrow {}^4I_{9/2}$	0.9825	0.9955	0.9966	0.9979	0.9994
Complex 11					
$^4F_{3/2} \leftarrow {}^4I_{9/2}$	0.9913	0.9913	0.9933	0.9928	0.9940
$^4F_{5/2} \leftarrow {}^4I_{9/2}$	0.9915	0.9929	0.9920	0.9946	0.9982
$^4F_{7/2} \leftarrow {}^4I_{9/2}$	0.9840	0.9829	0.9888	0.9904	0.9974
$^4F_{9/2} \leftarrow {}^4I_{9/2}$	0.9916	0.9894	0.9925	0.9917	0.9994
$^4G_{5/2} \leftarrow {}^4I_{9/2}$	0.9977	0.9965	0.9986	0.9998	0.9750
$^4G_{7/2} \leftarrow {}^4I_{9/2}$	0.9949	0.9954	0.9956	0.9953	0.9962
$^4G_{9/2} \leftarrow {}^4I_{9/2}$	0.9949	0.9964	0.9979	0.9981	0.9996

Table 3b.8 Calculation of Sinha Parameter δ for complexes 9, 10, and 11.

Sinha Parameter δ					
Transitions	Acetonitrile	Ethanol	Pyridine	DMF	DMSO
Complex 9					
$^4F_{3/2} \leftarrow {}^4I_{9/2}$	0.9121	0.0191	0.8079	0.7281	0.6288
$^4F_{5/2} \leftarrow {}^4I_{9/2}$	0.8732	0.0016	0.7339	0.5411	0.1301
$^4F_{7/2} \leftarrow {}^4I_{9/2}$	1.6891	0.0295	1.1570	0.9051	0.2886
$^4F_{9/2} \leftarrow {}^4I_{9/2}$	0.1281	0.1332	1.1981	0.4689	0.1379
$^4G_{5/2} \leftarrow {}^4I_{9/2}$	0.2560	0.0424	0.3304	0.2761	2.5993
$^4G_{7/2} \leftarrow {}^4I_{9/2}$	0.4421	0.0220	0.5560	0.5614	0.4570
$^4G_{9/2} \leftarrow {}^4I_{9/2}$	0.6170	0.0445	0.3950	0.2935	0.1264
Complex 10					
$^4F_{3/2} \leftarrow {}^4I_{9/2}$	0.7074	0.8063	0.7762	0.6805	0.6570
$^4F_{5/2} \leftarrow {}^4I_{9/2}$	0.8926	0.7009	0.7145	0.5363	0.1438
$^4F_{7/2} \leftarrow {}^4I_{9/2}$	1.5864	1.7522	1.2785	0.9437	0.2095
$^4F_{9/2} \leftarrow {}^4I_{9/2}$	0.9088	1.7455	1.0567	0.0531	0.0439
$^4G_{5/2} \leftarrow {}^4I_{9/2}$	0.2584	0.2425	0.2819	0.3583	2.6316
$^4G_{7/2} \leftarrow {}^4I_{9/2}$	0.2548	0.4116	0.5369	0.5243	0.4607
$^4G_{9/2} \leftarrow {}^4I_{9/2}$	1.7835	0.4478	0.3378	0.2131	0.0575
Complex 11					
$^4F_{3/2} \leftarrow {}^4I_{9/2}$	0.8732	0.8751	0.6775	0.7254	0.6024
$^4F_{5/2} \leftarrow {}^4I_{9/2}$	0.8586	0.7114	0.8027	0.5411	0.1759
$^4F_{7/2} \leftarrow {}^4I_{9/2}$	1.6282	1.7438	1.1290	0.9650	0.2645
$^4F_{9/2} \leftarrow {}^4I_{9/2}$	0.8477	1.0669	0.7515	0.8369	0.0610
$^4G_{5/2} \leftarrow {}^4I_{9/2}$	0.2292	0.3516	0.1379	0.0175	2.5598
$^4G_{7/2} \leftarrow {}^4I_{9/2}$	0.5167	0.4608	0.4453	0.4703	0.3786
$^4G_{9/2} \leftarrow {}^4I_{9/2}$	0.5095	0.3592	0.2138	0.1931	0.0385

Table 3b.9 Calculation of Bonding parameter $b^{1/2}$ for complexes 9, 10, and 11.

Bonding parameter $b^{1/2}$					
Transitions	Acetonitrile	Ethanol	Pyridine	DMF	DMSO
Complex 9					
$^4F_{3/2} \leftarrow {}^4I_{9/2}$	0.0672	0.0098	0.0633	0.0601	0.0559
$^4F_{5/2} \leftarrow {}^4I_{9/2}$	0.0658	0.0028	0.0604	0.0519	0.0255
$^4F_{7/2} \leftarrow {}^4I_{9/2}$	0.0911	0.0122	0.0756	0.0670	0.0379
$^4F_{9/2} \leftarrow {}^4I_{9/2}$	0.0253	0.0258	0.0769	0.0483	0.0262
$^4G_{5/2} \leftarrow {}^4I_{9/2}$	0.0357	0.0146	0.0406	0.0371	0.1125
$^4G_{7/2} \leftarrow {}^4I_{9/2}$	0.0469	0.0105	0.0526	0.0528	0.0477
$^4G_{9/2} \leftarrow {}^4I_{9/2}$	0.0554	0.0149	0.0444	0.0383	0.0251
Complex 10					
$^4F_{3/2} \leftarrow {}^4I_{9/2}$	0.0593	0.0632	0.0621	0.0581	0.0571
$^4F_{5/2} \leftarrow {}^4I_{9/2}$	0.0665	0.0590	0.0596	0.0516	0.0268
$^4F_{7/2} \leftarrow {}^4I_{9/2}$	0.0884	0.0928	0.0794	0.0684	0.0323
$^4F_{9/2} \leftarrow {}^4I_{9/2}$	0.0671	0.0926	0.0723	0.0163	0.0148
$^4G_{5/2} \leftarrow {}^4I_{9/2}$	0.0359	0.0348	0.0375	0.0422	0.1132
$^4G_{7/2} \leftarrow {}^4I_{9/2}$	0.0356	0.0453	0.0517	0.0511	0.0479
$^4G_{9/2} \leftarrow {}^4I_{9/2}$	0.0936	0.0472	0.0410	0.0326	0.0170
Complex 11					
$^4F_{3/2} \leftarrow {}^4I_{9/2}$	0.0658	0.0659	0.0580	0.0600	0.0547
$^4F_{5/2} \leftarrow {}^4I_{9/2}$	0.0652	0.0594	0.0631	0.0519	0.0296
$^4F_{7/2} \leftarrow {}^4I_{9/2}$	0.0895	0.0926	0.0747	0.0691	0.0363
$^4F_{9/2} \leftarrow {}^4I_{9/2}$	0.0648	0.0727	0.0611	0.0644	0.0175
$^4G_{5/2} \leftarrow {}^4I_{9/2}$	0.0338	0.0419	0.0262	0.0093	0.1117
$^4G_{7/2} \leftarrow {}^4I_{9/2}$	0.0507	0.0479	0.0471	0.0484	0.0434
$^4G_{9/2} \leftarrow {}^4I_{9/2}$	0.0503	0.0423	0.0327	0.0310	0.0139

Table 3b.10 Calculation of Angular Overlap parameter η for complexes 9, 10, and 11.

Angular Overlap parameter η					
Transitions	Acetonitrile	Ethanol	Pyridine	DMF	DMSO
Complex 9					
$^4F_{3/2} \leftarrow {}^4I_{9/2}$	0.0046	0.0001	0.0040	0.0036	0.0031
$^4F_{5/2} \leftarrow {}^4I_{9/2}$	0.0044	0.0000	0.0037	0.0027	0.0007
$^4F_{7/2} \leftarrow {}^4I_{9/2}$	0.0084	0.0001	0.0058	0.0045	0.0014
$^4F_{9/2} \leftarrow {}^4I_{9/2}$	0.0006	0.0007	0.0060	0.0023	0.0007
$^4G_{5/2} \leftarrow {}^4I_{9/2}$	0.0013	0.0002	0.0017	0.0014	0.0129
$^4G_{7/2} \leftarrow {}^4I_{9/2}$	0.0022	0.0001	0.0028	0.0028	0.0023
$^4G_{9/2} \leftarrow {}^4I_{9/2}$	0.0031	0.0002	0.0020	0.0015	0.0006
Complex 10					
$^4F_{3/2} \leftarrow {}^4I_{9/2}$	0.0035	0.0040	0.0039	0.0034	0.0033
$^4F_{5/2} \leftarrow {}^4I_{9/2}$	0.0045	0.0035	0.0036	0.0027	0.0007
$^4F_{7/2} \leftarrow {}^4I_{9/2}$	0.0079	0.0087	0.0064	0.0047	0.0010
$^4F_{9/2} \leftarrow {}^4I_{9/2}$	0.0045	0.0087	0.0053	0.0003	0.0002
$^4G_{5/2} \leftarrow {}^4I_{9/2}$	0.0013	0.0012	0.0014	0.0018	0.0131
$^4G_{7/2} \leftarrow {}^4I_{9/2}$	0.0013	0.0021	0.0027	0.0026	0.0023
$^4G_{9/2} \leftarrow {}^4I_{9/2}$	0.0089	0.0022	0.0017	0.0011	0.0003
Complex 11					
$^4F_{3/2} \leftarrow {}^4I_{9/2}$	0.0044	0.0044	0.0034	0.0036	0.0030
$^4F_{5/2} \leftarrow {}^4I_{9/2}$	0.0043	0.0036	0.0040	0.0027	0.0009
$^4F_{7/2} \leftarrow {}^4I_{9/2}$	0.0081	0.0087	0.0056	0.0048	0.0013
$^4F_{9/2} \leftarrow {}^4I_{9/2}$	0.0042	0.0053	0.0038	0.0042	0.0003
$^4G_{5/2} \leftarrow {}^4I_{9/2}$	0.0011	0.0018	0.0007	0.0001	0.0127
$^4G_{7/2} \leftarrow {}^4I_{9/2}$	0.0026	0.0023	0.0022	0.0023	0.0019
$^4G_{9/2} \leftarrow {}^4I_{9/2}$	0.0025	0.0018	0.0011	0.0010	0.0002

Positive numbers of the bonding parameter and minimal alteration imply covalent bonding through limited participation of *4f*-orbitals in synthesised complexes in all the solvents where the nephelauxetic effect values lie between 0.9743 to 1.001. The Sinha parameter (δ%) values and angular overlap parameter (η) values, which both demonstrate electron delocalisation across *4f* orbital as well as covalency, have been identified to be positive for all complexes, indicating a similar extent of covalent bonding as would be expected given the similar coordination number [28,44,45].

Figure 3b.17 shows a spectrum analysis of these recently synthesized compounds employing solid-state emission spectra ($\lambda_{excited}$ = 290 nm) and electronic absorption in a 10^{-6} M ethanolic solution at room temperature. When measured at the wavelengths listed in Table 3b.11, all three complexes, 9, 10, and 11, exhibit electronic n→π*, π→π*, and LMCT transitions. Furthermore, all three complexes show three emission peaks. The emission of light from $^{2}D_{3/2}$, $^{2}H_{11/2}$→$^{4}I_{9/2}$ is what causes the emission peaks that are seen at wavelengths of 330 (complex 9), 329.4 (complex 10), and 330.3 (complex 11) nm. Similarly, peaks at 467.3 (complex 9), 467.7 (complex 10), and 468.5 (complex 11) nm indicate $^{4}G_{11/2}$→$^{4}I_{9/2}$ transition, while those at 493.4 (complex 9), 494.2 (complex 10), and 493.4 (complex 11) nm indicates $^{4}G_{7/2}$→$^{4}I_{9/2}$ transition. The results of the analysis of absorption and emission spectrum peak are shown in Table 3b.11 [46]. In all these neodymium compounds, a small vibrational shifting is observed [46].

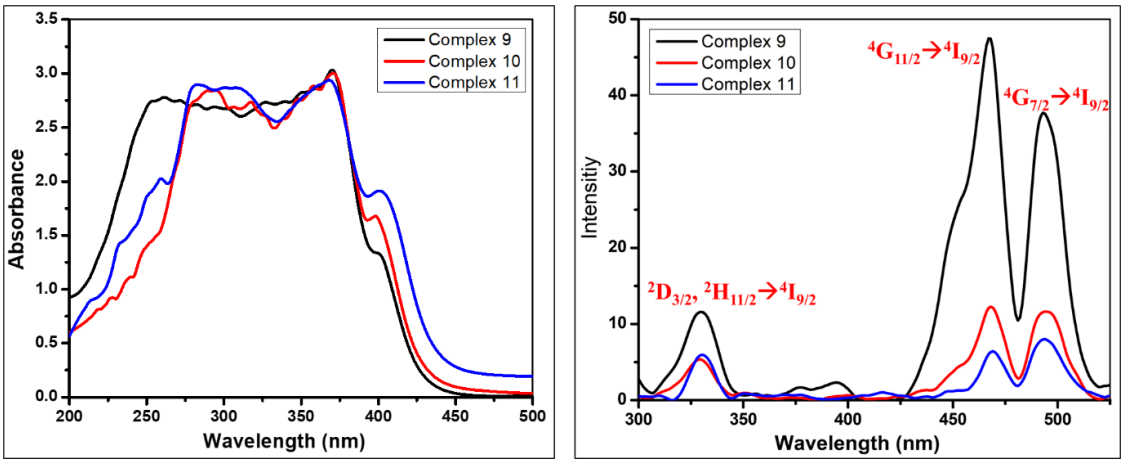

Figure 3b.17 The spectra of (a) Electronic absorption and (b) Emission for complexes 9, 10 and 11.

Table 3b.11 Absorption and emission peak analysis for complexes 9, 10 and 11.

Complex	Absorption	Emission	Shifting
9	261.6 (n→π*)	330 ($^2D_{3/2}$, $^2H_{11/2}$→$^4I_{9/2}$)	68.4
	370.3 (π→π*)	467.3 ($^4G_{11/2}$→$^4I_{9/2}$)	97
	398 (LMCT)	493.4 ($^4G_{7/2}$→$^4I_{9/2}$)	95.4
10	290 (n→π*)	329.4 ($^2D_{3/2}$, $^2H_{11/2}$→$^4I_{9/2}$)	39.4
	370.5 (π→π*)	467.7 ($^4G_{11/2}$→$^4I_{9/2}$)	97.2
	398.6	494.2 ($^4G_{7/2}$→$^4I_{9/2}$)	95.6
11	283 (n→π*)	330.3 ($^2D_{3/2}$, $^2H_{11/2}$→$^4I_{9/2}$)	47.3
	368 (π→π*)	468.5 ($^4G_{11/2}$→$^4I_{9/2}$)	100.5
	401 (LMCT)	493.4 ($^4G_{7/2}$→$^4I_{9/2}$)	92.4

The widely recognized energy diagram is reported [47], shown in Figure 3b.18, illustrates how energy is absorbed by the acylpyrazolone ligand, known as the "CL (central ligand)", transferred to the metal ion, and then returned to the ground state. The emission process of neodymium ions can be explained using this diagram [48,49]. Because of its $4f^3$ configuration of Nd^{3+}, splitting of the spectrum states caused by interelectronic repulsion, spin-orbit coupling, and ligand field influence will take place to partially or completely remove the J degeneracy, making the transition "allowed". Energy travels through a path that begins with the central ligand absorbing energy into its excited singlet state, which is subsequently transferred to a triplet state by the ISC before arriving at the Ln ion's energy levels. The functional group connected to the phenyl rings of acylpyrazolone, a NL (neutral ligand) that provides stability, fluorescence efficacy, absorption efficacy, and LMCT efficacy, is seen to have an impact on this light energy conversion diagram, which is also referred to as the "antenna effect" (See Figure 3b.18).

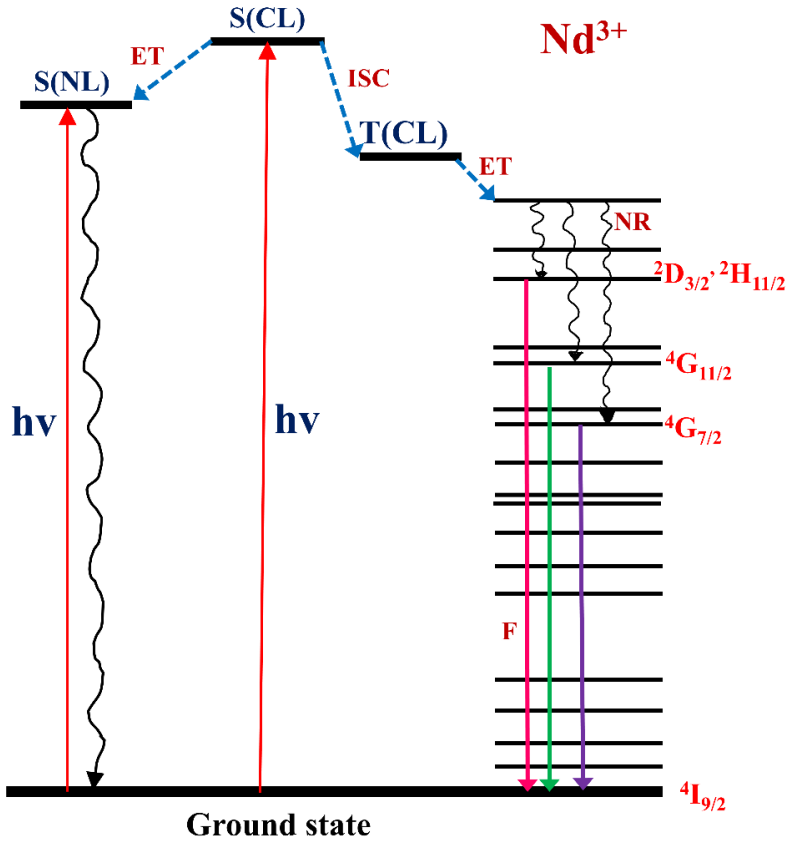

Energy level diagram for Nd^{3+} complex, where CL = central ligand, NL = neutral ligand, S = singlet excited state, T = triplet excited state, ET = intramolecular energy transfer, ISC = intersystem crossing, F = Fluorescence decay, NR = Non-radiative pathway

Figure 3b.18 "Antenna effect" diagram showing the mechanism of the emission process in complexes 9, 10 and 11.

3b.4 Conclusions

The main goals of the present research aimed to (i) measure the intensity of the hypersensitive transitions of chemically associated Nd(III)-acylpyrazolone complexes as well as pseudo-hypersensitive transitions across different solvents, (ii) show how the hypersensitive transition (oscillator strength, band shapes, and Judd-Ofelt parameters) responds to structural variations between the ligand in several complexes, and (iii) show the impact of various coordinating and non-coordinating solvents (iv) calculate the degree of covalency using various covalency parameters. Three neodymium-acylpyrazolone complexes—9, 10, and 11—had eight-coordinated distorted square antiprism geometry, which was held in space by three σ-donating acylpyrazolone ligands, one water molecule, and one ethanol molecule. The structure of all three

complexes was investigated using ESI-mass, FT-IR, thermogravimetric, and single-crystal X-ray diffraction methods. The $^4G_{5/2} \leftarrow {}^4I_{9/2}$ transition in the electronic spectra of complexes follows the electric-quadrupolar selection principles and is hypersensitive, as demonstrated by the larger value of oscillator strength and Ω_2 parameter. These findings unequivocally demonstrate that, among the solvents examined, DMF promotes the *4f-4f* strength the most. Additionally, in three solvents with strong coordination (pyridine, DMF, DMSO), three complexes exhibit the sequence 9 > 10 > 11. Lower consistent Ω_4 values and Hirshfeld analysis, indicating long-ranging secondary π···π stacking or H-bonding interactions. Calculating the covalency parameters demonstrates both the electron delocalization across the *4f* orbital and the covalency, both of which have been found to be positive for all complexes, suggesting an analogous degree of covalent bonding. The functional group attached to the phenyl rings of acylpyrazolone, an NL (neutral ligand) that provides stability, fluorescence efficacy, absorption efficacy, and LMCT efficacy, significantly impacts the intensity of emission spectra as seen in antenna effect energy diagrams. The potential to alter the acylpyrazolone's chemical and spectroscopic properties in order to synthesise multi-dentate Nd(III) complexes, which have special appeal in a variety of potential applications in the fields of material sensing and scanning that may help with understanding biological mechanisms or disease diagnosis.

References

[1] F. Marchetti, C. Pettinari, R. Pettinari, Acylpyrazolone ligands: Synthesis, structures, metal coordination chemistry and applications, Coord Chem Rev. 249 (2005) 2909–2945. https://doi.org/10.1016/j.ccr.2005.03.013.

[2] F. Marchetti, R. Pettinari, C. Pettinari, Recent advances in acylpyrazolone metal complexes and their potential applications, Coord Chem Rev. 303 (2015) 1–31. https://doi.org/10.1016/j.ccr.2015.05.003.

[3] F. Marchetti, C. Pettinari, C. Di Nicola, A. Tombesi, R. Pettinari, Coordination chemistry of pyrazolone-based ligands and applications of their metal complexes, Coord Chem Rev. 401 (2019) 213069. https://doi.org/10.1016/j.ccr.2019.213069.

[4] A.K. Patel, R.N. Jadeja, H. Roy, R.N. Patel, S.K. Patel, R.J. Butcher, Pseudo-tetrahedral copper(II) complex derived from N'-[(2E,3Z)-4-hydroxy-4-phenylbut-3-en-2-ylidene]acetohydrazide: Synthesis, molecular structure, quantum chemical investigations, antioxidant and antiproliferative properties, J Mol Struct 1185 (2019) 341–350. https://doi.org/10.1016/j.molstruc.2019.03.004.

[5] G.M. Sheldrick, SHELXT - Integrated space-group and crystal-structure determination, Acta Crystallogr A. 71 (2015) 3–8. https://doi.org/10.1107/S2053273314026370.

[6] G.M. Sheldrick, Crystal structure refinement with SHELXL, Acta Crystallogr C Struct Chem. 71 (2015) 3–8. https://doi.org/10.1107/S2053229614024218.

[7] I. Shaikh, R.N. Jadeja, R. Patel, Three mixed ligand mononuclear Zn(II) complexes of 4-acyl pyrazolones: Synthesis, characterization, crystal study and anti-malarial activity, Polyhedron 183 (2020) 114528. https://doi.org/10.1016/j.poly.2020.114528.

[8] W.J. Geary, The use of conductivity measurements in organic solvents for the characterisation of coordination compounds, Coord Chem Rev 7 (1971) 81–122. https://doi.org/10.1016/S0010-8545(00)80009-0.

[9] R. Ilmi, K. Iftikhar, Structure elucidation by sparkle/RM1, effect of lanthanide contraction and photophysical properties of lanthanide(III) trifluoroacetylacetonate complexes with 1,10-phenanthroline, J Photochem Photobiol A Chem 325 (2016) 68–82. https://doi.org/10.1016/j.jphotochem.2016.03.018.

[10] R. Ilmi, K. Iftikhar, Luminescent nine-coordinate lanthanide complexes derived from fluorinated β-diketone and 2,4,6-tris (2-pyridyl)-1,3,5-triazine, J Coord Chem 65 (2012) 403–419. https://doi.org/10.1080/00958972.2011.649737.

[11] P.R. Patel, T. Thaker, S. Zele, Preparation and characterisation of some lanthanide complexes involving a heterocyclic β-diketone, Indian J Chem A. 38 (1999) 563–567. https://nopr.niscpr.res.in/bitstream/123456789/15786/1/IJCA%2038A%286%29%20563-567.pdf.

[12] E.C. Okafor, The Metal Chelates of Heterocyclic β-Diketones and their Derivatives, Part IV New Mixed Ligand Tetrakis Complexes of Lanthanides Derived from tris-Acetylacetonates and Some 4-Acyl Pyrazolones, Z Naturforsch B. 35 (1980) 715–718. https://doi.org/10.1515/znb-1980-0615.

[13] N.M. Shavaleev, R. Scopelliti, F. Gumy, J.C.G. Bünzli, Near-infrared luminescence of nine-coordinate neodymium complexes with benzimidazole-substituted 8-hydroxyquinolines, Inorg Chem. 47 (2008) 9055–9068. https://doi.org/10.1021/ic8010585.

[14] Z. Ahmed, H.C. Avila, R.S. Carvalho, J. Kai, J.A.L.C. Resende, E. Bandini, A. Barbieri, M. Cremona, Bright neodymium complexes for efficient near infra-red organic light emitting diodes, New J Chem 44 (2020) 14161–14170. https://doi.org/10.1039/d0nj00403k.

[15] G. Bombiere, A. Polo, W. Jia-Fu, W. Jinguang, X. Guang-Xian, Synthesis and characterization of a ytterbium complex with diphenylacetylpyrazolone $Yb(DPAP)_3 \cdot (H_2O)_2 \cdot 3EtOH$, Inorganica Chim Acta. 132 (1987) 263–271. https://doi.org/10.1016/S0020-1693(00)81753-3.

[16] E. C. Okafor, The metal complexes of heterocyclic β-diketones and their derivatives—IX. Lanthanon chelates of 3-methyl-1-phenyl-4-trifluoroacetylpyrazol-5-one (HPMTFP). ^{1}H, ^{13}C and ^{19}F NMR, i.r. and u.v.-visible spectral studies, Spectrochim Acta A Mol Spectrosc. 38 (1982) 981–987. https://doi.org/10.1016/0584-8539(82)80049-4.

[17] V.F. Shul'Gin, S. V. Abkhairova, O. V. Konnik, S.B. Meshkova, Z.M. Topilova, E.B. Rusanov, G.G. Aleksandrov, I.L. Eremenko, Anionic lanthanide complexes with 3-

methyl-4-formyl-1-phenyl-5-pyrazolone, Russ J Inorg Chem. 58 (2013) 678–683. https://doi.org/10.1134/S0036023613060223.

[18] Z. Ahmed, R.E. Aderne, J. Kai, H.I.P. Chavarria, M. Cremona, Ytterbium β-diketonate complexes for near infra-red organic light-emitting devices, Thin Solid Films. 620 (2016) 34–42. https://doi.org/10.1016/j.tsf.2016.07.076.

[19] D. Zhou, Q. Li, C. Huang, G. Yao, S. Umetani, M. Matsui, L. Ying, A. Yu, X. Zhao, Room-temperature fluorescence, phosphorescence and crystal structures of 4-acyl pyrazolone lanthanide complexes: $Ln(L)_3.2H_2O$, Polyhedron. 16 (1997) 1381–1389. https://doi.org/10.1016/S0277-5387(96)00382-8.

[20] Q. Liu, S. Zhang, K. Du, W. Li, Q. Yin, P. jun Cai, Structure and photoluminescence properties study of neodymium complexes containing fluorine ligands, J Fluor Chem. 212 (2018) 161–165. https://doi.org/10.1016/j.jfluchem.2018.03.015.

[21] C.F. Yao, Y.S. Chen, W.C. Chen, R.S. Sheu, J.K. Lai and C.H. Ueng, 1,3-Diphenyl-2-tricyclo[3.3.1.$1^{3,7}$]dec-2-ylidenepropane-1,3-diimine, and its -1-imino-3-one and -1,3-dione Derivatives, Acta Cryst, C53 (1997) 956–959. https://doi.org/10.1107/S0108270197002746.

[22] Q. Liu, P. Cai, X. Wan, S. Zhang, K. Du, Q. Yin, Neodymium ternary complexes with 2,4,6-tri(2-pyridyl)-1,3,5-triazine: Synthesis, crystal structure and fluorescence property, J Mol Struct. 1193 (2019) 151–157. https://doi.org/10.1016/j.molstruc.2019.05.008.

[23] C.F. Mackenzie, P.R. Spackman, D. Jayatilaka, M.A. Spackman, CrystalExplorer model energies and energy frameworks: Extension to metal coordination compounds, organic salts, solvates and open-shell systems, IUCrJ. 4 (2017) 575–587. https://doi.org/10.1107/S205225251700848X.

[24] B. Dziuk, B. Ośmiałowski, B. Zarychta, K. Ejsmont, L. Chęcińska, Symmetric fluoroborate and its boron modification: Crystal and electronic structures, Crystals (Basel) 9 (2019) 662. https://doi.org/10.3390/cryst9120662.

[25] K. Klai, K. Kaabi, W. Kaminsky, C. Jelsch, F. Lefebvre, C. Ben Nasr, A Hirshfeld surface analysis, crystal structure and physicochemical studies of a new Cd(II) complex

with the 2-amino-4-methylpyrimidine ligand, J Mol Struct 1128 (2017) 378–384. https://doi.org/10.1016/j.molstruc.2016.09.002.

[26] A.P. Novikov, M.A. Volkov, A.V. Safonov, M.S. Grigoriev, Synthesis, Crystal Structure, and Hirshfeld Surface Analysis of Hexachloroplatinate and Tetraclorouranylate of 3-Carboxypyridinium—Halogen Bonds and π-Interactions vs. Hydrogen Bonds, Crystals (Basel) 12 (2022). https://doi.org/10.3390/cryst12020271.

[27] R. Ilmi, K. Iftikhar, Pyrazine bridged Ln_2 (La, Nd, Eu and Tb) complexes containing fluorinated β-diketone, Inorg Chem Commun 20 (2012) 7–12. https://doi.org/10.1016/j.inoche.2012.01.037.

[28] H. Debecca Devi, Ch. Sumitra, Th. David Singh, N. Yaiphaba, N. Mohondas Singh, N. Rajmuhon Singh, Calculation and Comparison of Energy Interaction and Intensity Parameters for the Interaction of Nd(III) with DL-Valine, DL-Alanine and β-Alanine in Presence and Absence of Ca^{2+} / Zn^{2+} in Aqueous and Different Aquated Organic Solvents Using 4f-4f Transition Spectra as Probe , Int J Spectrosc 2009 (2009) 1–9. https://doi.org/10.1155/2009/784305.

[29] R. Ilmi, K. Iftikhar, Luminescent nine-coordinate lanthanide complexes derived from fluorinated β-diketone and 2,4,6-tris (2-pyridyl)-1,3,5-triazine, J Coord Chem 65 (2012) 403–419. https://doi.org/10.1080/00958972.2011.649737.

[30] W.T. Carnall, P.R. Fields, B.G. Wybourne, Spectral intensities of the trivalent lanthanides and actinides in solution. I. Pr^{3+}, Nd^{3+}, Er^{3+}, Tm^{3+}, and Yb^{8+}, J Chem Phys 42 (1965) 3797–3806. https://doi.org/10.1063/1.1695840.

[31] P. Hervé, L.K.J. Vandamme, General relation between refractive index and energy gap in semiconductors, Infrared Phys Technol 35 (1994) 609–615. https://doi.org/10.1016/1350-4495(94)90026-4.

[32] P. Ahlawat, S. Bhayana, V. Lather, S. Khatri, P. Kumari, M. Kumar, M.S. Shekhawat, V.B. Taxak, S.P. Khatkar, R. Kumar, Judd-Ofelt, urbach energy and geometrical optimization study of orange light emitting samarium (III) complexes with heterocyclic ligands for application in optoelectronic devices, Opt Mater (Amst) 133 (2022) 112940. https://doi.org/10.1016/j.optmat.2022.112940.

[33] Y. Tian, B. Chen, R. Hua, J. Sun, L. Cheng, H. Zhong, X. Li, J. Zhang, Y. Zheng, T. Yu, L. Huang, H. Yu, Optical transition, electron-phonon coupling and fluorescent quenching of $La_2(MoO_4)_3:Eu^{3+}$ phosphor, J Appl Phys 109 (2011) 053511. https://doi.org/10.1063/1.3551584.

[34] W. Luo, J. Liao, R. Li, X. Chen, Determination of Judd–Ofelt intensity parameters from the excitation spectra for rare-earth doped luminescent materials, Phys Chem Chem Phys 12 (2010) 3276–3282. https://doi.org/10.1039/B921581F.

[35] M. Luo, B. Chen, X. Li, J. Zhang, S. Xu, X. Zhang, Y. Cao, J. Sun, Y. Zhang, X. Wang, Y. Zhang, D. Gao, L. Wang, Fluorescence decay route of optical transition calculation for trivalent rare earth ions and its application for Er^{3+}-doped $NaYF_4$ phosphor, Phys Chem Chem Phys 22 (2020) 25177–25183. https://doi.org/10.1039/D0CP04379F.

[36] Y. Zhang, B. Chen, S. Xu, X. Li, J. Zhang, J. Sun, X. Zhang, H. Xia, R. Hua, A universal approach for calculating the Judd–Ofelt parameters of RE^{3+} in powdered phosphors and its application for the β-$NaYF_4:Er^{3+}/Yb^{3+}$ phosphor derived from auto-combustion-assisted fluoridation, Phys Chem Chem Phys 20 (2018) 15876–15883. https://doi.org/10.1039/C8CP02317D.

[37] G.S. Opelt, Intensities of crystal spectra of rare-earth ions, J Chem Phys 37 (1962) 511–520. https://doi.org/10.1063/1.1701366.

[38] B.R. Judd, Optical Absorption Intensities of Rare-Earth Ions, 127 (1962) 750–761. https://doi.org/10.1103/PhysRev.127.750.

[39] P. Goldner, F. Auzel, Application of standard and modified Judd-Ofelt theories to a praseodymium-doped fluorozirconate glass, J Appl Phys 79 (1996) 7972–7977. https://doi.org/10.1063/1.362347.

[40] M. İlhan, L.F. Güleryüz, Boron doping effect on the structural, spectral properties and charge transfer mechanism of orthorhombic tungsten bronze β-$SrTa_2O_6:Eu^{3+}$ phosphor, RSC Adv 13 (2023) 12375–12385. https://doi.org/10.1039/D3RA00618B.

[41] M. İlhan, M.İ. Katı, İ.Ç. Keskin, L.F. Güleryüz, Evaluation of structural and spectroscopic results of tetragonal tungsten bronze $MTa_2O_6:Eu^{3+}$ (M = Sr, Ba, Pb) phosphors and comparison on the basis of Judd-Ofelt parameters, J Alloys Compd 901 (2022) 163626. https://doi.org/10.1016/j.jallcom.2022.163626.

[42] J.H.S.K. Monteiro, I.O. Mazali, F.A. Sigoli, Determination of Judd-Ofelt Intensity Parameters of Pure Samarium(III) Complexes, J Fluoresc 21 (2011) 2237–2243. https://doi.org/10.1007/s10895-011-0928-x.

[43] C.K. Jørgensen, R. Reisfeld, Judd-Ofelt parameters and chemical bonding, J Less-Common Met 93 (1983) 107–112. https://doi.org/10.1016/0022-5088(83)90454-X.

[44] K. Iftikhar, Hypersensitivity in the 4f–4f absorption spectra of lanthanide(III) complexes, Inorganica Chim Acta. 129 (1987) 261–264. https://doi.org/10.1016/S0020-1693(00)86672-4.

[45] M.C. Chavan, P. V Vaidya, N.R. Lokhande, M.N. Ghoshal, Bonding and Energy Parameters for Some Praseodymium(III) Mixed Ligand Complexes, Asian J Chem 22 (2010) 2575–2578. https://asianpubs.org/index.php/ajchem/article/view/11445.

[46] I. Ameen, A.K. Tripathi, R.L. Mishra, A. Siddiqui, U.N. Tripathi, Aging effect on bonding properties of fluorescent neodymium materials, Karbala International Journal of Modern Science 4 (2018) 258–273. https://doi.org/10.1016/j.kijoms.2018.05.001.

[47] N. Sabbatini, M. Guardigli, J.-M. Lehn, Luminescent lanthanide complexes supramolecular devices as photochemical, Coord Chem Rev. 123 (1993) 201–228. https://doi.org/10.1016/0010-8545(93)85056-A.

[48] M. Mirzaei, H. Eshtiagh-Hosseini, N. Lotfian, A. Salimi, A. Bauzá, R. Van Deun, R. Decadt, M. Barceló-Oliver, A. Frontera, Syntheses, structures, properties and DFT study of hybrid inorganic–organic architectures constructed from trinuclear lanthanide frameworks and Keggin-type polyoxometalates, Dalton Trans 43 (2014) 1906–1916. https://doi.org/10.1039/C3DT51971F.

[49] M. Samaniyan, M. Mirzaei, R.M. Gomila, H. Eshtiagh-Hosseini, N. Lotfian, J.T. Mague, A.N. Pour, A. Frontera, Supramolecular network of a framework material supported by the anion–π linkage of Keggin-type heteropolyoxotungstates: experimental and theoretical insights, Dalton Trans 50 (2021) 1895–1900. https://doi.org/10.1039/D0DT03891A.

Published Papers:

ChemistrySelect | Research Article
doi.org/10.1002/slct.202302438
Chemistry Europe
European Chemical Societies Publishing

www.chemistryselect.org

Structural Features, Emission Analysis, and Covalency Comparison of Neodymium Acylpyrazolone Complexes using Oscillator Strengths, Covalency and Judd-Ofelt Parameters**

Maitrey Travadi,[a] Rajendrasinh N. Jadeja,*[a] and Ray J. Butcher[b]

Three distorted square antiprismatic eight coordinated neodymium acylpyrazolone complexes were synthesized having the compositions $[Nd(L_1)_3(H_2O)(EtOH)]$ (**NdL_1**), $[Nd(L_2)_3(H_2O)(EtOH)]$ (**NdL_2**), and $[Nd(L_3)_3(H_2O)(EtOH)]$ (**NdL_3**). The structure of all three complexes was examined using ESI-mass, FT-IR, and thermogravimetric methods. According to the single crystal analysis of NdL_1, the complex was found eight coordinated (NdO8) with a distorted square antiprismatic geometry. A powder XRD pattern confirmed a similar structural arrangement of the other two complexes. In electronic absorption spectra, the transition $^4G_{5/2}\leftarrow{}^4I_{9/2}$, which is close to the centre of the visible spectrum (~17,500 cm^{-1}), exhibits hypersensitivity, which stands out in stark contrast to the behaviour of many other typically weak and reliably unchanging, typical 4f–4f transitions. Through a comparative analysis of calculated oscillator strength, Judd-Ofelt parameters, root mean square deviation, radiative lifetime and covalency parameters in various solvents, hypersensitivity, symmetry characteristics, and covalency have been thoroughly investigated. The promotion of 4f–4f electric-dipole intensity has been found to be particularly successful with ethanol, pyridine, DMF, and DMSO. Utilizing Judd-Ofelt Ω_4 values and Hirshfeld analysis, long-range secondary π···π stacking or H-bonding interactions were investigated. The intensity of emission spectra, quantum yield, stokes shift, and antenna effect energy diagram was examined using solid-state emission spectra.

Introduction

The coordination chemistry of lanthanide ions has attracted a lot of interest over the past two decades due to their advantageous magnetic, thermal, cytotoxic, redox, and optical properties as well as their enormous coordination numbers, which enable highly complex and dimensional networks to be produced.[1–8] Due to their diverse variety of distinctive properties, they have found usage in NMR imaging, sensors, the lighting sector, fibres, display devices, lasers, and biological assays.[7] Due to the low impact of the environment on 4f electrons – which are shielded by $5s^2$ and $5p^6$ orbitals and ion-specific emission – lanthanides normally do not promote higher covalency with ligands. The distinctive 4f–4f electronic transition of Ln(III) is sharp because of the modest stokes shift brought on by the intrinsic nature of 4f electrons, which is protected from the 5s and 5p electrons and restricts the disruption of the 4f electrons by the ligand field. Since it is difficult to pinpoint the characteristics of lanthanide complexes and covalency forms the basis for explaining the bonding of lanthanide complexes, it is necessary to investigate the type and degree of covalency.[9] Even though there are limitations imposed by the Laporte ($\triangle L = \pm 1$) and Spin ($\triangle S = 0$) rules for 4f–4f transitions, a small number of spectral transitions exhibit higher intensities (known as hypersensitive transitions) and greatly affect covalency because they are extremely sensitive to the ligand's environment. Judd-Ofelt intensity parameters (Ω_2, Ω_4, Ω_6) and oscillator strength calculations are essential since their values give the ligand a distinctive impact on the intra-configurational transition of the Ln(III)-ions according to factors of covalency, number and magnitude of lines, and the ratio of transition intensities.[10,11] These factors reveal details about the rigidity, long-range distance, symmetry, and coordination number of complexes.

Among all the lanthanides, neodymium is known for forming alloys to make strong permanent magnets. Neodymium can be extracted using various techniques, including ion exchange, flash pyrolysis,[12] solvent extraction,[13] etc. Neodymium compounds and nanomaterials are known for anticandidal,[14] nano catalytic,[15] chemo selective,[15] optical limiting,[16] antibacterial,[17] wastewater treatment,[18] structural, optical, and electrical[19] activities. Perovskite strontium doped neodymium manganite is known for effectively removing Fast Green Dye.[20] Neodymium complexes with a β-diketone backbone containing ligands generally prefer distorted square antiprism geometry.[21] Dynamic coupling mechanism provides major contribution to the intensity of hypersensitive transition in Nd-β -diketone complexes.[22] NIR-emitting ternary neodymium tris β-diketonate complexes have excellent organic

[a] M. Travadi, Dr. R. N. Jadeja
Department of Chemistry, Faculty of Science, The Maharaja Sayajirao University of Baroda, Vadodara 390002, India
E-mail: rjadeja-chem@msubaroda.ac.in
[b] Prof. R. J. Butcher
Department of Inorganic & Structural Chemistry, Howard University, Washington, DC, 22031, USA
[**] A previous version of this manuscript has been deposited on a preprint server (https://doi.org/10.2139/ssrn.4425346).
Supporting information for this article is available on the WWW under https://doi.org/10.1002/slct.202302438

Inorganica Chimica Acta 559 (2024) 121766

Contents lists available at ScienceDirect

Inorganica Chimica Acta

journal homepage: www.elsevier.com/locate/ica

Neodymium based acylpyrazolone complexes: Synthesis and physicochemical characterizations

Maitrey Travadi [a], Rajendrasinh N. Jadeja [a,*], Ray J. Butcher [b], Manoj S. Shekhawat [c]

[a] Department of Chemistry, Faculty of Science, The Maharaja Sayajirao University of Baroda, Vadodara 390002, India
[b] Department of Inorganic & Structural Chemistry, Howard University, Washington, DC 22031, USA
[c] Department of Physics, Engineering College Bikaner, Bikaner 334001, India

ARTICLE INFO

Keywords:
Neodymium acylpyrazolone
4f-4f transition and hypersensitivity
Oscillator strength
Judd-Ofelt and covalency parameter
Antenna effect energy diagram

ABSTRACT

The electronic spectra of three neodymium acylpyrazolone complexes with the compositions [Nd(DMBPMP)$_3$(H_2O)(EtOH)] (**Nd1**), [Nd(DMMCPMP)$_3$(H_2O)(EtOH)] (**Nd2**), and [Nd(DMBPTMP)$_3$(H_2O)(EtOH)] (**Nd3**) have been analyzed. Utilizing ESI-mass, FT-IR, thermogravimetric, and single crystal X-ray diffraction methods, the structure of the DMBPTMP ligand and all three complexes were investigated. According to the single crystal analysis of Nd2, the complex is mononuclear and eight-coordinate (NdO_8) with a distorted square antiprismatic geometry. A powder XRD pattern confirmed a similar structural arrangement of the other two complexes. The transition $^4G_{5/2} \leftarrow {}^4I_{9/2}$, which is close to the centre of the visible spectrum (~17,500 cm^{-1}), exhibits hypersensitivity, which stands out in stark contrast to the behaviour of many other typically weak and reliably unchanging, typical *4f-4f* transitions. Through a comparative analysis of calculated oscillator strength, Judd-Ofelt parameters, and covalency parameters in various solvents, hypersensitivity, symmetry characteristics, and covalency have been thoroughly investigated. The promotion of *4f-4f* electric-dipole intensity has been found to be particularly successful with DMF, DMSO, pyridine and ethanol. Utilizing Judd-Ofelt parameter Ω_4 values and Hirshfeld analysis, long-range secondary π···π stacking or H-bonding interactions were investigated. Using solid-state emission spectra, intensity of emission spectra and antenna effect energy diagram was examined.

1. Introduction

Due to the beneficial magnetic, redox, and optical properties of lanthanoids as well as their enormous coordination numbers, which allow for high complexity and dimensionality of the resulting networks, the coordination chemistry of lanthanoids has received a lot of attention over the past two decades [1–4]. Lanthanoids typically do not favour greater covalency with ligands because of the minimal effect of the environment on *4f* electrons, which are protected by $5s^2$ and $5p^6$ orbitals and ion-specific emission. Due to varied binding and ligand coordination, several complexes with pyrazine or pyridine derivatives [5,6], carboxylates [7], have diverse characteristics. Numerous inorganic–organic hybrids based on Keggin polyoxometalates were created using various 5-membered *N*-bidentate ligands with lanthanides and had varying coordination properties [8]. It is reported that developments in the field of metal–organic frameworks, utilising suitable functional groups and guest molecules, offer properties such host–guest interactions, photosensitization, exciton diffusion, etc. that are adequate [9]. Other features, including as non-covalent interactions and binding energies, are essential for the stabilisation of crystals in various geometries according to research that has reportedly been done in this field [10–13]. Since it is difficult to pinpoint the characteristics of lanthanoid complexes and since covalency forms the basis for explanations of the bonding of Ln-acylpyrazolones, it is necessary to investigate the type and degree of covalency [14]. Even though there are limitations imposed by the Laporte ($\Delta L = \pm 1$) and Spin ($\Delta S = 0$) rules for *4f-4f* transitions, a small number of spectral transitions exhibit higher intensities (known as hypersensitive transitions) are affected by covalency because they are extremely sensitive to the ligand's environment. Judd-Ofelt intensity parameters (Ω_2, Ω_4, Ω_6) and oscillator strength

Abbreviations: DMBPMP, (4-(3,5-dimethyl benzoyl) 1-phenyl 3-methyl 5-pyrazolone ligand; DMBMCPMP, (4-(3,5-dimethyl benzoyl) 1-(m-chlorophenyl) 3-methyl 5-pyrazolone) ligand; DMBPTMP, (4-(3,5-dimethyl benzoyl) 1-(p-tolyl) 3-methyl 5-pyrazolone) ligand.

* Corresponding author.
E-mail address: rjadeja-chem@msubaroda.ac.in (R.N. Jadeja).

https://doi.org/10.1016/j.ica.2023.121766
Received 19 July 2023; Received in revised form 4 September 2023; Accepted 14 September 2023
Available online 21 September 2023